

Aus dem Pathologischen Institut der Ludwig-Maximilians-Universität München

Direktor: Prof. Dr. med. Thomas Kirchner

in der Arbeitsgruppe Experimentelle und Molekulare Pathologie

Leiter: Prof. Dr. rer. nat. Heiko Hermeking

Genetic analysis of *Ap4* in the *Apc^{Min}* mouse model

Dissertation zum Erwerb des Doktorgrades der
Naturwissenschaften (Dr. rer. nat.) an der Medizinischen Fakultät
der Ludwig-Maximilians-Universität München

vorgelegt von

Stephanie Jaeckel

aus Flensburg

2018

**Gedruckt mit der Genehmigung der Medizinischen Fakultät
der Ludwig-Maximilians-Universität München**

Erstgutachter: Prof. Dr. rer. nat. Heiko Hermeking

Zweitgutachter: Priv. Doz. Dr. rer. nat. Andreas Herbst

Dekan: Prof. Dr. med. dent. Reinhard Hickel

Tag der mündlichen Prüfung: 04.04.2019

Meiner Mutter und Großmutter

Eidesstattliche Versicherung

Stephanie Jaeckel

Ich erkläre hiermit an Eides statt, dass ich die vorliegende Dissertation mit dem Thema

“Genetic analysis of *Ap4* in the *Apc^{Min}* mouse model”

selbständig verfasst, mich außer der angegebenen keiner weiteren Hilfsmittel bedient und alle Erkenntnisse, die aus dem Schrifttum ganz oder annähernd übernommen sind, als solche kenntlich gemacht und nach ihrer Herkunft unter Bezeichnung der Fundstelle einzeln nachgewiesen habe.

Ich erkläre des Weiteren, dass die hier vorgelegte Dissertation nicht in gleicher oder in ähnlicher Form bei einer anderen Stelle zur Erlangung eines akademischen Grades eingereicht wurde.

Ort, Datum: München, 11.04.2019

Unterschrift: Stephanie Jaeckel

Publications

Publications

Parts of this thesis have been published in the article:

Stephanie Jaeckel, Markus Kaller, Rene Jackstadt, Ursula Götz, Susanna Müller, Sophie Boos, David Horst, Peter Jung and Heiko Hermeking. *Ap4* is rate limiting for intestinal tumor formation by controlling the homeostasis of intestinal stem cells. ***Nature Communications***; 2018; 9: 3573.

Abbreviations

Abbreviations

ABC	Avidin-Biotin complex
AEC	3-Amino-9-ethylcarbazole
AP4	Activating enhancer binding protein 4
APC	Adenomatous polyposis coli
APC ^{Min}	APC ^{Multiple intestinal neoplasia}
APS	Ammonium peroxodisulfate
bHLH-LZ	basic-Helix-loop-helix leucine zipper
cDNA	complementary DNA
ChIP	Chromatin immuno-precipitation
ChIP-seq	ChIP-sequencing
CMS	Consensus molecular <i>subtypes</i>
CRC	Colorectal cancer
Cre	Cyclization recombination or “causes recombination”
CSC	Cancer stem cell
CSL	CBF1/suppressor of Hairless/LAG-1
CTTNB1	Catenin beta 1, gene encoding β -catenin
DAB	3,3'-diaminobenzidine
DAPI	2-(4-Amidinophenyl)-6-indolecarbamide-dihydrochloride
DBZ	Dibenzazepine (inhibitor of γ -secretase)
DCS	Deep crypt secretory cells
DIG	Digoxigenin
DMEM	Dulbecco`s modified Eagles medium
DMSO	Dimethyl-sulfoxide
DNA	Deoxyribonucleic acid
DOX	Doxycycline
dNTPs	Deoxynucleotides triphosphate
E-Box	Enhancer box
<i>E.coli</i>	<i>Escherichia coli</i>
ECL	Enhanced chemiluminescence
EDTA	Ethylene-diamine-tetra-acetic acid
EGF	Epidermal growth factor
eGFP	enhanced Green fluorescent protein
EM	Electron microscopy
EMT	Epithelial-mesenchymal transition
EMT-TF	EMT-inducing transcription factor
ER	Endoplasmatic reticulum
ERT2	Estrogen receptor tamoxifen inducible 2
ES cells	Embryonic stem cells
FAP	Familial adenomatous polyposis
FBS	Fetal bovine serum
FFPE	Formalin-fixed, paraffin-embedded
FITC	Flourescein
fl	Floxed, flanked by loxP
flp	Flippase
frt	flp recognition target

Abbreviations

GSEA	Gene set enrichment analysis
HBSS	Hank's balanced salt solution
HE	Hematoxylin and eosin
HES	Hairy and enhancer of split
HRP	Horse-radish-peroxidase
IEC	Intestinal epithelial cell
IF	Immunofluorescence
IgG	Immunoglobulin G
IHC	Immunohistochemistry
ISC	Intestinal stem cell
ISH	<i>In situ</i> hybridization
IVC	Individually ventilated cages
Kbp	Kilo base pair
KD=kDa	Kilo dalton
KEGG	Kyoto Encyclopedia of Genes and Genomes
Ko	Knockout
LGR5	Leu-rich repeat-containing G protein-coupled Receptor 5
loxP	Locus of X-over P1
LRC	Label retaining cell
LSM	Laser scanning microscopy
MEF	Mouse embryonic fibroblast
MET	Mesenchymal-epithelial transition
mRNA	Messenger RNA
MSigDB	Molecular signatures database
NEO	Neomycin
NGS	Next-generation sequencing
NICD	Notch intracellular domain
4-OHT	4-hydroxytamoxifen
OLFM4	Olfactomedin 4
ORF	Open reading frame
PAGE	Polyacrylamide gel electrophoresis
PAS	Periodic acid-Schiff
PBS	Phosphate buffered saline
PCR	Polymerase chain reaction
PFA	Paraformaldehyde
P/S	Penicillin Streptomycin
qPCR	Quantitative real-time PCR
RBP-J κ	Recombination signal binding protein for immunoglobulin kappa J region
RNA	Ribonucleic acid
RNA-Seq	RNA-Sequencing
Rpkm	Reads per kilobase million
RSEM	RNA-Seq by expectation maximization
RSPO1	R-spondin-1
SD	Standard deviation
SDS	Sodium dodecyl sulfate
siRNA	Small interfering RNA
SMOC2	SPARC-related modular calcium-binding protein 2
TAM	Tamoxifen

Abbreviations

TA unit	Transient-amplifying unit
TCF	T-cell factor
TCGA	The cancer genome atlas
TEMED	Tetramethylethylenediamin, 1,2-bis (dimethylamino) - ethan
TFAP4	Transcription factor AP4
TMA	Tissue microarray
TSS	Transcriptional start site
Vil-Cre	Villin-Cre
VSV	Vesicular stomatitis virus (tag)
WB	Western blot analysis
WNT	Wingless/Int-1
Wt	Wild-type

Table of contents

Table of contents

Eidesstattliche Versicherung	I
Publications	II
Abbreviations	III
1. Introduction	1
1.1 Cancer incidence	1
1.2 The hallmarks of cancer	2
1.3 The genetics of colorectal cancer	3
1.4 Canonical Wnt-signaling in colorectal cancer	4
1.5 The Notch signaling in colorectal cancer	5
1.6 The transcription factor AP4	8
1.7 The role of AP4 in colorectal cancer	10
1.8 The homeostasis of the intestinal epithelium	11
1.9 The role of the Wnt and Notch pathway in intestinal homeostasis	13
2. Aims of the study	16
3. Materials	17
3.1 Chemicals and reagents	17
3.2 Enzymes	19
3.3 Kits	19
DAB+ Substrate Chromogen System	19
3.4 Antibodies	20
3.4.1 Primary antibodies	20
3.4.2 Secondary antibodies	21
3.5 Buffers and solutions	22
3.6 Oligonucleotides	26
3.6.1 Oligonucleotides used for genotyping	26
3.6.2 Oligonucleotides used for qPCR	26
3.6.3 Oligonucleotides used for qCHIP	27
3.7 siRNAs	29
3.8 Vectors	29

Table of contents

3.9 Mice	29
3.10 Cell lines.....	30
3.11 Software	30
3.12 Laboratory equipment	31
4. Methods	32
4.1 Generation and husbandry of mice.....	32
4.2 Tissue preparation and adenoma counting.....	32
4.3 HE and PAS/Alcian blue staining.....	33
4.4 Immunohistochemistry	33
4.5 <i>In situ</i> hybridization.....	34
4.6 Isolation of IECs	34
4.7 Crypt isolation and organoid culture.....	34
4.8 Tissue microarrays and IHC (immunohistochemistry) analysis of clinical samples	36
4.9 RNA expression profiling by RNA-Seq	36
4.10 Bioinformatics analyses of RNA-Seq and ChIP-Seq data.....	36
4.11 <i>In silico</i> analysis of human colorectal patient samples	37
4.12 Indirect immunofluorescence detection and confocal laser-scanning microscopy.....	38
4.13 Electron microscopy.....	38
4.14 RNA isolation and quantitative real-time PCR (qPCR)	38
4.15 DBZ treatment of mice.....	38
4.16 Cell lines / culture and reagents	39
4.17 Chromatin immunoprecipitation (ChIP) assay.....	39
4.18 Generation of cell pools stably expressing conditional alleles	40
4.19 Plasmids and RNAi.....	40
4.20 Cell-Based Reporter Assays.....	40
4.21 Western blot analysis	41
4.22 Statistical analysis	41
4.23 Data availability statement.....	41
5. Results	42

Table of contents

5.1 Role of <i>Ap4</i> in intestinal adenoma formation.....	42
5.2 mRNA expression profiling of <i>Ap4</i> -deficient adenomas.....	49
5.3 Analysis of tumor organoids from <i>Ap4</i> -deficient <i>Apc^{Min}</i> mice.....	57
5.4 <i>Ap4</i> regulates the homeostasis of intestinal stem cells.....	62
5.5 Analysis of <i>Ap4</i> function in intestinal organoids.....	73
5.6 Gene expression profiling of <i>Ap4</i> -deficient organoids.....	74
5.7 Regulation of the NOTCH pathway by AP4 in human CRC cells.....	80
5.8 Role of AP4 in human CRCs.....	86
6. Discussion.....	90
7. Summary.....	97
8. Zusammenfassung.....	98
9. Acknowledgements.....	99
10. References.....	100
11. Supplements.....	113
11.1 Supplemental Data 1.....	113
11.2 Supplemental Data 2.....	128
11.3 Supplemental Data 3.....	146

Introduction

1. Introduction

1.1 Cancer incidence

Today, cancer is the second major reason for global death: 9,6 million people have died of cancer in 2018, while 18,1 million new cases have been registered (Figure 1) (as of 12th of September 2018 at (www.who.int/cancer/PRGlobocanFinal.pdf?ua=1)).

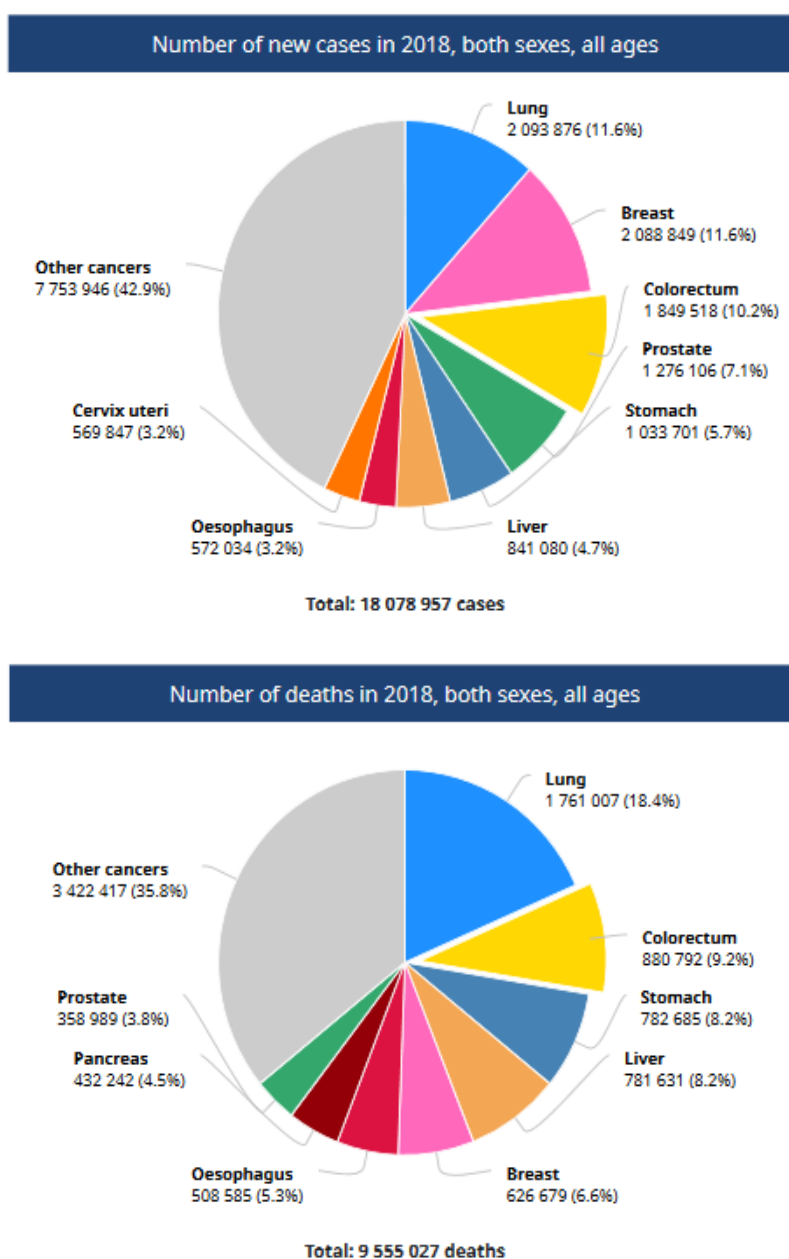


Figure 1 Cancer incidence in 2018. Number of new cases (upper panel) and cancer related deaths (lower panel) in 2018. Colorectal cancer is highlighted. Taken from: http://gco.iarc.fr/today/data/factsheets/cancers/10_8_9-Colorectum-fact-sheet.pdf. As of 12th of September 2018.

Introduction

Colorectal cancers (CRCs) constitute about 1.8 million new cases and 10.2% of all new cancer cases in 2018 worldwide, while CRC related deaths include 881.000 cases and 9,2% of all cancer related deaths. CRC is the third most frequent cause of new cancer cases and the second most frequent cause of cancer related deaths worldwide (Figure 1).

1.2 The hallmarks of cancer

Cancer develops after an accumulation of mutations in genes leading to constant activation of cancer promoting oncogenes or inactivation of tumor suppressor genes. While tumor promoting oncogenes only require a single mutation for activation, tumor suppressor genes require two mutations for inactivation - one mutation in both alleles. These mutations are responsible for the six so-called hallmarks of cancer that leads to survival and proliferation of cancer cells followed by metastasis to other tissues and organs in the body: sustaining proliferation, evading growth suppressors, resisting apoptosis, inducing angiogenesis, enabling replicative immortality and activation of invasion and metastasis (Figure 2) (Hanahan and Weinberg, 2000, 2011).

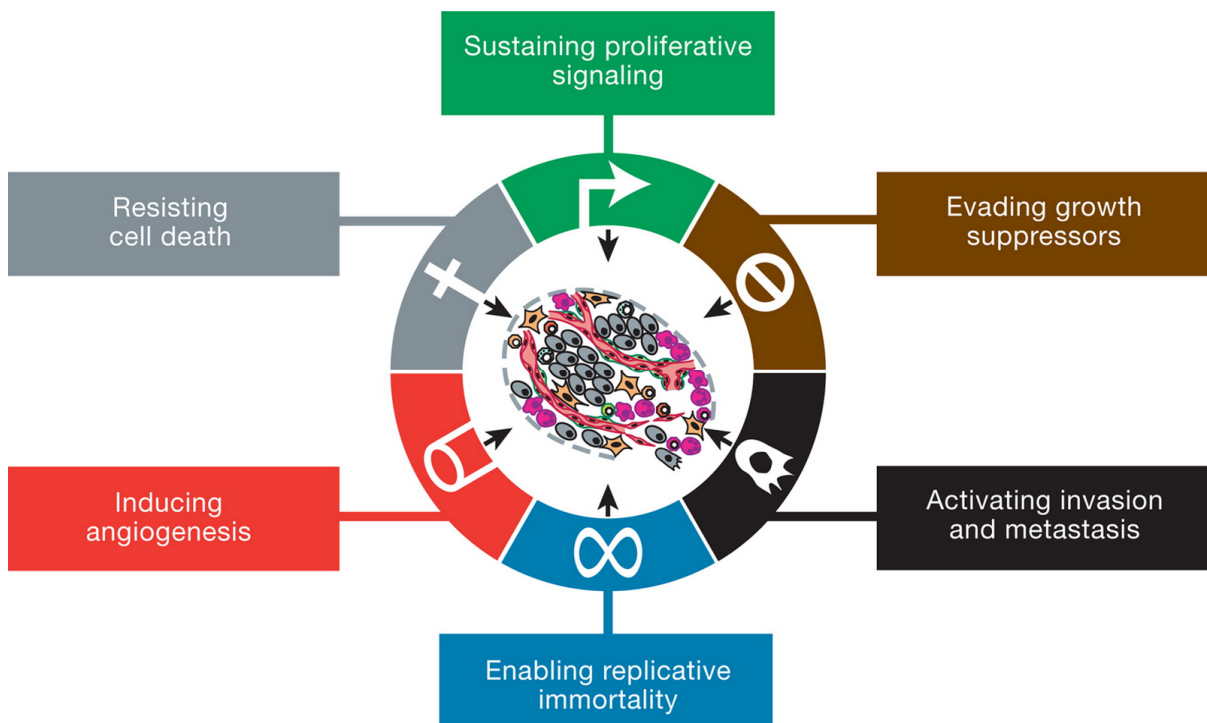


Figure 2 The Hallmarks of Cancer. Schematic representation of the six hallmarks of cancer. Taken from (Hanahan and Weinberg, 2011).

Introduction

1.3 The genetics of colorectal cancer

Around 85% of all human colorectal cancers have mutations in the *APC* (Adenomatous polyposis coli) gene (Kinzler and Vogelstein, 1996), which is true for both sporadic CRC (Payne, 1990) and inherited CRC (Powell et al., 1993). An activation of the WNT (Wingless/Int-1)-signaling pathway by mutations in *APC* or *CTNNB1* (Catenin Beta 1, gene encoding β -CATENIN) is the initiating event in CRC (Figure 3). The β -CATENIN/TCF4 (T-cell factor 4) complex induces the expression of a large number of genes, which maintain intestinal stem cells (ISCs) in an undifferentiated state. Uncontrolled proliferation of these cells results in benign adenomas, which progress to malignant intestinal cancer with almost 100% probability (Clevers and Nusse, 2012). During progression, additional mutations occur, as for example the oncogenic activation of *K-RAS* and the inactivation of the tumor-suppressor gene *p53* (Fearon and Vogelstein, 1990; Kinzler and Vogelstein, 1996; Sancho et al., 2004).

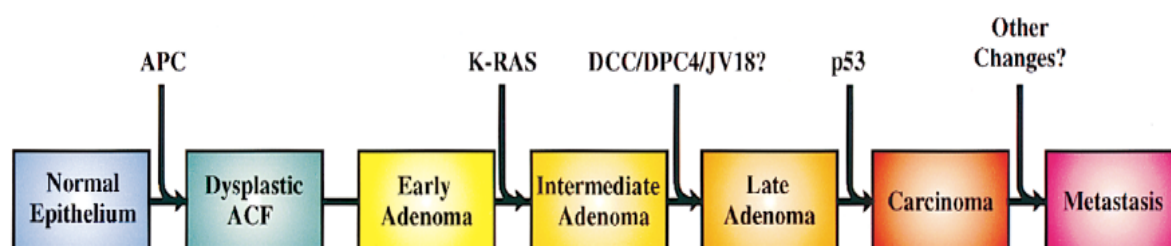


Figure 3 Genetic mutations correlated with colorectal tumorigenesis. Mutation in the *APC* gene initiate the process of colorectal tumorigenesis. Mutations in additional, indicated genes result in further progression. Taken from (Kinzler and Vogelstein, 1996).

The *Apc*^{Min} (Multiple intestinal neoplasia) mouse model is commonly used for the study of genes involved in colorectal cancer. These mice harbor a mutation in codon 850 in the *Apc* gene leading to a premature stop in translation resulting in an incomplete *Apc* protein, which is no longer able to inactivate Wnt signaling. The consequence is the development of about 100 adenomas in the small intestine and few adenomas in the colon which represent the early stage of colorectal cancer (Moser et al., 1990; Su et al., 1992). The human and mouse *Apc* genes display sequence similarity of around 90% (Su et al., 1992). The *Apc*^{Min} mouse model and the human inherited human familial adenomatous polyposis (FAP) syndrome show high genetic and phenotypic similarities. In humans the FAP syndrome leads to 100-1000 benign tumors in the

Introduction

colon which ultimately develop into malignant colorectal cancer in all cases. Since the *APC* gene is mutated in almost all human colorectal cancers, *Apc^{Min}* mice represent a relevant mouse model of colorectal cancer (Su et al., 1992). Due to high tumor burden and a consequently short lifespan of mice with a C57BL/6 background, tumor cells in the adenomas do not accumulate further mutations necessary for progression into adenocarcinomas and metastasis (Halberg et al., 2009). Only in a mixed background causing lower tumor burden and subsequent longer survival time, the adenomas progress into malignant cancer (Halberg et al., 2009). Early detection of CRC is critical for curing cancer and the understanding of the earliest mechanisms in the development of CRC is necessary. The mutation of *Apc* is modelling the initiation of human CRC, which makes it possible to study the early steps of cancer progression.

1.4 Canonical Wnt-signaling in colorectal cancer

The canonical Wnt signaling pathway is highly conserved between species. In the absence of Wnt ligands, β -catenin is phosphorylated by the destruction complex. The destruction complex consists of Axin (axis inhibition protein), which functions as a scaffold protein, the tumor suppressor protein *Apc* (adenomatous polyposis coli) as well as the protein kinases Ck1 (Casein kinase 1) and Gsk3 (Glycogen synthase kinase 3), which phosphorylate β -catenin. The phosphorylation of β -catenin leads to its degradation by the β -transducin-repeat-containing protein (β TrCP). In the absence of β -catenin, Tcf transcription factors bind to Groucho corepressors resulting in repression of transcription of Wnt target genes (Figure 4, left panel). When the Wnt ligand binds to the complex of the receptor Frizzled (Fz) and its coreceptor Lrp (lipoprotein receptor-related protein), Axin as well as Ck1 and Gsk3 are recruited to the Lrp receptor and no destruction complex is formed. β -catenin enters the nucleus, where it displaces the Groucho repressors by binding to Tcf-transcription factor proteins to promote the transcription of Wnt target genes (Figure 4, right panel).

Introduction

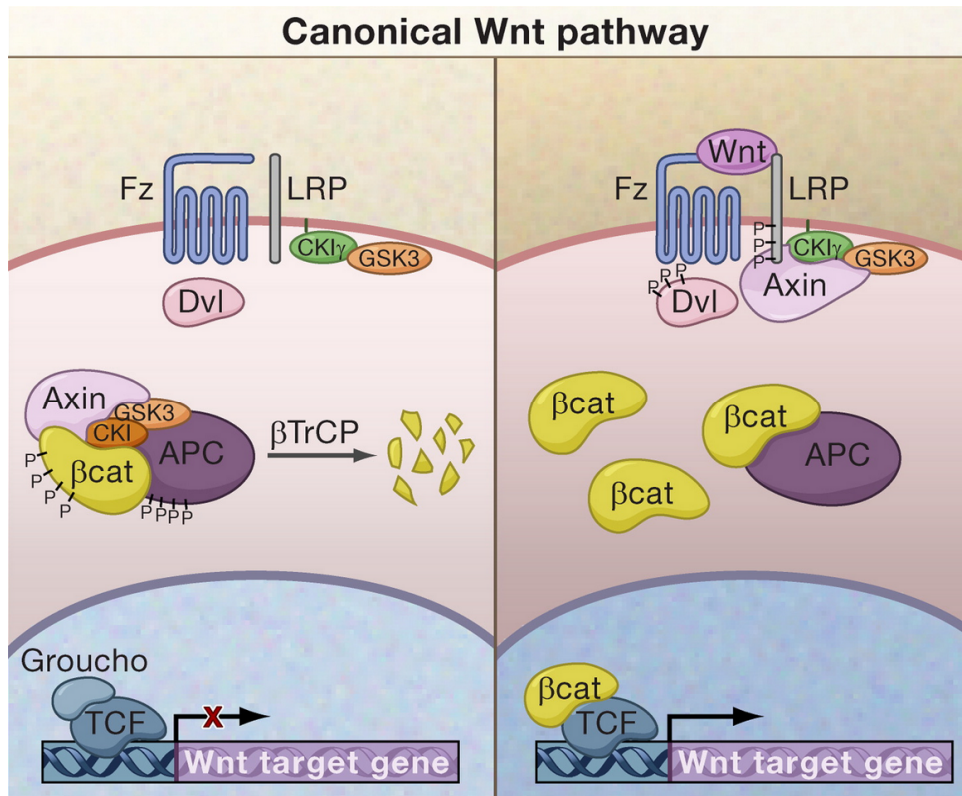


Figure 4 Canonical Wnt signaling. Molecular processes in the Wnt signaling pathway are illustrated. See main text for further explanation. Taken from (Clevers, 2006).

1.5 The Notch signaling in colorectal cancer

The Notch signaling pathway consists of four different Notch receptors (Notch1-4) and five Notch ligands from the Dsl (Delta/Serrate/Lag-2) transmembrane protein family, three are delta like (ligand) proteins (Dll1, Dll3 and Dll4) and two are the Jagged proteins (Jag1 and Jag2). Three cleavages (S1-S3) of the native Notch protein occur during maturation and signaling activation (Figure 5). For maturation, the immature Notch receptor is glycosylated by the proteins Pofut1 (protein O-fucosyltransferase 1) and Fringe in the endoplasmic reticulum (ER) which leads to cleavage by a furin-like convertase (S1). After binding of the DSL ligand presented by the signal-sending cell to the Notch receptor at the membrane of the signal-receiving cell, Adam (a disintegrin and metalloprotease peptidase) cleaves the Notch receptor (S2), after which the Notch extracellular domain is endocytosed by the signal-sending cell. The gamma (γ)-secretase cleaves the intracellular domain of the Notch receptor (S3), which releases the Notch intracellular domain (Nicc) into the cytoplasm. In the nucleus, Nicd forms a transcriptional complex with the DNA binding protein Rbp-Jk (recombination signal binding protein for immunoglobulin kappa J region), also known as Csl

Introduction

(Cbf1/suppressor of hairless/Lag-1), as well as other transcriptional coactivators such as Maml1 (mastermind like transcriptional coactivator 1). This complex mediates target gene regulation (Noah and Shroyer, 2013). A known Notch target gene is *Hes1* (hairy and enhancer of split-1), whose gene transcription is activated in response to an active Notch signaling (Fre et al., 2005; Jarriault et al., 1995; Jarriault et al., 1998). For inactivation, Nicd is ubiquitinated by Fbw7 (F-box and WD repeat domain-containing 7). The ubiquitination targets Nicd for degradation (Noah and Shroyer, 2013). Another function of the DSL on the signal-sending cell is to inhibit their own Notch receptor. Furthermore, the DSL ligand undergoes proteolytic cleavage by Adam and γ -secretase, whereafter it binds to Rbp-Jk (Csl) in combination with corepressors (CoR) to inhibit Notch target gene expression. The lack of *Hes1* expression leads to expression of *Atoh1* (protein atonal homolog 1), which induces transcription of new DSL ligands (Noah and Shroyer, 2013).

Introduction

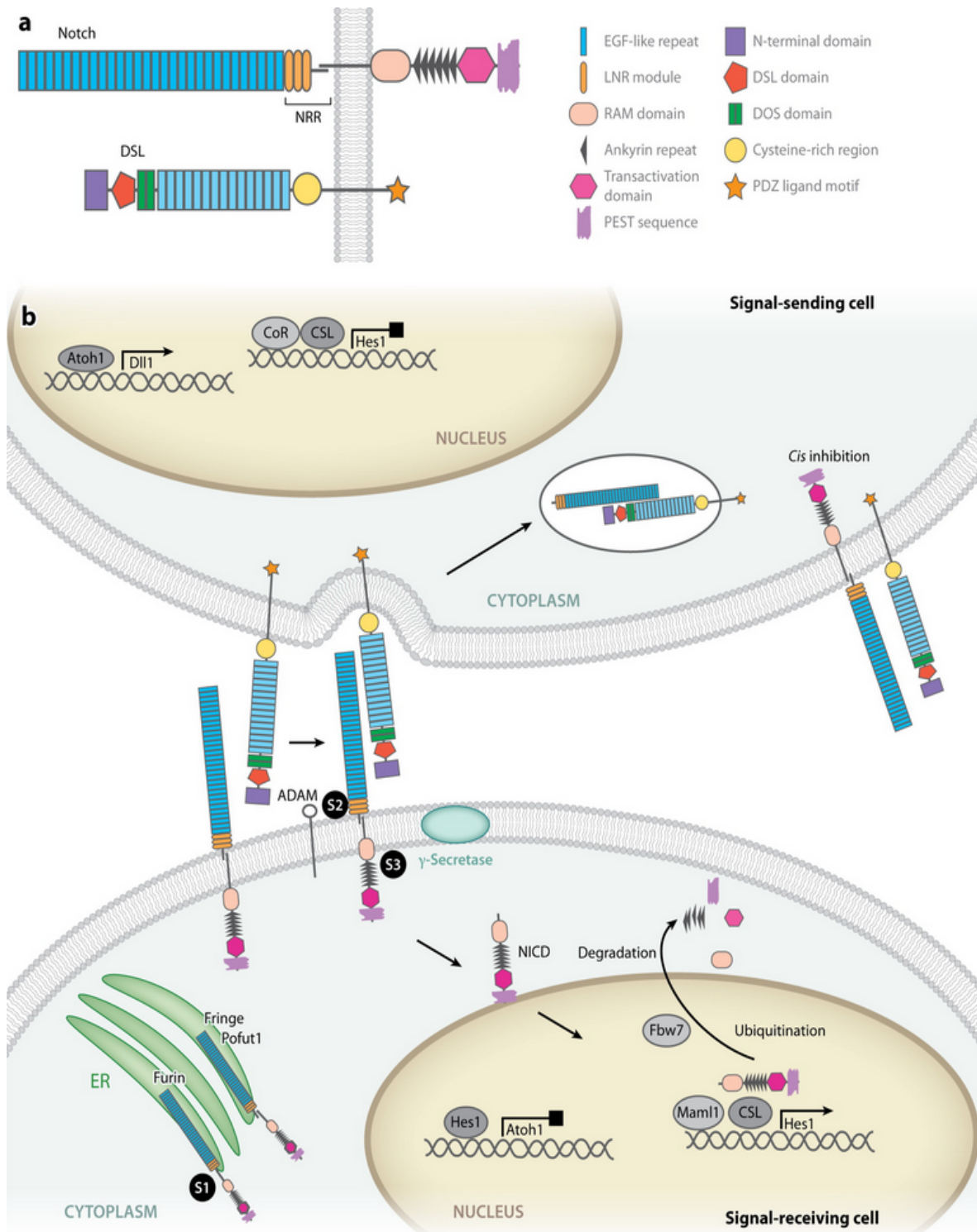


Figure 5 The Notch signaling pathway. a Schematic representation of the Notch receptors and ligands (Delta/Serrate/Lag-2: DSL). NRR: negative regulatory region, EGF-like repeat: epidermal growth factor-like repeat, LNR module: Lin12-Notch repeat module, RAM domain: RBP-Jkappa-associated module domain, PEST sequence: a peptide sequence rich in proline (P), glutamic acid (E), serine (S) and threonine (T), DOS domain: Dll4 delta and Osm-11 domain, PDZ ligand motif: domain present in Psd-95, Dlg, and Zo-1/2. **b** Molecular processes in the Notch signaling pathway. See main text for further explanation. ER: endoplasmic reticulum. Taken from (Noah and Shroyer, 2013).

Introduction

NOTCH signaling is deregulated in human CRCs and is active during the whole process of tumor formation (Wu et al., 2013). In tumor development, NOTCH1-4 seems to have different functions. Upregulation of NOTCH1 (Chu et al., 2011) and NOTCH3 (Serafin et al., 2011) positively correlates with poor survival in patients with CRC. In addition, ectopic expression of NOTCH1 (Wu et al., 2013; Zhang et al., 2010) or NOTCH3 (Serafin et al., 2011) promotes tumor progression and metastasis. However, NOTCH1 and NOTCH2 negatively correlate with each other and NOTCH2 expression negatively correlates with poor survival in contrast to NOTCH1 (Chu et al., 2011). Ectopic NOTCH4 expression in human CRC cell lines leads to a decreased proliferation rate as well as decreased migration and invasion (Zhang et al., 2018). This means, while NOTCH1 and NOTCH3 support tumorigenesis and metastasis in human CRC, NOTCH2 and NOTCH4 inhibit the same event. However, high expression of both NOTCH1 and NOTCH2 is associated with the poorest survival (Chu et al., 2011). Therefore, an interplay of different NOTCH receptors results in other effects than elevated expression of a single receptor.

Like in humans, Notch signaling plays a role in tumorigenesis in mice, since activated Notch in intestinal epithelial cells of *Apc^{Min}* mice leads to an increase in intestinal adenomas and a shortened lifespan (van Es et al., 2005b). Furthermore, there is a link between the cancer initiating Wnt/ β -catenin pathway activation and Notch signaling, since a high level of β -catenin activates the transcription of the Notch ligand Jag1 in *Apc^{Min}* mice (Rodilla et al., 2009), which could be, at least in part, the cause for activation of both pathways in intestinal tumorigenesis.

1.6 The transcription factor AP4

The TFAP4/AP4 (transcription factor activating enhancer binding protein 4) protein belongs to the class of basic-helix-loop-helix leucine zipper (bHLH-LZ) transcription factors. AP4 exclusively forms homodimers via interaction of the three protein dimerization sites HLH, LZ1 and LZ2. The AP4 homodimers use the N-terminal basic region to bind to the E-box motif CA(G/C)CTG in the promoter, thereby activating the expression of target genes. For repression of target genes the AP4 homodimer binds to a geminin-SMRT complex to recruit HDAC3 (Histone deacetylase 3) or it binds directly to HDAC1. The AP4 protein contains a highly conserved TIV motif consisting of the amino acids Threonine (T), Isoleucine (I) and Valine (V), but its function is

Introduction

unknown (Figure 6) (reviewed in (Jung and Hermeking, 2009)). The gene encoding AP4 was previously identified as a direct transcriptional target of c-MYC (Jung et al., 2008). c-MYC also belongs to the bHLH-LZ transcription factors, but binds to the E-box motif CA(C/T)GTG as a heterodimer with MAX (reviewed in (Jung and Hermeking, 2009)).

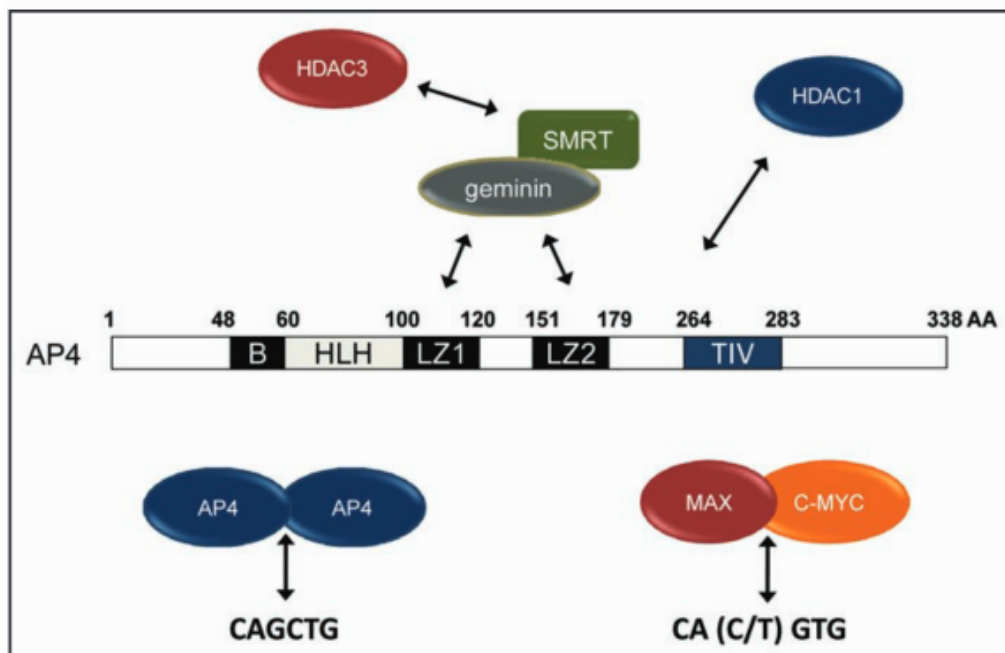


Figure 6 Scheme of the structure of the AP4 protein and its molecular interactions.

B: basic region, HLH: helix-loop-helix, LZ: leucine zipper, HDAC: histone deacetylase, AA: amino acid position. Taken from (Jung and Hermeking, 2009).

In human CRC cells AP4 directly represses the gene encoding the CDK-inhibitor p21 (encoded by the gene *CDKN1A*) to block differentiation and to induce proliferation and apoptosis. This result points to an important role of AP4 in mediating the repressing effect of c-MYC on p21 expression. In addition, AP4 is expressed in progenitor/transient amplifying cells in human colonic crypts as well as in colorectal cancer in a pattern similar to c-MYC and in a converse pattern to p21, indicating an identical or at least similar function of AP4 in human tissue as in human cell lines (Jung et al., 2008).

Introduction

1.7 The role of AP4 in colorectal cancer

The prototypic oncogene *c-MYC* is a direct target of the APC/WNT pathway (He et al., 1998) and an essential mediator of tumor formation induced by inactivation of *Apc* in the intestine of mice (Sansom et al., 2007; Sur et al., 2012). Deletion of one *c-Myc* allele decreases the tumor load in *Apc^{Min}* mice (Sur et al., 2012), while a complete loss of *c-Myc* prevents adenoma formation caused by homozygous *Apc* deletion in mice (Sansom et al., 2007). In addition, both human and murine *c-MYC* are direct targets of the Notch pathway (Palomero et al., 2006; Weng et al., 2006). Therefore, c-MYC may be an important effector of APC/WNT-induced and/or NOTCH-induced tumor formation in the intestine and direct target genes of c-MYC could have an important influence in the development and progression of cancer. High expression of the c-MYC target gene *AP4* positively correlated with survival and formation of distant metastases in the liver in two different colorectal cancer patient cohorts (Jackstadt et al., 2013c). Additionally, high expression of AP4 also correlated with poor survival in other tumor entities, such as gastric cancer, non-small cell lung carcinomas and hepatocellular tumors (Gong et al., 2014; Hu et al., 2013; Xinghua et al., 2012). Moreover, a genome-wide analysis of AP4-regulated genes and AP4 DNA binding has been performed in a human colon cancer (CRC) cell line (Jackstadt et al., 2013c). Interestingly, AP4 could be identified as an epithelial-mesenchymal transition inducing transcription factor (EMT-TF), which regulates a large number of genes controlling EMT, stemness and proliferation. AP4 was required for metastases formation by CRC lines in a xenograft mouse model (Jackstadt et al., 2013c). Furthermore, a double negative feedback-loop between AP4 and the tumor-suppressor microRNA-15a/16-1 controls the balance of EMT and MET (mesenchymal-epithelial transition) during metastases formation of human CRCs (Shi et al., 2014). In addition, microRNA-302c directly targets *AP4* and represses the transcription of *AP4*, thereby repressing EMT and metastasis formation of CRC cell lines (Ma et al., 2018). On the other hand, the ubiquitin specific peptidase 22 (USP22) binds to the promoter of *AP4* to activate its transcription to enhance EMT and metastasis formation of CRC cell lines (Li et al., 2017).

In mouse embryonic fibroblasts (MEFs) loss of *Ap4* leads to premature senescence through induction of the known target *p21* as well as the additional CDK (Cyclin dependent kinase)-inhibitor *p16*. *c-Myc* activation is not able to repress *p21* and *p16* in the absence of *Ap4*, indicating that *Ap4* is necessary for the regulation of proliferation

Introduction

by c-Myc (Jackstadt et al., 2013a). Ectopic expression of both Ap4 and Ras (Rat sarcoma protein) combined with loss of p53 leads to cellular transformation of MEFs (Jackstadt et al., 2013a). In addition, AP4 is regulated on posttranscriptional level, since it is a target for proteasome-dependent degradation by the β TrCP ubiquitin ligase (D'Annibale et al., 2014). This degradation takes place in the G2 phase of the cell cycle and is mediated by phosphorylation of a conserved degron. Furthermore, the ectopic expression of a non-degradable stabilized AP4 mutant revealed that β TrCP-dependent degradation of AP4 is required for the fidelity of mitotic division, as it increase chromosomal instability leading to cancer initiating mutations.

These results indicate an important role of AP4 in cancer development and progression. However, the organismal function of AP4 in the intestinal epithelium and its relevance for intestinal tumor formation has so far not been analysed using a genetic approach.

1.8 The homeostasis of the intestinal epithelium

The intestinal epithelium is one of the fastest dividing tissues in the body. The small intestine contains crypts and villi, where each villus is surrounded by at least 6 crypts (Figure 7). In contrast to the small intestine the colon does not contain villi. In the small intestine the crypt base harbors 4-6 intestinal stem cells (ISCs) surrounded by supporting Paneth cells (Barker et al., 2007). Paneth cells are differentiated cells, which are exclusively located in the base of the crypt (Clevers and Bevins, 2013). Lgr5 (Leu-rich repeat-containing G protein-coupled receptor 5)-positive ISCs generate all differentiated cells in the intestine (Barker et al., 2007). The Lgr5+ ISCs divide asymmetrically to self-renew and to generate highly proliferative, Lgr5-negative transit amplifying (TA) cells, which differentiate into absorptive enterocytes or secretory cells, such as goblet, Tuft and entero-endocrine cells (Barker, 2014; Barker et al., 2007; Beumer and Clevers, 2016; Sancho et al., 2004). Goblet cells are located in both the crypt and the villus, and function as mucus producing cells. Paneth cells are derived from Lgr5+ precursors generated by asymmetric division of ISCs, which proliferate slowly and therefore represent label-retaining cells (LRCs) (Buczacki et al., 2013). Paneth cells control the maintenance of the ISCs by secretion of Wnt and Notch ligands, which suppress differentiation into the secretory lineage, and protect ISCs from bacteria and fungi through secretion of Lysozyme and Cryptdin (Clevers and

Introduction

Bevins, 2013; Sato et al., 2011b). However, the presence of Paneth cells in the colon is currently unknown. So-called deep crypt secretory (DCS) cells were identified in colonic crypts, which may have Paneth cell like functions (Sasaki et al., 2016). DCS cells are positive for Reg4 (Regenerating Family Member 4) and intermingled with ISCs.

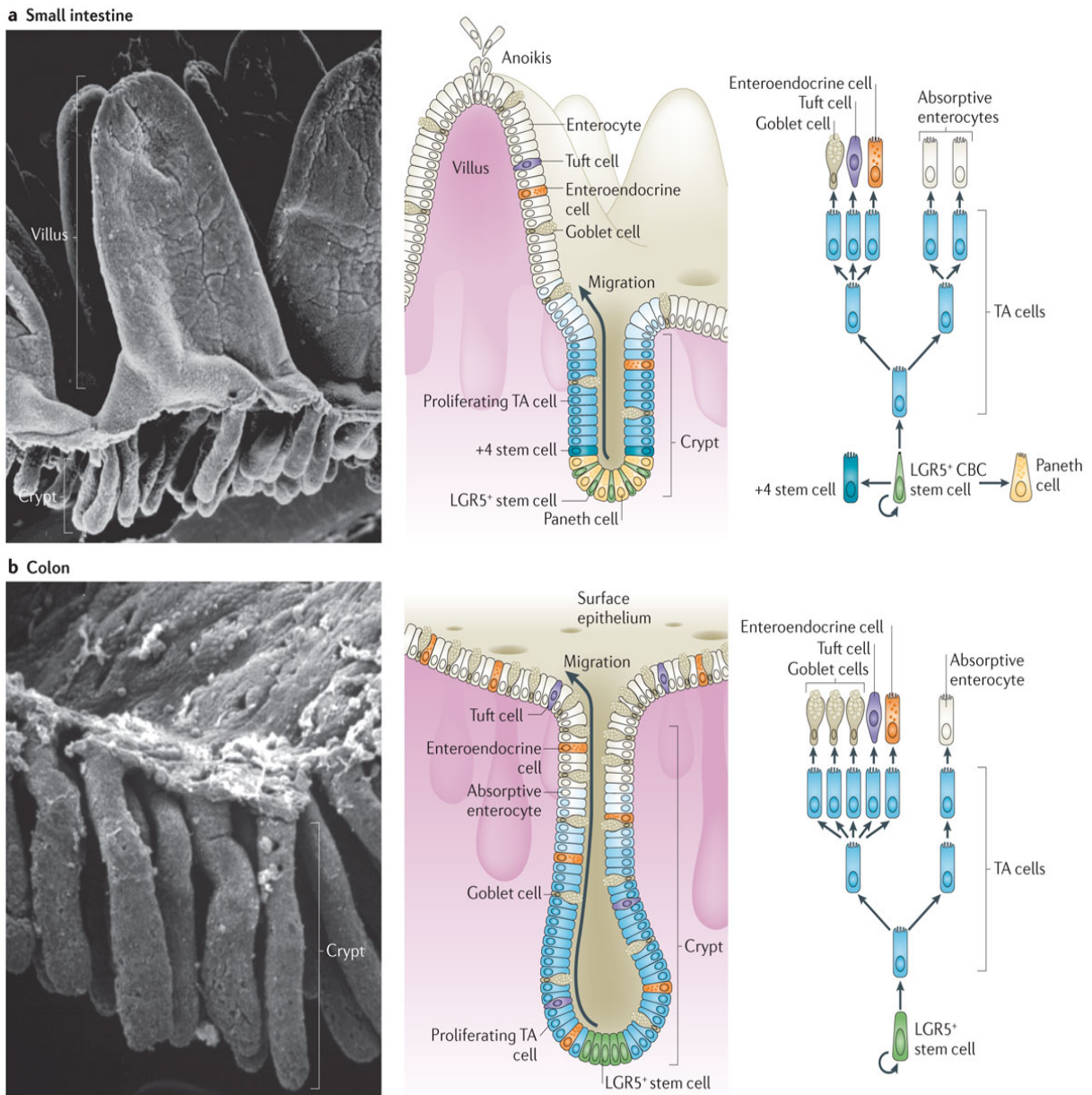


Figure 7 The structural organization and homeostasis of the intestinal epithelium. Left panels: structural organization of the small intestine (a) and colon (b) shown by electron microscopy. Middle panels: Schematic representation of the cellular organization in the small intestine (a) or colon (b). Right panels: Schematic representation of cellular differentiation in the small intestine (a) and colon (b). Taken from (Barker, 2014).

LGR5+ stem cell: Leu-rich repeat-containing G protein-coupled receptor 5-expressing stem cell, CBC stem cells: crypt base columnar stem cells, TA cell: transit-amplifying cell.

Introduction

The homeostasis of the intestinal epithelium is regulated mainly by the Wnt/ β -catenin and Notch pathways, which control ISC maintenance and differentiation (Beumer and Clevers, 2016; Sancho et al., 2004). During the upward migration of cells these signals become weaker and cells differentiate to replace the epithelial cells lost by anoikis (Figure 7) (Clevers and Bevins, 2013). The turnover of epithelial cells occurs every 3-5 days in the small intestine and every 5-7 days in the colon, while Paneth cells are long-lived cells surviving 3-6 weeks (Barker, 2014). In addition to the fast cycling ISCs quiescent Bmi1+ (B lymphoma Mo-MLV insertion region 1 homolog) ISCs reside at position +4 above the crypt base (Sangiorgi and Capecchi, 2008). These cells start to proliferate to rebuild the Lgr5+ ISC pool after tissue injury (Tian et al., 2011).

1.9 The role of the Wnt and Notch pathway in intestinal homeostasis

The maintenance of intestinal stem cells is positively controlled by the Wnt, Notch and Egf (epidermal growth factor) pathway as well as negatively controlled by the Bmp (bone morphogenetic protein) pathway (Figure 8) (Sato and Clevers, 2013). Wnt/ β -catenin signaling activity is strongest in the intestinal crypt base and decreases as a gradient in the direction towards the villi (Batlle et al., 2002; Munoz et al., 2012; Van der Flier et al., 2007), suggesting an important role at the crypt base. Paneth cells are the main source of Wnt ligands to activate Wnt signaling in ISCs, which is important for the stem cell maintenance and self-renewal capability (Figure 8) (Clevers et al., 2014; Gregorieff and Clevers, 2005; Sato and Clevers, 2013; Sato et al., 2011b). However, also stroma cells provide Wnt signals to the ISCs (Clevers et al., 2014).

Introduction

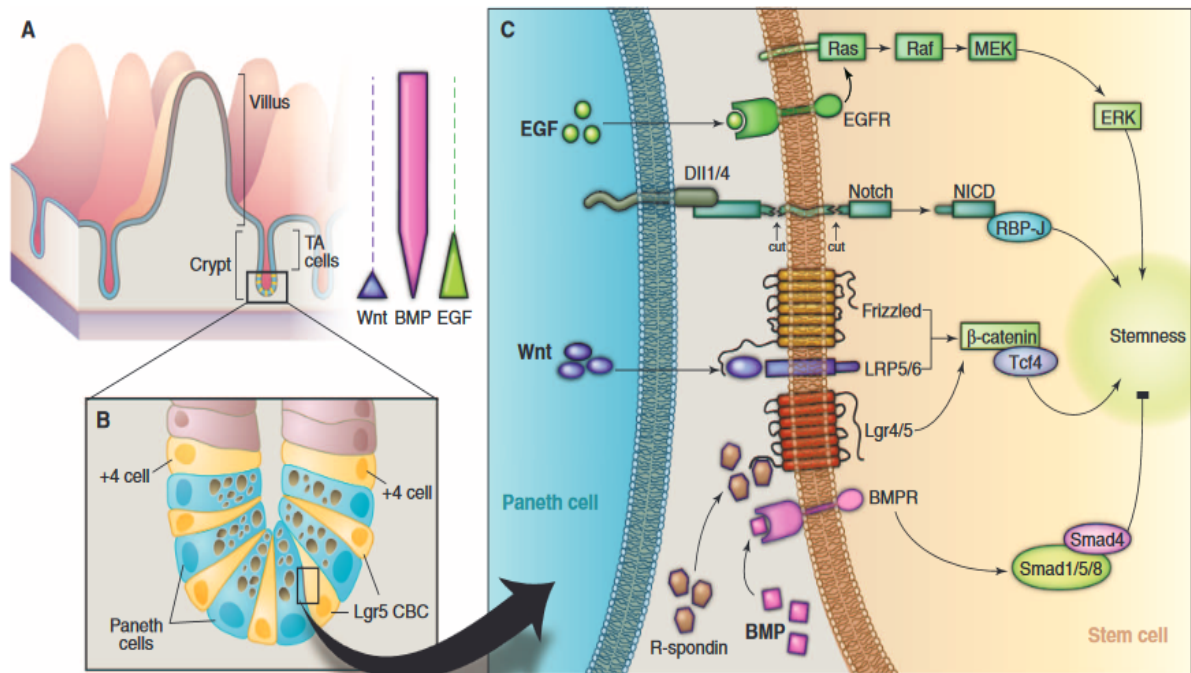


Figure 8 Interaction of intestinal stem cells with their niche. **A** Schematic representation of the localization of small intestinal crypts. Gradients of expression of Wnt, Bmp, and EGF signals are acting along the crypt axis. **B** Scheme of the stem cell niche. **C** Egf, Notch and Wnt signals positively control stem cell characteristics/stemness, whereas Bmp signals negatively control stem cell characteristics of intestinal epithelial cells. Taken from (Sato and Clevers, 2013).

A complete abrogation of Wnt signaling by deletion of *Tcf4* results in a complete loss of Lgr5+ ISCs (Korinek et al., 1998; van Es et al., 2012), while inactivation of *Ctnnb1/β-catenin* results in loss of ISCs due to increased differentiation and as a consequence loss of all intestinal crypts (Fevr et al., 2007). However, partial inhibition of Wnt signaling results only in a reduction of ISCs (Huels et al., 2018). Furthermore, overexpression of the Wnt inhibitor Dkk1 (Dickkopf-related protein 1) results in decreased proliferation and loss of intestinal crypts (Kuhnert et al., 2004; Pinto et al., 2003). However, a constitutively active Wnt signaling in intestinal stem cells, but not in progenitors or differentiated cells of mice can effectively initiate colorectal cancer (Barker et al., 2009; Zhu et al., 2009). These results confirm the importance of a well-balanced Wnt/β-catenin signaling in the homeostasis and tumorigenesis in the intestine.

Both the Notch receptor and the Notch target gene *Hes1* are expressed in ISCs at the base of intestinal crypts as well as in some cells of the TA unit, suggesting a critical role of active Notch signaling in ISCs and their progenitors (Fre et al., 2005; Jensen et

Introduction

al., 2000; Kayahara et al., 2003; Riccio et al., 2008). In the intestinal crypt base Paneth cells present the Notch ligands to the Notch receptors present on ISCs, thereby activating Notch signaling and maintaining the stemness character (Figure 8) (Sato and Clevers, 2013; Sato et al., 2011b). The main ligands mediating the activation of Notch signaling important for the homeostasis of ISCs in the intestine probably are the Dll1 and Dll4 ligands. Mutation of these two ligands reduced proliferation of ISCs and forced them to differentiate, while mutation of the ligand Jag1 had no effect on proliferation and differentiation (Pellegrinet et al., 2011).

Since the Notch1 and Notch2 receptor are expressed in the crypt base of the intestine, while the Notch3 and Notch4 receptor are mostly expressed in the villus, only Notch1 and Notch2 seems to play a role in the maintenance of ISCs (Riccio et al., 2008). Partial Notch inhibition by the γ -secretase inhibitor Dibenzazepine (DBZ) or by deleting *Notch1* (but not *Notch2*) leads to a decrease of ISCs, an increase in secretory cells such as goblet and Paneth cells, a decrease in the expression of the Notch target gene *Olfm4* (Olfactomedin 4) as well as reduced stem cell proliferation (Carulli et al., 2015; VanDussen et al., 2012). Notch1 may be the main factor regulating intestinal homeostasis, since conditional deletion of *Notch1* leads to the known phenotype of Notch inhibition as well as a decreased expression of the Notch target genes *Hes1*, *Olfm4* and *c-Myc*, while no differences can be seen after conditional deletion of *Notch2* alone (Carulli et al., 2015). However, a complete loss of Notch signaling, e.g. by simultaneous *Notch1* and *Notch2* receptor deletion or by *Rbp-Jk (Csl)* deletion results in a complete loss of ISCs (Riccio et al., 2008; van Es et al., 2010; van Es et al., 2005b; VanDussen et al., 2012). In addition, complete loss of Notch signaling results in more hyperplasia in goblet and Paneth cells as seen after deletion of *Notch1* alone (Carulli et al., 2015), indicating a role of Notch2 in stem cell maintenance and secretory cell differentiation in combination with Notch1. Taken together, these results show that intestinal homeostasis is dependent on a functional Notch signaling pathway.

Aims of the study

2. Aims of the study

The present study had the following aims:

- Genetic analysis of *Ap4* in an *Apc^{Min}* mouse model
- Characterization of pathways and mechanisms by which *Ap4* influences tumorigenesis and intestinal homeostasis

Materials

3. Materials

3.1 Chemicals and reagents

Application	Chemical compound	Supplier
IHC, IF, Histology	30% H ₂ O ₂	Carl Roth
	Rabbit serum	PAA Laboratories
	Roti®-Histokitt II	Carl Roth
	Antibody diluent, background-reducing	Dako
	Pro taqs IX pH10	BioCyc
	Target retrieval solution, citrate pH 6	Dako
	TRS (Target retrieval solution) pH 6	Dako
	DAPI	Carl Roth
	ProLong gold antifade reagent	Life Technologies
	Hematoxylin	Vector Laboratories
	Hematoxylin	Waldeck
	Eosin	Sigma-Aldrich
	Alcian blue	BioOptica
	Periodic acid	Merck Millipore
Schiff's reagent	Sigma-Aldrich	
WB	Rotiphorese gel 30 (37,5:1)	Carl Roth
	Ammonium peroxodisulfate (APS)	Carl Roth
	Tetramethylethylenediamine (TEMED)	Carl Roth
	Sodium dodecyl sulfate (SDS)	Carl Roth
	β-mercaptoethanol	Sigma-Aldrich
	Complete mini protease inhibitor cocktail	Roche Diagnostics
	Bradford reagent	Bio-Rad
	PageRuler™ plus prestained protein ladder	Thermo Fisher Scientific
	Immobilon-P PVDF,0.45µm membrane	Merck Millipore
	Skim milk powder	Sigma-Aldrich
	Methanol	Carl Roth
	Tween-20	Sigma-Aldrich
	Nonidet®P40 substitute	Sigma-Aldrich
	ECL/HRP substrate	Merck Millipore
Western lightning plus ECL	Perkin Elmer	
Organoids	Growth factor reduced, phenol red-free matrigel	Corning
	Advanced DMEM/F12	Gibco/Life Technologies
	Penicillin-streptomycin	Gibco/Life Technologies
	Glutamax	Gibco/Life Technologies
	Hepes	Gibco/Life Technologies
	Noggin	Preprotech
	N2	Gibco/Life Technologies
	B27	Gibco/Life Technologies
	EGF	Preprotech
	RSPO1	Sinobiological
	Y-27632	MedBiochem Express
	Wnt-3a	Abcam
	4-hydroxytamoxifen (4-OHT)	Sigma-Aldrich
	Hank's Balanced Salt Solution (HBSS)	Gibco/Life Technologies

Materials

Application	Chemical compound	Supplier
ISH	Kaiser glycerine gelatin	Merck Millipore
	Formamide	Sigma-Aldrich
	Paraformaldehyd	Merck Millipore
	3-[(3-cholamidopropyl)dimethyl-ammonio]-1-propane sulfonate (CHAPS)	Sigma-Aldrich
	Diethyl pyrocarbonate (DEPC)	Sigma-Aldrich
	Blocking solution	Roche Diagnostics
	NBT/BCIP solution, ready to use	Sigma-Aldrich
	RNA from Yeast	Sigma-Aldrich
	Heparin sodium	Sigma-Aldrich
qChIP	Protein G agarose/salmon sperm DNA	Merck Millipore
	Fatty acid-free BSA	Sigma-Aldrich
	37% formaldehyde	Merck Millipore
Cell culture	FBS (Fetal Bovine Serum)	Invitrogen
	Penicillin-streptomycin	Gibco/Life Technologies
	DMEM–Dulbecco's Modified Eagle Media	Gibco/Life Technologies
	McCoy's 5A (Modified) media	Gibco/Life Technologies
	RPMI 1640 media without L-glutamine	Gibco/Life Technologies
	Hank's Balanced Salt Solution (<i>HBSS</i>)	Gibco/Life Technologies
	DMSO (Dimethyl Sulfoxide)	Carl Roth
	FuGENE® HD transfection reagent	Promega Corporation
	HiPerFect transfectin reagent	QIAGEN
	Lipofectamine® 2000 transfection reagent	Invitrogen
	Opti-MEM™ reduced serum media	Gibco/Life Technologies
	Doxycycline (DOX)	Sigma-Aldrich
	Puromycin dihydrochloride	Sigma-Aldrich
Cloning / generation of vectors	Ampicillin	Carl Roth
	LB agar (Lennox)	Carl Roth
	LB medium (Luria/Miller)	Carl Roth
	Universal agarose PeqGold	PeqLab
	Ethidium bromide	Carl Roth
	Gene ruler 1kb DNA ladder	Thermo Fisher Scientific
PCR, Gel electrophoresis, q-PCR	Deoxynucleotides (dNTPs)	Thermo Fisher Scientific
	Gene ruler low range DNA ladder	Thermo Fisher Scientific
	Gene ruler 100bp plus DNA ladder	Thermo Fisher Scientific
	Gene ruler 1kb DNA ladder	Thermo Fisher Scientific
	Universal agarose PeqGold	PeqLab
	Ethidium bromide	Carl Roth
	Fast SYBR® green master mix	Applied Biosystems
	Trizol	Invitrogen
Luciferase reporter assays	Ampicillin	Sigma-Aldrich
	LB-Agar (Lennox)	Carl Roth
	LB-Medium (Luria/Miller)	Carl Roth
	Hi-Di™ Formamide	Applied Biosystems
	Universal agarose PeqGold	PeqLab
	Gene Ruler 1kb DNA ladder	Thermo Fisher Scientific
	Ethidium bromide	Carl Roth
	FuGENE® HD transfection reagent	Promega Corporation
	Opti-MEM® Reduced Serum Medium	Gibco/Life Technologies
Electron microscopy	Osmium tetroxide	Serva Electrophoresis
	EPON 812 glycid ether 100	Serva Electrophoresis

Materials

Application	Chemical compound	Supplier
DBZ-treatment	Tween-80	Sigma-Aldrich
	Methocel® MC low viscosity	Sigma-Aldrich
	Dibenzazepine (DBZ)	Axon Medchem

3.2 Enzymes

Application	Enzyme	Supplier
Organoids	Collagenase Type IV	Merck Millipore
	Dispase Type II	Sigma-Aldrich
ISH	Proteinase K	Sigma-Aldrich
Cell culture	Trypsin-EDTA (0.5%, 10x, phenol-red free)	Gibco/Life Technologies
Generation of vectors	restriction endonucleases	New England Biolabs
	T4 DNA ligase	Thermo Fisher Scientific
qPCR	DNase I (RNase-free)	Sigma-Aldrich
PCR	FIREPol® DNA Polymerase	Solis BioDyne
	Hot FIREPol® DNA Polymerase	Solis BioDyne

3.3 Kits

Application	Kit	Supplier
IHC	DAB Substrate Chromogen System	Vector laboratories
	DAB+ Substrate Chromogen System	Dako
	Vectastain <i>Elite</i> ABC HRP detection Kit	Vector laboratories
	AEC Substrate Chromogen System	Thermo Fisher Scientific
	Impress HRP Anti Goat Ig	Vector laboratories
	Impress HRP Anti Rabbit Ig	Vector laboratories
	Impress Excel Staining Kit, Anto Rabbit-Ig	Vector laboratories
	Impress HRP Anti Mouse Ig	Vector laboratories
	M.O.M. (mouse on mouse) Kit	Vector laboratories
WB	BCA Protein Assay Kit	Thermo Fisher Scientific
ISH	DIG Northern Starter Kit	Roche Diagnostics
	BCIP/NBT substrate system	Sigma Aldrich
Cloning / generation of vectors	QIAquick Gel Extraction Kit	QIAGEN
	Pure Yield™ Plasmid Midiprep System	Promega Corporation
	QIAprep Spin Miniprep Kit	QIAGEN
	BigDye Terminator v1.1 cycle sequencing Kit	Applied Biosystems
	Dye Ex 2.0 Spin Kit	QIAGEN
qPCR	High Pure RNA Isolation Kit	Roche Diagnostics
	RNeasy Kit	QIAGEN
	Verso cDNA Synthesis Kit	Thermo Fisher Scientific
Luciferase reporter assays	Dual-Luciferase® Reporter Assay System	Promega Corporation

Materials

3.4 Antibodies

3.4.1 Primary antibodies

epitope	source	company	catalog no.	use	dilution mouse	dilution human
α -Tubulin	mouse	Sigma-Aldrich	#T9026	WB	1:1000	1:1000
β -catenin	mouse	BD Pharmingen	610154	IHC	1:300	
BrdU	rat	AbD Serotec	MCA2060	IHC	1:400	
Cleaved caspase-3	rabbit	Cell signaling	#9661	IHC	1:100	
c-myc	rabbit	Merck Millipore	#06-340	IHC	1:300	
GFP	rabbit	Santa Cruz	SC-8334	IHC; IF	1:700; 1:700	
Hes1	rabbit	Cell signaling	#11988	IHC; WB	1:50; 1:1000	1:50; 1:1000
Ki67	rat	Dako	E0468	IHC	1:500	
Lysozyme	rabbit	Biozol, Lifespan Biosciences	LS-C138144-100	IHC; IF	1:4000; 1:4000	
NICD1	rabbit	Cell Signaling	#4147	IHC; WB	1:50; 1:1000	1:100; 1:1000
TFAP4	mouse	AbD Serotec	MCA4993Z	IHC; IF; WB; ChiP	1:100; 1:100; 1:1000; 3 μ g	1:400; 1:1000
VSV	rabbit	Sigma-Aldrich	#4888	WB		1:7500
Rabbit IgG		Biozol Diagnostica	BZL04060	IHC; IF		
Rabbit (DA1E) mAB IgG		Cell Signaling	3900	IHC		
Mouse IgG2a		Biozol Diagnostica	SER-MCA929-100	IHC; IF		
Mouse IgG1		Southern Biotech	SBA-0102-01	IHC		
Rat IgG2a		Biozol Diagnostica	BZL01284	IHC		
Mouse IgG		Sigma-Aldrich	M7023	ChiP		

ChiP: Chromatin Immunoprecipitation; IF: Immunofluorescence; IHC: Immunohistochemistry; WB: Western Blotting;

Materials

3.4.2 Secondary antibodies

name	source	company	catalog no.	use	dilution	Used for pAB
Anti-mouse-HRP	goat	Promega Corporation	#4021	WB	1:10000	α -Tubulin, TFAP4
Anti-Rabbit-HRP	goat	Sigma-Aldrich	#A0545	WB	1:10000	c-Myc, NICD1, Hes1
Anti-mouse-Alexa 555	goat	Invitrogen	A-21422	IF	1:500	TFAP4
Anti-Rabbit-FITC	donkey	Jackson Immuno Research	711-095-152	IF	1:500	GFP, Lysozyme
Anti-Rat-biotinylated	rabbit	Dako	E0468	IHC	1:500	Ki67

ChiP: Chromatin Immunoprecipitation; IF: Immunofluorescence; IHC: Immunohistochemistry; WB: Western Blotting;

Materials

3.5 Buffers and solutions

Immunohistochemistry:

10x PBS (1l):

80g NaCl; 1 g KCl; 14.42 g Na₂HPO₄*2H₂O; 2 g KH₂PO₄; ad 1 l ddH₂O

Tris-Buffer:

43.90 g NaCl; 34.25 g Tris-HCL; 4.50 g Tris-Base; add ddH₂O to 5 l

Western Blotting:

2x Laemmli buffer:

125 mM Tris/HCl (pH 6.8); 4% SDS; 20% glycerol; 0.05% bromophenol blue (in H₂O); 10% β-mercaptoethanol (added right before use)

RIPA lysis buffer (for protein lysates):

1% NP40 (Nonidet P-40); 0.5% sodium deoxycholate; 0.1% SDS; 150 mM NaCl; 50 mM Tris/HCl (pH 8.0), add 1 tablet of protease (Roche Diagnostics) to 10 ml of RIPA buffer

10x Tris-glycine-SDS running buffer (5l, for SDS-PAGE):

720 g Glycin; 150 g Tris; 50 g SDS; pH 8.3-8.7; ad 5 l ddH₂O

Towbin buffer (for Western blotting):

200 mM glycine; 20% methanol; 25 mM Tris (pH 8.6)

10x TBS-T (5l):

500 ml 1M Tris (pH 8.0); 438.3 g NaCl; 50 ml Tween20; ad 5 l ddH₂O

Genotyping of mice:

10x Gitschier`s Buffer (10x GB):

1675 µl of 2M Tris (pH 8.8); 830 µl of 1M (NH₄)₂SO₄; 670 µl of 0.5M MgCl₂; 1825 µl ddH₂O

Materials

Soriano Buffer:

5040 µl of ddH₂O; 600 µl of 10x GB; 300 µl of 10% Triton X-100; 60 µl 2-Mercaptoethanol

10x Vogelstein PCR buffer:

166 mM (NH₄)₂SO₄; 670 mM Tris/HCL (pH 8.8); 67 mM MgCl₂; 100 mM β-mercaptoethanol

In situ Hybridization

Acetic anhydride solution:

0.2 % acetic anhydride in 0.1 M trietanolamine (pH 8.0)

Tris/NaCl Buffer:

0.1 M Tris/HCl (pH 7.5); 0.15 M NaCl; 0.1% Tween20

Blocking Solution:

1 % blocking powder (Roche Diagnostics) in 1x Tris/NaCl buffer (heat to 65°C to dissolve)

DEPC-H₂O:

1 ml Diethyl-Pyrokarbonat (DEPC) (Sigma) in 1 L H₂O (autoclave to inactivate DEPC)

Hybridization solution:

50% formamide, 5x SSC (pH 4.5); 2% Blocking Powder (Roche Diagnostics); 0.05% CHAPS (Sigma); 5 mM EDTA; 50 µg/ml heparin; 1 µg/ml yeast RNA (heat to 65°C to dissolve)

NBT/BCIP Solution:

10 mg of NBT (Sigma) in 1ml of DEPC-H₂O

NTM Buffer:

0.1 M Tris/HCl (pH 9.5); 0.1 M NaCl, 0.05 M MgCl₂

PFA:

4% Paraformaldehyde (PFA) in PBS (heat to 65°C and add NaOH to dissolve)

1x PBS

8g NaCl; 0.2g KCl; 1.78g Na₂HPO₄*2H₂O; 0.24g KH₂PO₄; add DEPC-H₂O to 1l

Materials

SSC, 20X:

175.3g NaCl; 88.2g sodium citrate*2H₂O; add DEPC-H₂O to 1l (adjust pH to 7.5 or 4.5)

qChIP:

TE buffer:

10 mM Tris/HCL (pH 7.5); 1 mM EDTA

Glycine buffer:

1 M glycine in ddH₂O

Triton X-100 dilution buffer:

100 mM Tris/HCl (pH 8.6); 100 mM NaCl; 5 mM EDTA (pH 8.0); 0.2 % NaN₃; 5 % Triton X-100

SDS buffer:

50 mM Tris (pH 8.1); 0.5% SDS; 100 mM NaCl; 5 mM EDTA

Immunoprecipitation (IP) buffer:

Mix 1 part of Triton X-100 dilution buffer and 2 parts of SDS buffer

LiCl/detergent wash:

0,5 % deoxycholic acid (sodium salt); 1 mM EDTA; 250 mM LiCl; 0.5 % NP-40; 10 mM Tris/HCl (pH 8.0); 0.2 % NaN₃

Buffer 500:

0.1 % deoxycholic acid; 1 mM EDTA; 50 mM HEPES (pH 7.5); 500 mM NaCl; 1 % Triton X-100; 0.2 % NaN₃

Mixed micelle buffer:

150 mM NaCl; 20 mM Tris/HCl (pH 8.1); 5 mM EDTA (pH 8.0); 5.2 % Sucrose; 0.02 % NaN₃, 1 % Triton X-100; 0.5 % SDS

Materials

Elution buffer:

10 mM EDTA, 1 % SDS; 50 Mm Tris/HCl (pH 8.0)

1x TBS:

1.5 M NaCl; 0.1 M Tris/HCl (pH 7.4)

1x PBS:

13.7 mM NaCl; 2.7 mM KCl; 80.9 mM Na₂HPO₄; 1.5 mM KH₂PO₄ (pH 7.4)

Materials

3.6 Oligonucleotides

3.6.1 Oligonucleotides used for genotyping

Name	Sequence (5'-3')
<i>Ap4</i> Primer a	GCCTAAGAGTAGGTGCTCTGC
<i>Ap4</i> Primer b	GCGAGCAAATGAACTGTTGAC
<i>Ap4</i> Primer c	CGTACGCCGGCTTAAGTGTA
<i>Apc</i> ^{Min} wt	GCCATCCCTTCACGTTAG
<i>Apc</i> ^{Min} com	TTCCACTTTGGCATAAGGC
<i>Apc</i> ^{Min} mut	TTCTGAGAAAGACAGAAGTTA
<i>Vil-Cre</i> Fwd	CGCGAACATCTTCAGGTTCT
<i>Vil-Cre</i> Rev	CAAGCCTGGCTCGACGGCC
<i>Lgr5</i> com	CTGCTCTCTGCTCCCAGTCT
<i>Lgr5</i> wt rev	ATACCCCATCCCTTTTGAGC
<i>Lgr5</i> mut rev	GAAC TTCAGGGTCAGCTTGC
<i>Cmv-Cre</i> trans1	GCGGTCTGGCAGTAAAACTATC
<i>Cmv-Cre</i> trans2	GTGAAACAGCATTGCTGTCACTT
<i>Cmv</i> Int Con Fwd	CTAGGCCACAGAATTGAAAGATCT
<i>Cmv</i> Int Con Rev	GTAGGTGGAATTCTAGCATCATCC

3.6.2 Oligonucleotides used for qPCR

Name	Sequence (5'-3')
mouse <i>B2m</i> Fwd	CCGGCCTGTATGCTATCC
mouse <i>B2m</i> Rev	CTTGCTGAAGGACATATCTGACA
mouse <i>Ap4</i> Fwd	TCAAGCGCTTTATCCAGGAG
mouse <i>Ap4</i> Rev	CAATGCCCTCATCCTTGTCT
mouse <i>Spdef</i> Fwd	AACATGTATCCCGACGATAGCAGC
mouse <i>Spdef</i> Rev	TCAATATCTTTTCAGGACCTCGCCC
mouse <i>EpCam</i> Fwd	TTGCTCCAAACTGGCGTCTA
mouse <i>EpCam</i> Rev	ACGTGATCTCCGTGTCCTTGT
mouse <i>Lysozyme</i> Fwd	ATGGAATGGCTGGCTACTTATGGAG
mouse <i>Lysozyme</i> Rev	CTCACCACCCTCTTTGCACATTG
mouse <i>Cryptdin</i> Fwd	AGGAGCAGCCAGGAGAAG
mouse <i>Cryptdin</i> Rev	ATGTTTCAGCGACAGCAGAG
mouse <i>Gob5</i> Fwd	TGAAATTGTGCTGCTGACCGATGG
mouse <i>Gob5</i> Rev	TGCTGCGAAAGCATCAACAAGACC
mouse <i>Muc2</i> Fwd	TGTGGGACTTTTGCCATGTACT
mouse <i>Muc2</i> Rev	GCAAGAGCACCTGTGATCCA
mouse <i>Smoc2</i> Fwd	GAAGAAGATATTGCCTCACG
mouse <i>Smoc2</i> Rev	TTCCTCAAGAGCTGACTGAT
mouse <i>Lgr5</i> Fwd	GAGGAAGCGCTACAGAATTTGAGA
mouse <i>Lgr5</i> Rev	GTGGCACGTAGCTGATGTGG
mouse <i>Olfm4</i> Fwd	TGGCCCTTGGAAAGCTGTAGT
mouse <i>Olfm4</i> Rev	ACCTCCTTGGCCATAGCGAA
mouse <i>Cdkn1a</i> (p21) Fwd	AACATCTCAGGGCCGAAA
mouse <i>Cdkn1a</i> (p21) Rev	TGCGCTTGGAGTGATAGAAA
mouse <i>Ctnnb1</i> Fwd	TGCTGAAGGTGCTGTCTGTC
mouse <i>Ctnnb1</i> Rev	AGTCGCTGCATCTGAAAGGT
mouse <i>Sox4</i> Fwd	GCTGCATCGTTCTCTCCAGA
mouse <i>Sox4</i> Rev	AAACAGGTAGACGCGCTTCA
mouse <i>Axin2</i> Fwd	ATGCTAGGCGGAATGAAGATG
mouse <i>Axin2</i> Rev	GGAGACAACGCTGTTGTTCTC

Materials

mouse <i>Ascl2</i> Fwd	GCCCCGTGAAGGTGCAAAC
mouse <i>Ascl2</i> Rev	ACAGGAAAAGTGCTCGCGA
mouse <i>Dll1</i> Fwd	CATGAACAACCTAGCCAATTGC
mouse <i>Dll1</i> Rev	GCCCCAATGATGCTAACAGAA
mouse <i>Notch1</i> Fwd	GCAGATGCTCAGGGTGTCTT
mouse <i>Notch1</i> Rev	GCCAGGATCAGTGGAGTTGT
mouse <i>Hes1</i> Fwd	TCAGCGAGTGCATGAACG
mouse <i>Hes1</i> Rev	TGCGCACCTCGGTGTTAAC
mouse <i>Jag1</i> Fwd	TCTCTGACCCCTGCCATAAC
mouse <i>Jag1</i> Rev	TTGAATCCATTCACCAGATCC
mouse <i>Jag2</i> Fwd	GGCAACTCCTTCTACCTGCC
mouse <i>Jag2</i> Rev	GTCATTGTCCCAGTCCCAGG
mouse <i>Dll4</i> Fwd	CCCTCACCTGGATTACCTAC
mouse <i>Dll4</i> Rev	GAATCTGCTTGTTAGGGATG
mouse <i>Hey1</i> Fwd	TGAGCTGAGAAGGCTGGTAC
mouse <i>Hey1</i> Rev	ACCCCAAACCTCCGATAGTCC
mouse <i>Tcf7 (Tcf1)</i> Fwd	TGCAGCTATACCCAGGCTGG
mouse <i>Tcf7 (Tcf1)</i> Rev	CCTCGACCGCCTCTTCTTC
mouse <i>c-Myc</i> Fwd	TGACCTAACTCGAGGAGGAGCTGGAATC
mouse <i>c-Myc</i> Rev	AAGTTTGAGGCAGTTAAAATTATGGCTGAAGC
mouse <i>EphB3</i> Fwd	AAGAGACTCTCATGGACACGAAAT
mouse <i>EphB3</i> Rev	ACTTCCCGCCGCCAGATG
human β - <i>ACTIN</i> Fwd	TGACATTAAGGAGAAGCTGTGCTAC
human β - <i>ACTIN</i> Rev	GAGTTGAAGGTAGTTTCGTGGATG
human <i>AP4</i> Fwd	GCAGGCAATCCAGCACAT
human <i>AP4</i> Rev	GGAGGCGGTGTCAGAGGT
human <i>c-MYC</i> Fwd	GCTGCTTAGACGCTGCTGGATTT
human <i>c-MYC</i> Rev	TAACGTTGAGGGGCATCG
human <i>NOTCH1</i> Fwd	TGATGAGGTCCTCCAGCAT
human <i>NOTCH1</i> Rev	TGATGAGGTCCTCCAGCAT
human <i>NRARP_Fwd</i>	TTCGAACCCGAAATCCTG
human <i>NRARP_Rev</i>	GCCACAGAAACCAGGAAGG
human <i>HES1</i> Fwd	GAAGCACCTCCGGAACCT
human <i>HES1</i> Rev	GTCACCTCGTTCATGCACTC

3.6.3 Oligonucleotides used for qCHIP

Name	Sequence (5'-3')
mouse <i>Sox4</i> (A) Fwd	TTCATGGGCGCCTTGATGT
mouse <i>Sox4</i> (A) Rev	CAACAACGCGGAGAACACTG
mouse <i>Sox4</i> (B) Fwd	CGCGTGCAATGAGAAGCTC
mouse <i>Sox4</i> (B) Rev	CACACACACAGAGGCCAAACG
mouse <i>Ascl</i> (A) Fwd	GCAGAGGTCAGTCAGCACTT
mouse <i>Ascl</i> (A) Rev	TTCTTCACAGCTGCATCCCT
mouse <i>Ascl</i> (B1) Fwd	ACAAACAAACGCCGGTCTTG
mouse <i>Ascl</i> (B1) Rev	GCCTGACACTTAGCGCCA
mouse <i>Ascl</i> (B2) Fwd	CTCCATCGGGCTTAGCTCTC
mouse <i>Ascl</i> (B2) Rev	TCTCTGTCCTGCGCCTCTAC
mouse <i>Ascl</i> (C1) Fwd	GCGTGGCTCCAGAGATGG
mouse <i>Ascl</i> (C1) Rev	TTCTCACACTCAAGGGGCAC
mouse <i>Ascl</i> (C2) Fwd	GTGCCCTTGAGTGTGAGAA
mouse <i>Ascl</i> (C2) Rev	GCATGAGGGGCTAAATGGGT
mouse <i>Tcf7</i> (A) Fwd	TCTTTGGGTAGAAGGCAGCC

Materials

mouse <i>Tcf7</i> (A) Rev	GCCTCAGCCAAAGTCATTCTG
mouse <i>Tcf7</i> (B) Fwd	AATCAGCCATCACCACCACC
mouse <i>Tcf7</i> (B) Rev	TGAGGGCAGAGGAGGAAGAA
mouse <i>Notch1</i> (A) Fwd	ACACTCAGCTCCCCGGAT
mouse <i>Notch1</i> (A) Rev	ACAATGGGCCGCTCTGATTC
mouse <i>Notch1</i> (B) Fwd	CCTACCTCTTGCGGCGAG
mouse <i>Notch1</i> (B) Rev	CCGGTGGTGTGCGTCAAC
mouse <i>Dll1</i> (A) Fwd	GTTTGGTGTGTGTCGTTCCG
mouse <i>Dll1</i> (A) Rev	AGCTCTTTCTCTCCGCATTGT
mouse <i>Dll1</i> (B) Fwd	ACATGAGAAAAGGGGAGGCG
mouse <i>Dll1</i> (B) Rev	AGGAAGGAGAGGCATAGGGG
mouse <i>Jag1</i> (A) Fwd	CTCGCGCTCCCCTTCTTTTA
mouse <i>Jag1</i> (A) Rev	CATTGTGTTACCTGCAGCCG
mouse <i>Jag1</i> (B) Fwd	CTTGCAAGCCCCAGGTGTAG
mouse <i>Jag1</i> (B) Rev	CTCTGGGCTCGCTTGCTG
mouse <i>Jag2</i> (A) Fwd	CAAGAGCACGCGCCCCAGG
mouse <i>Jag2</i> (A) Rev	CTTTCAGTTCGCCTGGCCGGTAC
mouse <i>Jag2</i> (B) Fwd	CTCAGCAGCTCCCCGTTT
mouse <i>Jag2</i> (B) Rev	CACTCTGCGCTGCCTTATTT
mouse <i>Jag2</i> (C) Fwd	GGGACGAGACTGACAGCTC
mouse <i>Jag2</i> (C) Rev	CTCGCCTCCTTTAAAGCTCG
mouse <i>Hes1</i> Fwd	CACACACCCCACACGCAG
mouse <i>Hes1</i> Rev	CCAAGAAGGTAAATAGCAGCTG
mouse <i>Dll4</i> (A) Fwd	TGTA CTCCCTCACTAGCCCG
mouse <i>Dll4</i> (A) Rev	GTAATCCAGGTGAGGGCGAC
mouse <i>Dll4</i> (B) Fwd	CTCCTTCTCTCGGTCCCTGT
mouse <i>Dll4</i> (B) Rev	GCAGATGCGGAAGAAAGTCC
mouse <i>Dll4</i> (C) Fwd	GGGACAAGAATAGCGGCAGT
mouse <i>Dll4</i> (C) Rev	GAAAGGAGCTCTGGTGTCCC
mouse <i>Cdkn1a</i> (A1) Fwd	AATTGAAGAGGTGGGGCTGC
mouse <i>Cdkn1a</i> (A1) Rev	TCTGGGGTCTCTGTCTCCAT
mouse <i>Cdkn1a</i> (A2) Fwd	TCCCCTTTGCCAGCAGAAT
mouse <i>Cdkn1a</i> (A2) Rev	CCAGGCACACACACAGAT
mouse <i>Cdkn1a</i> (B) Fwd	CCCAGAAGTGTGTGTGTGTG
mouse <i>Cdkn1a</i> (B) Rev	ACACCCGTCATCCACCTG
mouse <i>Cdkn1a</i> (C) Fwd	CCCCAGACGCTTCATCTCTT
mouse <i>Cdkn1a</i> (C) Rev	TACCACACACATACACACGC
mouse <i>EphB3</i> Fwd	AAGAGCGGCCAACTGAACTC
mouse <i>EphB3</i> Rev	CTGCCCGTCAACTCAGG
mouse <i>AchR</i> Fwd	AGTGCCCCCTGCTGTGTCAGT
mouse <i>AchR</i> Rev	CCCTTTCCTGGTGCCAAGA

Materials

3.7 siRNAs

The following siRNAs were purchased from Ambion:

AP4-specific siRNA: 5'-GUGAUAGGAGGGCUCUGUAG-3'

Silencer negative control siRNA: 5-UUGUCUUGCAUUCGACUAAUU-3

3.8 Vectors

Name	Insert	Source
Bluescript II plasmid p695-pBS-mOlfm4	Mouse <i>Olfm4</i> ORF	Prof. Dr. Hans Clevers
pCMV6-Entry-Lgr5	Mouse <i>Lgr5</i> ORF	Origene, cat.no. MR219702
pCMV6-Entry-Smoc2	Mouse <i>Smoc2</i> ORF	Origene, cat.no. MR207121
pBluescriptII-KS	empty	Promega Corporation
pRTR	empty	(Jackstadt et al., 2013c)
pRTR-Ap4-VSV	AP4-VSV ORF	(Jackstadt et al., 2013c)
pGA-RBPJ	Human <i>RBPJ</i> -ORF	(Oswald et al., 2001)
pGA	empty	(Oswald et al., 2001)

ORF: Open Reading Frame

3.9 Mice

Genotype	Background	Source
<i>Ap4^{fl/fl}</i>	C57BL/6	Our lab (Jackstadt et al., 2013a)
<i>Apc^{Min}</i>		Dr. Marlon Schneider (LMU)
<i>Lgr5-CreERT2</i>		Prof. Dr. Hans Clevers (Hubrecht Institute)
<i>Vil-Cre</i>		Prof. Dr. Klaus-Peter Janssen (TUM)
<i>Vil-CreERT2</i>		
<i>CMV-Cre</i>		
<i>Flp</i>		The Jackson Laboratory
<i>Prkdc-scid</i>	NOD	The Jackson Laboratory

Materials

3.10 Cell lines

Species	Cell lines	Medium	Supplier
Human CRC cell lines	SW620	DMEM Medium + 10% FBS + 1% P/S	--
	DLD-1	McCoy`s 5A Medium + 10% FBS + 1% P/S	--
	HCT15		--
	Colo320	RPMI1640 w/o glutamax + 1% Glutamax + 10% FBS + 1% P/S	--
Murine CRC cell line	CT26	RPMI1640 w/o glutamax + 1% Glutamax + 10% FBS + 1% P/S	ATCC
Human kidney cell line	HEK293	DMEM Medium + 10% FBS + 1% P/S	DSMZ

ATCC: The Global Bioresource Center; <https://www.atcc.org/>

DSMZ: Deutsche Sammlung von Mikroorganismen und Zellkulturen GmbH;
<https://www.dsmz.de/>

3.11 Software

application	software	Supplier
Data analysis and figure generation	Excel	Microsoft Cooperation
	Prism5	Graphpad Software Inc.
WB	Varioskan Flash Multimode Reader	Thermo Scientific
	KODAK MI SE software	Carestream Health
qPCR	ND1000 V3	PEQLAB
	LightCycler 480	Roche Diagnostics
Cell Culture	cFlow Software	Accuri
Sequencing analysis	DNA Sequencing Analysis Software v5	Applied Biosystems
	BioEdit	BioEdit
IF	ZEN 2009	Carl Zeiss
IHC, ISH, tumor counting	Axiovision	Carl Zeiss
Organoids	Nikon NIS-Elements	Nikon
Luciferase reporter assays	SIMPLICITY software package	DLR

Materials

3.12 Laboratory equipment

application	Device	Supplier
qPCR	ND 1000 NanoDrop Spectrophotometer	PEQLAB
	LightCycler480	Roche Diagnostics
WB	Mini-PROTEAN®-electrophoresis system	Bio-Rad
	HTU SONI130	G. Heinemann Ultraschall- und Labortechnik
	Varioskan Flash Multimode Reader	Thermo Scientific
	Mini Trans-Blot® Electrophoretic Transfer Cell	Bio-Rad
	Powerpac 300 Power Supply	Bio-Rad
	biophotometer plus	eppendorf
	EPS 600 power supply	Pharmacia Biotech
	440CF imaging system	Eastman Kodak
Cell culture	Herasafe KS class II safety cabinet	Thermo Fisher Scientific
	Neubauer counting chamber	Carl Roth
	BD Accuri™ C6 Flow Cytometer Instrument	BD Accuri
	Axiinvert 25 microscope equipped with an Axiocam 105 color camera	Carl Zeiss
Sequencing	ABI 3130 genetic analyzer capillary sequencer	Applied Biosystems
IF	LSM700 confocal microscope	Carl Zeiss
IHC, ISH	Axioplan 2 imaging microscope AxioCam HRc camera	Carl Zeiss
Electron microscopy	Libra 120 transmission electron microscope	Carl Zeiss
Organoids	Stemi 2000-C stereo microscope	Carl Zeiss
	Nikon AZ-100 macroscope equipped with a Nikon DS-Fi3 color camera equipped with a 5.9 megapixel CMOS image sensor.	Nikon
Tumor counting	Stemi 2000-C stereo microscope	Carl Zeiss
	Nikon D5100 digital camera equipped with a Nikon AF-S Nikkor 18-55mm 1:3.5-5.6G objective	Nikon
Luciferase reporter assays	Orion II Luminometer	Berthold Technologies

Methods

4. Methods

4.1 Generation and husbandry of mice

Ap4^{fl/fl} mice and germ-line *Ap4* knock-out mice were generated by the Hermeking lab as follows: targeted embryonic stem cells (ES-cells) with C57BL/6N background were obtained by homologous recombination with a vector containing the *Ap4* exons 2-4 flanked by *loxP* (locus of X-over P1) sites and an intronic neomycin resistance (*Neo*) cassette flanked by *frt* (*flp* recognition target) sites (scheme in (Jackstadt et al., 2013a)). *Ap4^{+/fl}* mice were generated by injection of targeted ES cells into C57BL/6N blastocyst. The *Neo* cassette was removed by crossing to *flp* (Flippase)-mice (Gronostajski and Sadowski, 1985) and germ-line *Ap4* knock-out mice were generated by crossing with *CMV* (cytomegalovirus)-*Cre*^{+/-} mice (Schwenk et al., 1995).

Ap4^{-/-} mice showed no overt phenotype and were born at normal Mendelian ratio. Oligonucleotides used for genotyping are listed in Table 3.6.1. For analysis of the effect of *Ap4* inactivation on the ISC number we used *Lgr5-eGFP-Cre-ERT2^{+/-}* mice (Barker and Clevers, 2007) (obtained from Hans Clevers, University Medical Center Utrecht, The Netherlands) and for specific deletion of *Ap4* in intestinal epithelial cells or derived organoids we used *Villin-Cre^{+/-}* or *Villin-Cre-ERT2^{+/-}* mice (el Marjou et al., 2004) (obtained from Klaus-Peter Janssen, Technical University Munich, Germany), respectively. *Apc^{Min/+}* mice (Moser et al., 1990; Su et al., 1992) (obtained from Marlon Schneider, Ludwig-Maximilians-Universität, München, Germany) were used to analyze the role of *Ap4* in intestinal adenoma development. Mice were kept in individually ventilated cages (IVC) with a 12-hour light/dark cycle and *ad libitum* access to water and standard rodent diet. For determination of proliferation rates 75 mg/kg BrdU (Bromdesoxyuridin) (Amersham) in PBS (phosphate-buffered saline) was i.p. (intraperitoneal) injected 1.5 hours before mice were sacrificed. All animal experimentations and analyses were approved by the Government of Upper Bavaria, Germany (AZ 55.2-1-54-2532-4-2014).

4.2 Tissue preparation and adenoma counting

After isolation of intestinal tissue, the colon and small intestine were separated and flushed with PBS to remove stool. The small intestine was dissected into duodenum, jejunum and ileum. The colon and small intestine were opened longitudinally and rolled

Methods

with the mucosa oriented outwards and fixed in formalin, dehydrated and embedded into paraffin. For evaluation of tumor numbers each part of the intestine was cut longitudinally and spread on Whatman 3 MM paper. After fixation in formalin adenomas were counted under a Stemi 2000-C stereo (dissection) microscope (Carl Zeiss) with 10x magnification. Pictures of intestines were taken with a Nikon D5100 digital camera with a Nikon AF-S Nikkor 18-55mm 1:3.5-5.6G objective.

4.3 HE and PAS/Alcian blue staining

Formalin-fixed, paraffin-embedded (FFPE) tissue was cut into 2 μm sections on a Microm HM355S rotating microtome (Thermo Fisher Scientific). For hematoxylin and eosin (HE)-staining the slides were de-paraffinized and stained with hematoxylin (Waldeck) for 6 minutes followed by eosin (Sigma-Aldrich) for 2.5 minutes in an automated slide staining device (Tissue-Tek, Prisma). Periodic acid Schiff (PAS)-staining was done by applying Alcian Blue pH 1 (Bio Optica) for 10 minutes followed by periodic acid (Merck Millipore) for 5 minutes, Schiff's reagent (Sigma Aldrich) for 5 minutes and counterstaining with hematoxylin (Waldeck).

4.4 Immunohistochemistry

FFPE tissue was cut into 2 μm sections on a microtome and de-paraffinized. After antigen retrieval slides were incubated with primary antibody (the primary antibodies used are listed in Table 3.4.1) for 1 hour at room temperature and washed with Tris-HCL (Tris hydrochloride) buffer (pH 7.5) followed by a secondary antibody. Antibodies were detected with the Vectastain *Elite* ABC (avidin-biotin complex) kit (Vector) using DAB (3,3'-diaminobenzidine) (Vector Laboratories and Dako) for brown stainings or AEC (3-Amino-9-ethylcarbazole) (Thermo Fisher Scientific) for red stainings. The slides were counterstained with hematoxylin (Vector Laboratories) and mounted with Roti®-Histokitt II (Carl Roth). All stainings were performed with the respective IgG (Immunoglobulin G) control (Table 3.4.1) as a negative control and without primary antibody as a system control. Images were captured on an Axioplan2 imaging microscope (Carl Zeiss) equipped with an AxioCamHRc Camera (Carl Zeiss). For analysis of cleaved Caspase-3 the AxioVision Software (Carl Zeiss) was used to measure the area for each tumor in mm^2 .

Methods

4.5 *In situ* hybridization

For detection of ISCs with an *Olfm4* mRNA probe, the Bluescript II plasmid p695-pBS-mOlfm4 (kindly provided by Prof. Hans Clevers) was linearized by using a NotI restriction enzyme (New England Biolabs). The pCMV6 entry plasmids containing the *Lgr5* or *Smoc2* open reading frame (ORF) were obtained from Origene with the catalog number MR219702 or MR207121, respectively. Both ORFs were cloned into the pBSII KS plasmid (Promega Corporation) by using the restriction enzymes NotI and KpnI. The pBSII KS-mSmoc2 was linearized with the KpnI restriction enzyme and the pBSII KS-mLgr5 was linearized with the BclI restriction enzyme. The *Olfm4*, *Lgr5* and *Smoc2* (SPARC-related modular calcium-binding protein 2) RNA probe was generated by an *in vitro* transcription reaction with a RNA-T7 Polymerase by using the DIG Northern Starter Kit (Roche Diagnostics). During the transcription reaction the probe was labeled with digoxigenin (DIG). The *in situ* hybridization was performed on freshly prepared 8 μ m paraffin sections as described (Gregorieff and Clevers, 2010).

4.6 Isolation of IECs

Each part of the intestine was dissected longitudinally and cut into small pieces. IECs were isolated by shaking the tissue in Hanks' balanced salt solution (HBSS)/ethylene-diamine-tetra-acetic acid (EDTA) at 37°C for 10 minutes. The supernatant including IECs was centrifuged and the pellet was washed with ice-cold PBS, frozen in liquid nitrogen and stored at -80°C until RNA isolation.

4.7 Crypt isolation and organoid culture

Crypt isolation and organoid culture was performed as described before (Sato et al., 2009). The small intestine was opened longitudinally, and the villi were scraped off under a dissection microscope by using a surgical blade. The intestine was cut into small pieces and incubated in 8 mM EDTA in HBSS for 5 minutes to remove the rest of the villi followed by an additional incubation in EDTA for 30 minutes at 4°C. Isolated crypts were washed in advanced DMEM (Dulbecco's Modified Eagle's Medium)/F12 (Gibco / Life Technologies) containing Glutamax (Gibco / Life Technologies) and HEPES (Gibco / Life Technologies), passed through a 100 μ m cell strainer and either frozen in liquid nitrogen (IEC) or counted and pelleted for culturing (organoids). 200 crypts were mixed with 50 μ l of growth factor reduced, phenol red-free matrigel. After

Methods

polymerization of the Matrigel 600 μ l of crypt culture medium was added. Crypt culture medium consists of advanced DMEM/F12 supplemented with 1:100 P/S (Penicillin/Streptomycin) (Gibco / Life Technologies), 1:100 HEPES, 1:100 Glutamax and the following growth factors: 100 ng/ml Noggin (Preprotech), 1:100 N2 (Gibco / Life Technologies), 1:50 B27 retinoic acid free (Gibco / Life Technologies), 50 ng/ml epidermal growth factor (EGF) (Preprotech), 500 ng/ml R-spondin-1 (RSPO1) (Sinobiological), 10 μ M Y-27632 (MedBiochem Express) was added only the first 2 days after isolation/culturing or passaging to avoid anoikis and 100 ng/ml Wnt-3a (Abcam) was added only the first two days after isolation/culturing. Crypt culture medium was changed every 2 days. Organoids were passaged at a 1:6 ratio once a week. For passaging organoids were removed from Matrigel and dissociated mechanically into single-crypt domains before they were transferred into fresh Matrigel. 4-OHT (4-hydroxytamoxifen) (Sigma-Aldrich), diluted in ethanol, was added to the crypt culture medium to a final concentration of 500 nM for at least 12 hours. RNA was isolated using Trizol (Invitrogen) and the RNeasy Mini Kit (QIAGEN).

For generation of tumoroids intestinal adenoma cells from 3 tumors for each *Apc*^{Min/+} mouse were isolated by lysis in DMEM containing 4000 units Collagenase Type IV (Merck Millipore) and 125 μ g/ml Dispase Type II (Sigma-Aldrich). Single cells were embedded in Matrigel and seeded in 24-well plates (15,000 single cells per 50 μ l Matrigel per well). The tumor organoid culture medium was formulated as described before (Sato et al., 2011a). Crypt culture medium (Advanced DMEM/F12 supplemented with 1:100 Penicillin/Streptomycin, 1:100 HEPES and 1:100 Glutamax and growth factors (1:100 N2, 1:50 B27, 50 ng/ml EGF)). 10 μ M Y-27632 was added only the first 2 days after isolation/culturing or passaging to avoid anoikis. Counting of the number of organoids per well (6 wells per mouse) was performed 6 days after isolation before the first passaging. Passaging was performed as described above for normal organoids. RNA was isolated using Trizol and the RNeasy Mini Kit. For Western blot analysis tumor organoids were lysed in RIPA lysis buffer (50 mM Tris/HCl, pH 8.0, 150 mM NaCl, 1% NP40, 0.5% sodium deoxycholate, 0.1% sodium dodecylsulfate, Complete Mini protease inhibitors (Roche Diagnostics)).

For tumoroid formation after acute loss of *Apc* or *Apc* and *Ap4* crypts were isolated as described above. For each well in a 6-well plate approximately 8 drops of 25 μ l matrigel and 50 crypts each were plated and overlaid with ENR media (containing EGF,

Methods

Noggin and RSPO1) as described above. 48 hours after isolation organoids were treated with 100 nM 4-OHT in ENR media for 48 hours. After passaging and additional 48 hours, the culture conditions were switched to EN devoid of RSPO1 to select for tumoroid growth. Pictures of tumoroids were taken with a Nikon AZ-100 microscope equipped with a Nikon DS-Fi3 color camera equipped with a 5.9 megapixel CMOS image sensor.

4.8 Tissue microarrays and IHC (immunohistochemistry) analysis of clinical samples

Colon cancer specimens from patients that underwent surgical resection at the University of Munich (LMU) were drawn from the archives of the Institute of Pathology. Specimens were anonymized, and the need for consent was waived by the institutional ethics committee of the Medical Faculty of the LMU. Tissue microarrays (TMAs) with samples of 225 (220 evaluable) stage II primary colorectal cancer cases were generated with 6 representative 1 mm cores of each case. 5 μ m TMA sections were deparaffinized and stained with primary antibodies (listed in Table 3.4.1) on a Ventana Benchmark XT Autostainer with UltraView Universal DAB and alkaline phosphatase detection kits (Ventana Medical Systems). The stainings were evaluated according to the score shown in Figure 30a.

4.9 RNA expression profiling by RNA-Seq

Total RNA from organoids or adenomas was used for RNA-Seq (RNA-sequencing). Random primed cDNA libraries were constructed and sequenced using the HiSeq2500 (Illumina) platform by GATC (Konstanz, Germany). Each sample was covered by at least 30 million single reads of 50 bp length.

4.10 Bioinformatics analyses of RNA-Seq and ChIP-Seq data

RNA-Seq FASTQ files were processed using the RNA-Seq module implemented in the CLC Genomics Workbench v8.0 software (QIAGEN Bioinformatics) with default settings and were mapped to the GRCm38/mm10 mouse reference genome and its associated gene and transcript annotation (ENSEMBL). RNA-Seq data were filtered to exclude weakly expressed transcripts with less than 5 mapped exon reads in all samples from the analysis and subjected to upper quartile normalization using the

Methods

R/Bioconductor *RUVSeq* (remove unwanted variation from RNA-Seq data) package as described in (Risso et al., 2014). Differential gene expression analysis was performed with *edgeR* (McCarthy et al., 2012; Robinson et al., 2010) or *DESeq2* (Love et al., 2014) after further normalization using the *RUVg* approach to remove variation between RNA samples resulting from differences in library preparation. Gene Set Enrichment Analysis (GSEA) was performed using the GSEA software (Subramanian et al., 2005). *Lgr5+* or *EphB2^{high}* stem cell gene sets were obtained from (Merlos-Suarez et al., 2011; Munoz et al., 2012; van der Flier et al., 2009). The Wnt/ β -catenin target gene sets were obtained from (Fevr et al., 2007). The Notch target gene set was obtained from (Li et al., 2012). Additional gene sets representing genes involved in Wnt/ β -catenin signaling, EMT or c-Myc target genes were obtained from the Molecular Signatures database (MSigDB) (Liberzon et al., 2015). Enrichment of Hallmark gene sets or Kyoto Encyclopedia of Genes and Genomes (KEGG) pathways among differentially regulated genes was analyzed with the Molecular Signatures database program (MSigDB) (Liberzon et al., 2015). Heatmaps were generated with GENE-E (Broad Institute).

ChIP-Seq (Chromatin immunoprecipitation-sequencing) data of genome-wide Ap4 occupancy in murine B and T cells (GEO accession nos. GSE80669 and GSE58075) and human CRC cells (GEO accession no. GSE46935) were obtained from previously published studies (Chou et al., 2014; Chou et al., 2016; Jackstadt et al., 2013c) and were analyzed with the UCSC genome browser (Kent et al., 2002).

4.11 *In silico* analysis of human colorectal patient samples

Normalized RNA expression (RNA-Seq by Expectation Maximization; RSEM) data from colorectal cancer patient samples were obtained from the publically available TCGA datasets (Cancer Genome Atlas, 2012) at <https://cancergenome.nih.gov/>. Association of TCGA patient samples with the different CMS (consensus molecular subtypes) categories was obtained from the Cancer Subtyping Consortium (CRCSC) at www.synapse.org. The CMS sub-types were described in (Guinney et al., 2015).

Methods

4.12 Indirect immunofluorescence detection and confocal laser-scanning microscopy

FITC (Fluorescein isothiocyanate) conjugated donkey anti-rabbit (Jackson Immuno Research) and AlexaFluor 555 conjugated goat anti-mouse (Invitrogen) antibodies were used for detection of primary rabbit or mouse antibodies, respectively. DNA was stained using DAPI (4',6-diamidino-2-phenylindole) (Carl Roth). Slides were mounted with ProLong Gold antifade reagent (Life technologies). Images were captured with a confocal microscope (LSM 700, Carl Zeiss) using a Plan Aplanachromat 20x/0.8 M27 objective, ZEN 2009 software (Carl Zeiss) and the following settings: Image size 2048x2048 and 16 bit; pixel/dwell of 25.2 μ s; pixel size 0.31 μ m; laser power 2%; master gain 600-1000. After image capturing the original LSM files were converted into TIFF files. Conditions for primary antibodies used here are listed in Table 3.4.1.

4.13 Electron microscopy

Small pieces from the middle of ileum were fixed in 6.25% glutaraldehyde, post-fixed with osmium tetroxide, dehydrated, embedded in EPON 812 (Serva Electrophoresis), polymerized at 80°C and cut into 60-80 nm sections with an ultra-microtome (Ultracut, Reichert Jung). The sections were stained with lead citrate and uranyl acetate. Images were captured on a transmission electron microscope (Libra 120, Carl Zeiss).

4.14 RNA isolation and quantitative real-time PCR (qPCR)

Total RNA was isolated using the High Pure RNA Isolation Kit (Roche Diagnostics) or RNAeasy Kit (QIAGEN). 5 adenomas per mouse were used for each *Apc^{Min}* tumor sample. cDNA was generated from 1 μ g total RNA per sample using anchored oligo-dT primers (Reverse-iT First Strand Synthesis; ABgene). qPCR was performed by using the LightCycler 480 (Roche Diagnostics) and the Fast SYBR Green Master Mix (Applied Biosystems) as described previously (Siemens et al., 2011). Oligonucleotides used as qPCR primers are provided in Table 3.6.2.

4.15 DBZ treatment of mice

DBZ (dibenzazepine) treatment was described elsewhere (van Es et al., 2005b). The γ -secretase inhibitor DBZ (Axon Medchem) was suspended in water with 0.5% Methocel and 0.1% Tween-80 (Sigma-Aldrich), and 40 μ mol/kg were injected i.p. on 5

Methods

consecutive days into NOD/SCID mice. The mice were sacrificed at day 6 for tissue collection.

4.16 Cell lines / culture and reagents

SW480, SW620, HT29 and HEK293T cell lines were maintained in Dulbecco's Modified Eagles Medium (DMEM, Gibco / Life Technologies). Colo320 and the mouse colon carcinoma cell line CT26 were cultured in RPMI (Roswell Park Memorial Institute) 1640 (Sigma-Aldrich, Gibco / Life Technologies). The colorectal cancer cell lines DLD-1 and HCT15 were maintained in McCoy's 5A Medium (Gibco / Life Technologies). The identity of SW480, SW620, Colo320, HT29, HCT15 and DLD-1 cell lines was confirmed by PCR-single-locus technology using 21 independent PCR amplicons (Eurofins Medigenomics, Ebersberg, Germany). CT26 cells were purchased from ATCC (the American Type Culture Collection) and HEK293T cells from DSMZ (Deutsche Sammlung von Mikroorganismen und Zellkulturen GmbH). All cells were cultivated in presence of 100 units/ml penicillin and 0.1 mg/ml streptomycin and 10% fetal bovine serum (FBS) (Invitrogen). Doxycycline (DOX) (Sigma-Aldrich) was dissolved in water (100 µg/ml stock solution) and always used at 100 ng/ml final concentration.

4.17 Chromatin immunoprecipitation (ChIP) assay

Cross-linking and harvesting of cells was performed as previously described (Jackstadt et al., 2013b). Briefly, cross-linking was performed by incubation of cells in 1% formaldehyde (Merck Millipore) and terminated after 5 minutes by addition of glycine at a final concentration of 0.125 M. Cells were harvested with SDS buffer (50 mM Tris/HCL pH 8.1, 0.5% SDS, 100 mM NaCl, 5 mM EDTA) and after pelleting resuspended in IP (Immunoprecipitation) buffer (2 parts of SDS buffer and 1 part Triton dilution buffer (100 mM Tris/HCl pH 8.6, 100 mM NaCl, 5 mM EDTA (pH 8.0), 0.2% NaN₃, 5% Triton X-100)). Chromatin was sheered by sonication (HTU SONI 130, G. Heinemann) to generate DNA fragments with an average size of 500 bp. Pre-clearing and incubation with an AP4-specific antibody or the respective IgG control (the antibodies used are listed in Table 3.4.1) was performed for 16 hours as previously described (Menssen et al., 2007). Washing and reversal of cross-linking was performed as described (Frank et al., 2001). Immunoprecipitated DNA was analyzed

Methods

by qPCR and the enrichment was expressed as percentage of the input for each condition (Frank et al., 2001). The sequences of oligonucleotides used as qChIP primers are listed in Table 3.6.3.

4.18 Generation of cell pools stably expressing conditional alleles

DLD-1 colorectal cancer cells were transfected with pRTR plasmids using Lipofectamin 2000 (Invitrogen) or FuGENE (Promega Corporation). After 24 hours cells were transferred into media containing 4 µg/ml Puromycin (Sigma-Aldrich) for one week. Homogeneity of the derived cell pools was determined by addition of 100 ng/ml DOX (Sigma-Aldrich) for 48 hours and evaluation of GFP expression by fluorescence microscopy by using an Axiovert 25 microscope equipped with an AxioCam 105 color camera (Carl Zeiss) and by flow cytometry using a BD Accuri™ C6 flow cytometer instrument (BD Accuri).

4.19 Plasmids and RNAi

The generation of pRTR-AP4-VSV was previously described (Jackstadt et al., 2013c). siRNAs (silencerRNAs) were transfected at a 40 nM final concentration using HiPerFect reagent (QIAGEN). siRNA target sequences were as follows: *AP4*-specific siRNA (Ambion): (5'-GUGAUAGGAGGGCUCUGUAG-3') as described in (Jung et al., 2008). As a control the Silencer negative control siRNA #1 (Ambion) was used.

4.20 Cell-Based Reporter Assays

HEK293T cells were seeded in 24-well format dishes at 50% confluence and transfected with FuGENE Reagent (Roche Diagnostics) for 24 hours with 100 ng of the indicated firefly luciferase reporter plasmid (pGA-RBPJ (Oswald et al., 2001)) and the respective control vector (pGA (Oswald et al., 2001)), 100 ng of the effector (dBR-AP4, AP4) or the respective control vector and 10 ng of *Renilla* reporter plasmid as a normalization control. The analyses were performed with the Dual Luciferase Reporter assay (Promega Corporation) according to manufacturer's instructions. Luminescence intensities were measured with an Orion II Luminometer (Berthold) in 96-well format and analyzed with the SIMPLICITY software package (DLR).

Methods

4.21 Western blot analysis

Cells or tumoroids were lysed in RIPA lysis buffer (50 mM Tris/HCl, pH 8.0, 150 mM NaCl, 1% NP40, 0.5% (w/v) sodium deoxycholate, 0.1% sodium dodecylsulfate, Complete Mini protease inhibitors (Roche Diagnostics)). Lysates were sonicated and centrifuged at 16.060 x g for 15 min at 4°C. Per lane 30 – 80 µg of whole cell lysate was separated using 10% or 12% SDS-acrylamide gels and transferred on Immobilon PVDF membranes (Merck Millipore). For immuno-detection membranes were incubated with primary antibodies (the primary antibodies used are listed in Table 3.4.1). Signals from HRP (horse-radish-peroxidase)-coupled secondary antibodies were generated by enhanced chemiluminescence (Perkin Elmer Life Sciences, Boston, MA) and recorded with a CCD camera (440CF imaging system, Eastman Kodak Co., Rochester, NY). Uncropped Western blot membranes are provided in Supplemental Data 3.

4.22 Statistical analysis

The Graph Pad Prism software was used for statistical analyses. A Student's *t* test (unpaired, two-tailed) was used for calculation of significant differences between two groups of samples or mice, with $p < 0.05$ considered significant. Asterices generally indicate: *: $p < 0.05$, **: $p < 0.01$ and ***: $p < 0.001$, n.s. = not significant. For calculation of correlation coefficients, Pearson's or Spearman's correlation analyses were applied. Kaplan Meier curves were analyzed by log-rank (Mantel-Cox) test.

4.23 Data availability statement

RNA-Seq data that support the findings of this study have been deposited in Gene Expression Omnibus (GEO) with the accession codes „GSE99434” and “GSE99437”. All other data are available from the corresponding author on reasonable request.

Results

5. Results

5.1 Role of *Ap4* in intestinal adenoma formation

Here we determined the effect of *Ap4*-deficiency on adenoma formation in the intestine of *Apc^{Min}* mice, which harbour an inactivating mutation in one adenomatous polyposis coli (*Apc*) allele (Jaeckel et al., 2018). Upon spontaneous loss of the second *Apc* allele these mice develop ~50-100 adenomas in the small intestine by the age of 4-6 months. As expected, adenomas in *Apc^{Min/+}/Ap4^{-/-}* mice did not display *Ap4* expression, whereas adenomas of *Apc^{Min}* mice showed elevated expression of *Ap4* (Figure 9a). ~50% of *Apc^{Min}* mice succumbed to intestinal adenomas by ~180 days of age (Figure 9b) which was in line with previous reports (Guillen-Ahlers et al., 2010; Hoshiko et al., 2013). However, in *Ap4*-deficient *Apc^{Min}* mice intestinal cancer-related death was delayed on average by 110 days, with heterozygous mice showing an intermediate delay.

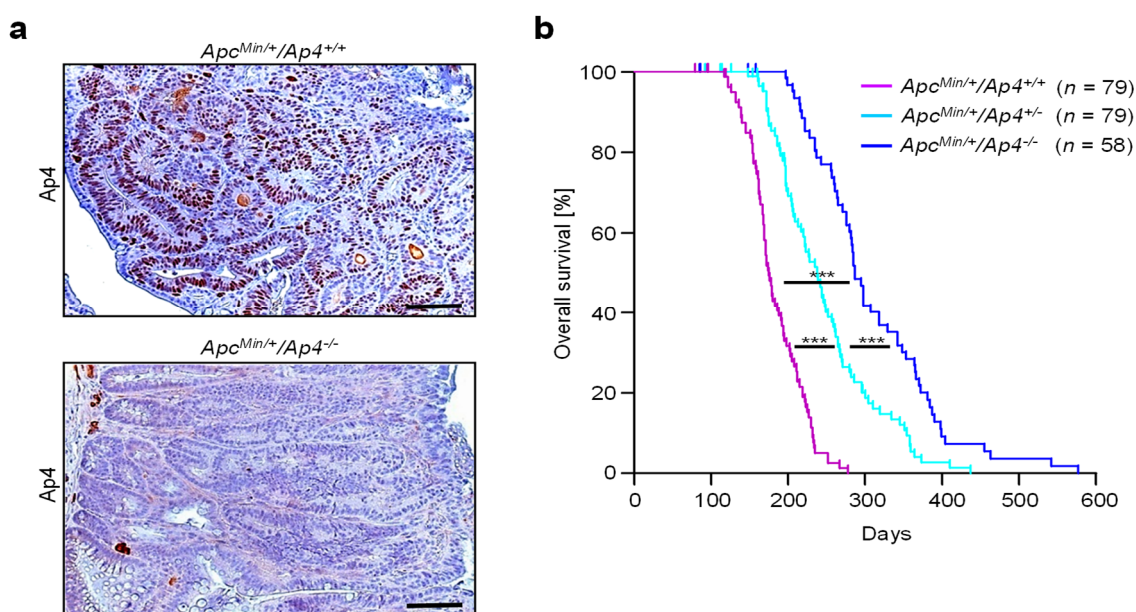


Figure 9 Deletion of *Ap4* in *Apc^{Min/+}* mice prolongs survival. **a** Immunohistochemical detection of *Ap4* in adenomas of moribund *Apc^{Min/+}* mice with the indicated genotype. Counterstaining with hematoxylin. Scale bar = 50 μ m. **b** Kaplan-Meier survival analysis of *Apc^{Min/+}* mice with the indicated genotypes. Censored mice without intestinal tumor related death are indicated on the Kaplan-Meier curve as tick marks. Results were subjected to a log rank test with p-values * < 0.05, ** < 0.01, *** < 0.001, n.s. = not significant

Ap4-deficiency was associated with a ~4-fold decrease in the number of adenomas in the small intestines of moribund *Apc^{Min}* mice, while the size of adenomas increased

Results

(Figure 10a-c). Unexpectedly, the proliferation rate within small intestinal adenomas of moribund *Apc^{Min}* mice was not affected by loss of *Ap4* (Figure 10d).

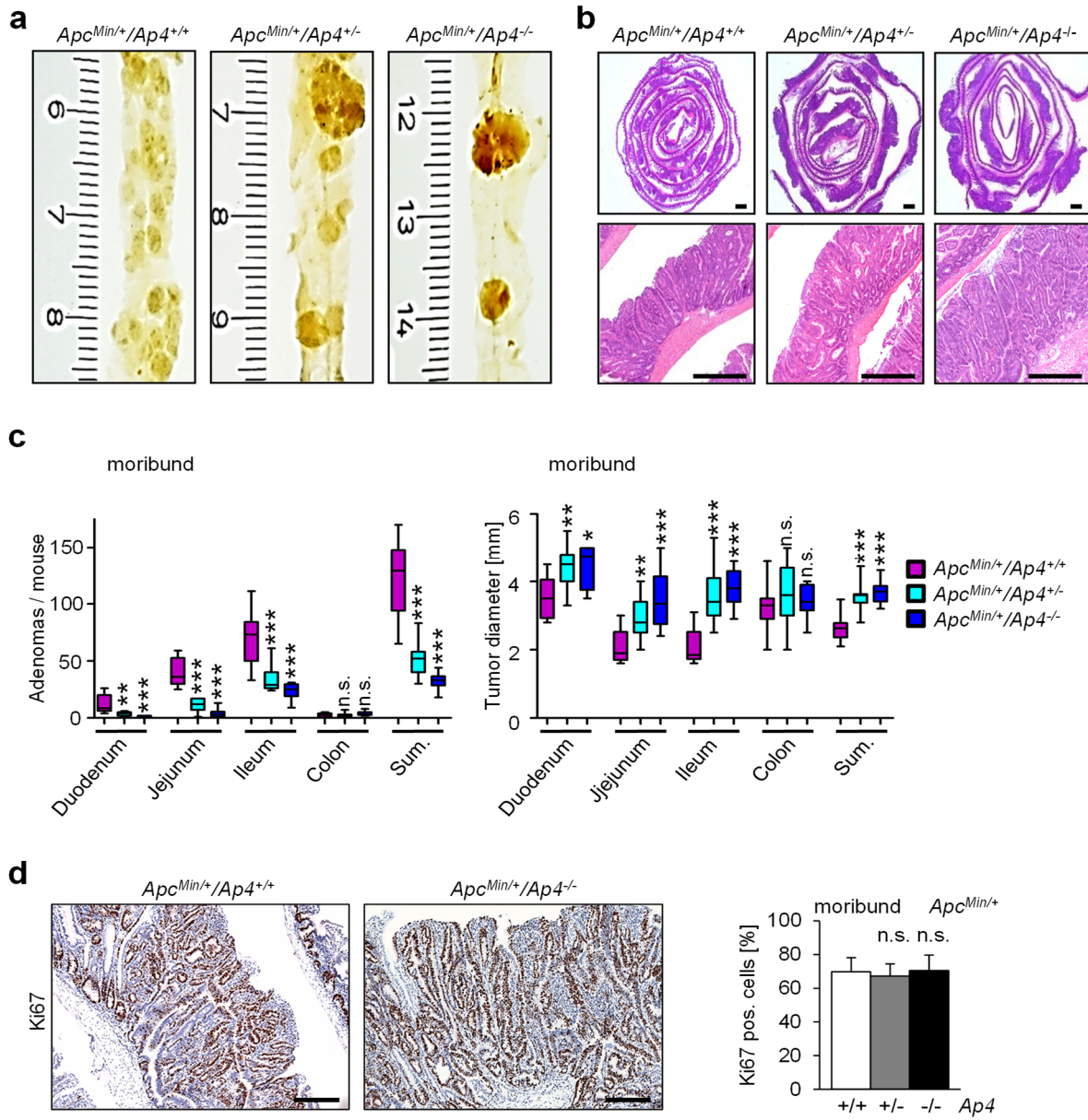


Figure 10 Deletion of *Ap4* in *Apc^{Min/+}* mice decreases the frequency of adenomas.

a Macroscopic pathology of representative polyps in the small intestine (ileum) of moribund *Apc^{Min/+}* mice with the indicated genotype, scale in cm. **b** Representative sections through rolls of the small intestine stained for hematoxylin and eosin (HE). Scale bar = 500 μ m. **c** Quantification of adenoma number/mouse (left panel) and tumor diameter (right panel) in the intestine of 6 male and 6 female (*Apc^{Min/+}/Ap4^{+/+}*), 5 male and 5 female (*Apc^{Min/+}/Ap4^{+/-}*) or 4 male and 4 female (*Apc^{Min/+}/Ap4^{-/-}*) moribund *Apc^{Min/+}* mice. The box plot extends from the 25th to 75th percentiles. The line in the middle of the box is plotted at the median. The whiskers underneath or above the boxes range from min. to max. value, respectively. **d** Left panel: Immunohistochemical detection of Ki67 in adenomas from moribund *Apc^{Min/+}* mice, scale bar = 200 μ m. Counterstaining with hematoxylin. Right panel: Ki67-positive cells were counted in at least 8 adenomas from 1 male and 2 female mice per genotype. c, d: Results represent the mean \pm SD. Results were subjected to an unpaired, two tailed Student's *t*-test with p-values * < 0.05, ** < 0.01, *** < 0.001, n.s. = not significant.

Results

When adenomas of age-matched, 120 days old *Apc^{Min}* mice were compared, the *Ap4*-deficient mice showed a ~5-fold decrease in the number of adenomas, whereas the size of the adenomas was not affected (Figure 11a-c). A decreased number of tumors was also detected in the colon of *Ap4*-deficient *Apc^{Min}* mice when compared to *Ap4*-wild-type *Apc^{Min}* mice (Figure 11d). However, due to the low incidence of adenomas in the colon of *Apc^{Min}* mice these differences did not reach statistical significance. The uniform tumor size and the unchanged proliferation rate of tumors in the small intestine (Figure 11e) in 120 days old mice suggested that the increase in adenoma size seen in moribund animals was most likely due to the increased lifespan of *Ap4*-deficient *Apc^{Min}* mice.

Results

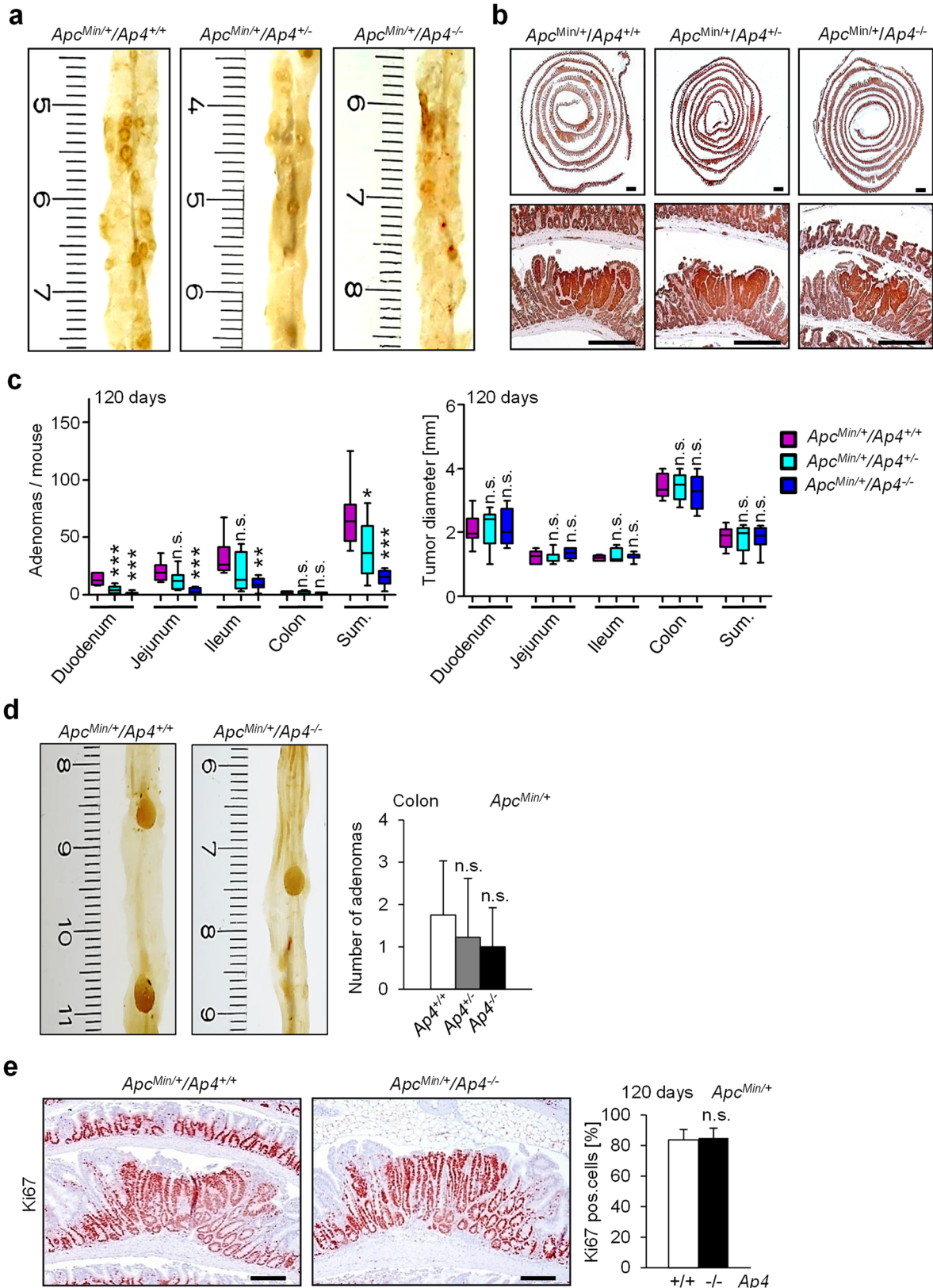


Figure 11 *Ap4* deletion decreases frequency but not size of adenomas in age-matched *Apc^{Min/+}* mice. **a** Macroscopic pathology of representative polyps in the small intestine (ileum) of 120 days old *Apc^{Min/+}* mice with the indicated genotype, scale in cm. **b** Representative sections through rolls of the small intestine were stained for β -catenin. Scale bar = 500 μ m

Results

(upper pictures) or 250 μm (lower pictures). **c** Quantification of adenoma number/mouse (left panel) and tumor diameter (right panel) in the intestine of 4 male and 4 female 120 days old $Apc^{Min/+}$ mice per genotype. The box extends from the 25th to 75th percentiles. The line in the middle of the box is plotted at the median. The whiskers represent the minimal and maximal values. **d** Left panel: Macroscopic pathology of representative polyps in the colon of 120 days old $Apc^{Min/+}$ mice with the indicated genotype, scale in cm. Right panel: Quantification of colonic adenomas of 120 days old $Apc^{Min/+}$ mice with the indicated genotype. **e** Left panel: Immunohistochemical detection of Ki67 in adenomas of 120 days old $Apc^{Min/+}$ mice of the indicated genotype. Scale bar = 100 μm . Counterstaining with hematoxylin. Right panel: Ki67-positive cells were counted in at least 9 adenomas derived from 1 male and 2 female mice per genotype. **c, d, e:** Results represent the mean \pm SD. Results were subjected to an unpaired, two tailed Student's *t*-test with p-values * < 0.05, ** < 0.01, *** < 0.001, n.s. = not significant.

The effects of *Ap4* loss on tumorigenesis observed in Apc^{Min} mice were independent of the gender (Figure 12a-c). When we analyzed Apc^{Min} mice with intestinal epithelial cell (IEC)-specific deletion of *Ap4*, which was achieved by crossing *Villin-Cre* with $Ap4^{fl/fl}$ mice, we obtained similar results as for Apc^{Min} mice with germ-line deletion of *Ap4*: i.e. in $Ap4^{\Delta IEC}/Apc^{Min}$ mice intestinal cancer-related death was significantly delayed by 110 days, with heterozygous mice showing an intermediate delay (Figure 13a). $Ap4^{\Delta IEC}/Apc^{Min}$ mice showed a 6-fold decrease in the number of adenomas in the small intestines of moribund and a 5-fold decrease in the small intestine of 120 days old Apc^{Min} mice, whereas the size of adenomas increases in moribund mice and the size of the adenomas was not affected in 120 days old mice (Figure 13b, c). Epithelial-specific deletion of *Ap4* in Apc^{Min} mice also resulted in a decreased number of adenomas in the colon, although this effect was not statistically significant (Figure 13d). Interestingly, deletion of *Ap4* in epithelial cells did not affect the proliferation rate of established adenomas of Apc^{Min} mice (Figure 13e). Therefore, the effects of *Ap4* deletion in the germ-line on adenoma formation are presumably intestinal epithelial cell-autonomous. Taken together, these results show that *Ap4* is rate limiting for adenoma initiation in Apc^{Min} mice. Since c-Myc is a required mediator of intestinal tumor formation in *Apc*-mediated tumorigenesis, the results imply a pivotal role of *Ap4* among the many known c-Myc target genes in mediating intestinal tumor formation.

Results

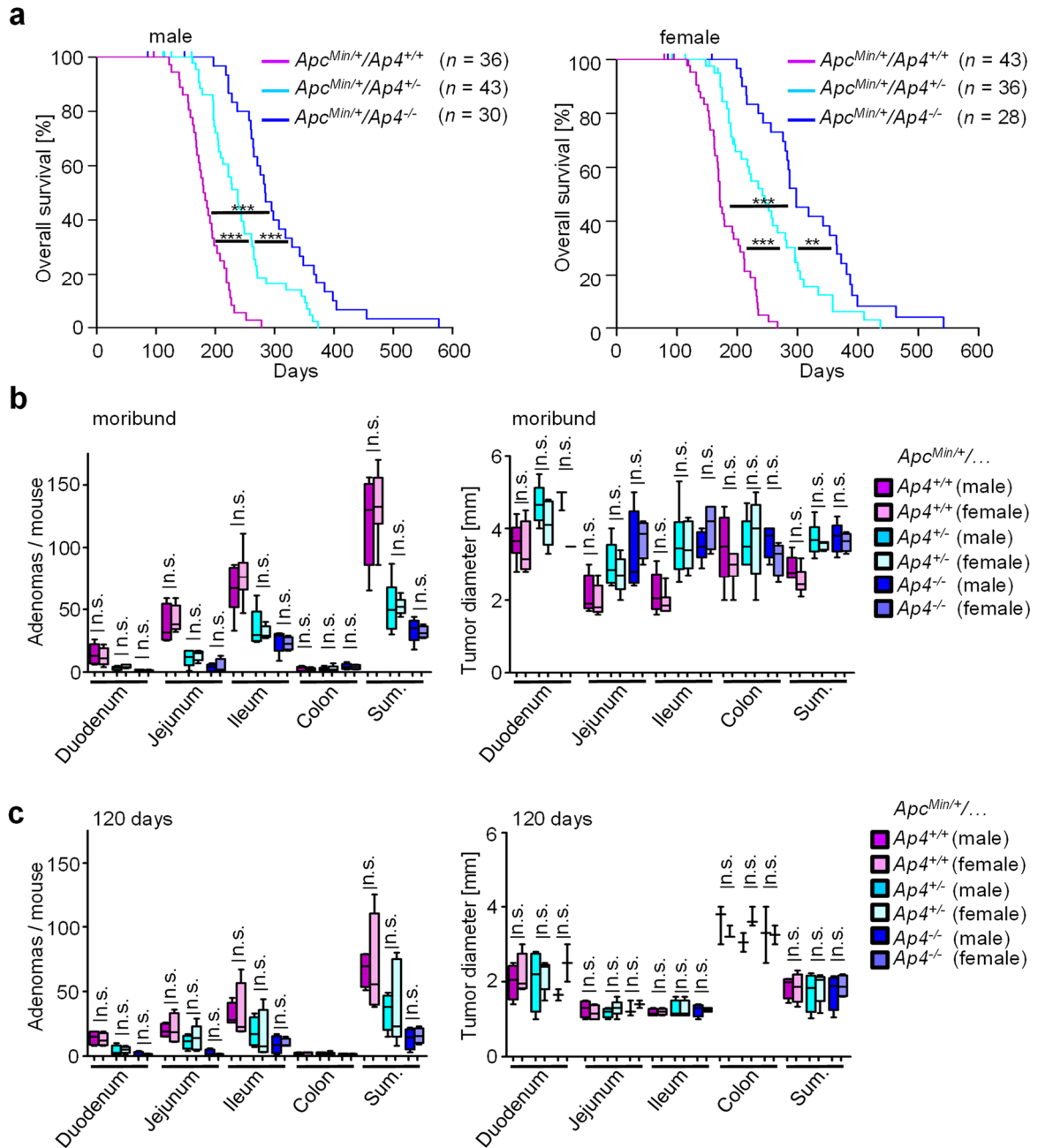
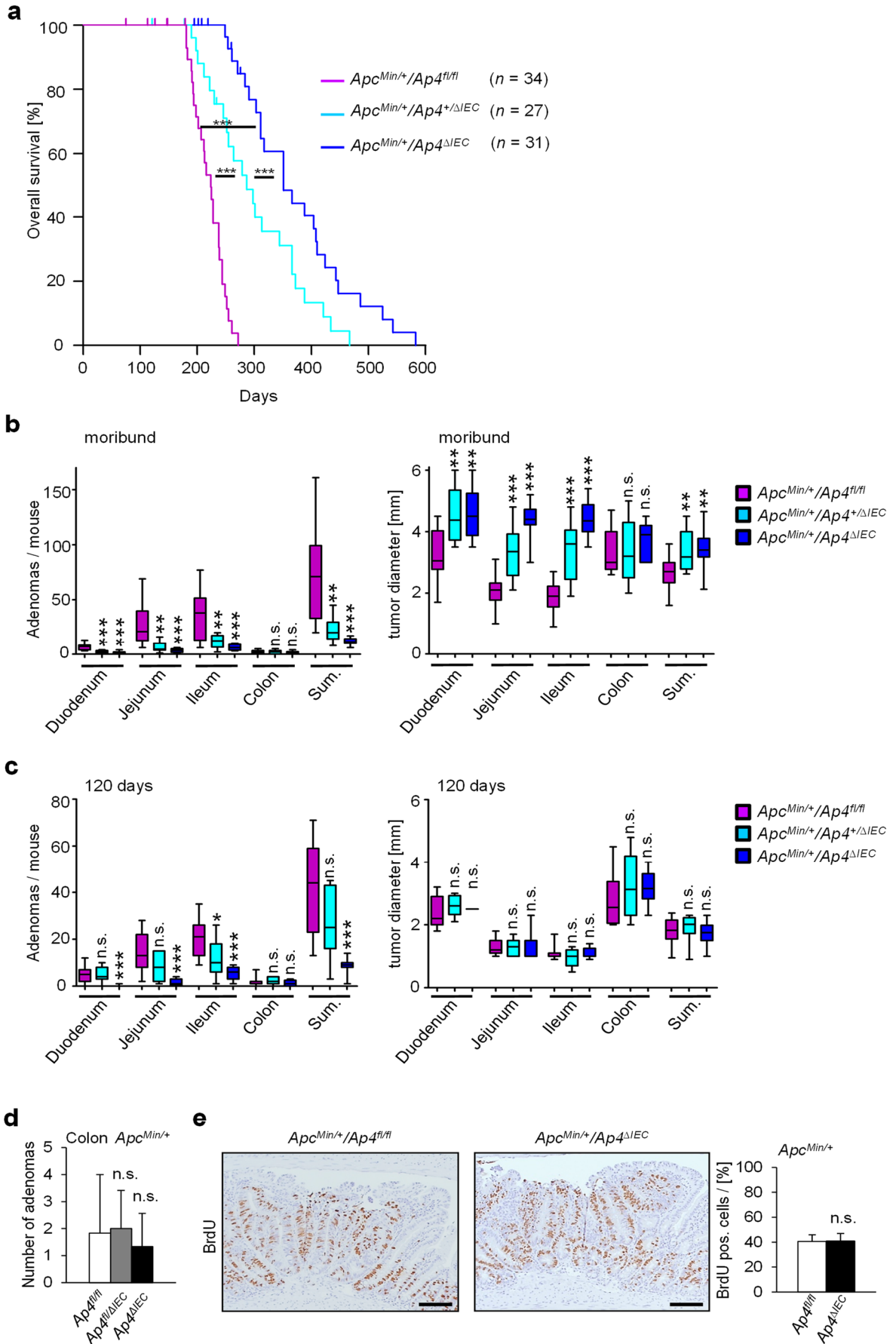


Figure 12 Effects of gender-specific deletion of *Ap4* on adenoma formation in *Apc^{Min/+}* mice. **a** Kaplan-Meier survival analysis of *Apc^{Min/+}* mice with the indicated genotypes. Male and female mice have been analyzed separately. Censored mice without intestinal tumor related death are indicated on the Kaplan-Meier curve as tick marks. **b** Quantification of adenoma number per mouse (left panel) and tumor diameter (right panel) in the intestine of 6 male and 6 female (*Apc^{Min/+}/Ap4^{+/+}*), 5 male and 5 female (*Apc^{Min/+}/Ap4^{+/-}*) or 4 male and 4 female (*Apc^{Min/+}/Ap4^{-/-}*) moribund *Apc^{Min/+}* mice. Male and female mice have been analyzed separately. The box extends from 25th to 75th percentile. The line in the middle of the box represents the median. The whiskers underneath or above the boxes depict the min. and max. value, respectively. **c** Enumeration of adenomas per mouse (left panel) and tumor diameter (right panel) in the intestine of 4 male and 4 female 120 days old *Apc^{Min/+}* mice per genotype as in (b). Male and female mice were analyzed separately. a: Results were subjected to a log rank test. b, c: Results represent the mean +/- SD with p-values * < 0.05, ** < 0.01, *** < 0.001, n.s. = not significant.

Results



Results

Figure 13 Effects of epithelial-specific deletion of *Ap4* on adenoma formation in *Apc^{Min/+}* mice. **a** Kaplan-Meier survival analysis of *Apc^{Min/+}* mice with the indicated genotypes. **b** Enumeration of adenomas/mouse (left panel) and tumor diameter (right panel) in the intestine of 7 male and 7 female (*Apc^{Min/+}/Ap4^{fl/fl}*) or 5 male and 5 female (*Apc^{Min/+}/Ap4^{+/-ΔIEC}*, *Apc^{Min/+}/Ap^{ΔIEC}*) moribund *Apc^{Min/+}* mice per genotype. **c** Enumeration of adenomas/mouse (left panel) and tumor diameter (right panel) in the intestine of 6 male and 6 female (*Apc^{Min/+}/Ap4^{fl/fl}*) or 4 male and 4 female (*Apc^{Min/+}/Ap4^{+/-ΔIEC}*, *Apc^{Min/+}/Ap^{ΔIEC}*) 120 days old *Apc^{Min/+}* mice per genotype. **d** Quantification of colonic adenomas of 120 days old *Apc^{Min/+}* mice with the indicated genotype. **e** Left panel: Immunohistochemical detection of BrdU incorporation in adenomas of 120 days old *Apc^{Min/+}* mice of the indicated genotype. Counterstaining with hematoxylin. Scale bar = 100 μm. Right Panel: Quantification of BrdU-positive cells in at least 9 adenomas of the ileum from 1 male and 2 female mice per genotype. **a**: Results were subjected to a log rank test. **b, c, d, e**: Results represent the mean +/- SD with p-values * < 0.05, ** < 0.01, *** < 0.001, n.s. = not significant.

5.2 mRNA expression profiling of *Ap4*-deficient adenomas

To identify pathways mediating the effects of *Ap4* we compared the mRNA expression profiles of intestinal adenomas that formed in *Apc^{Min}* mice with and without *Ap4* deletion. By applying next-generation sequencing (NGS) we identified 1459 mRNAs that were differentially regulated with a fold change in expression ≥ 1.5 ($p < 0.05$) due to deletion of *Ap4* (Figure 14a). Out of these, 954 mRNAs were significantly down-regulated, and 505 mRNAs were up-regulated in *Ap4*-deficient *Apc^{Min}* mice (Figure 14b, c). Notably, pathway analysis showed that mRNAs encoding for proteins involved in EMT (epithelial-mesenchymal transition), as well as cell-cycle regulatory proteins (e.g. E2f targets) were significantly enriched among the down-regulated mRNAs (Figure 14d, Supplemental Data 1).

Results

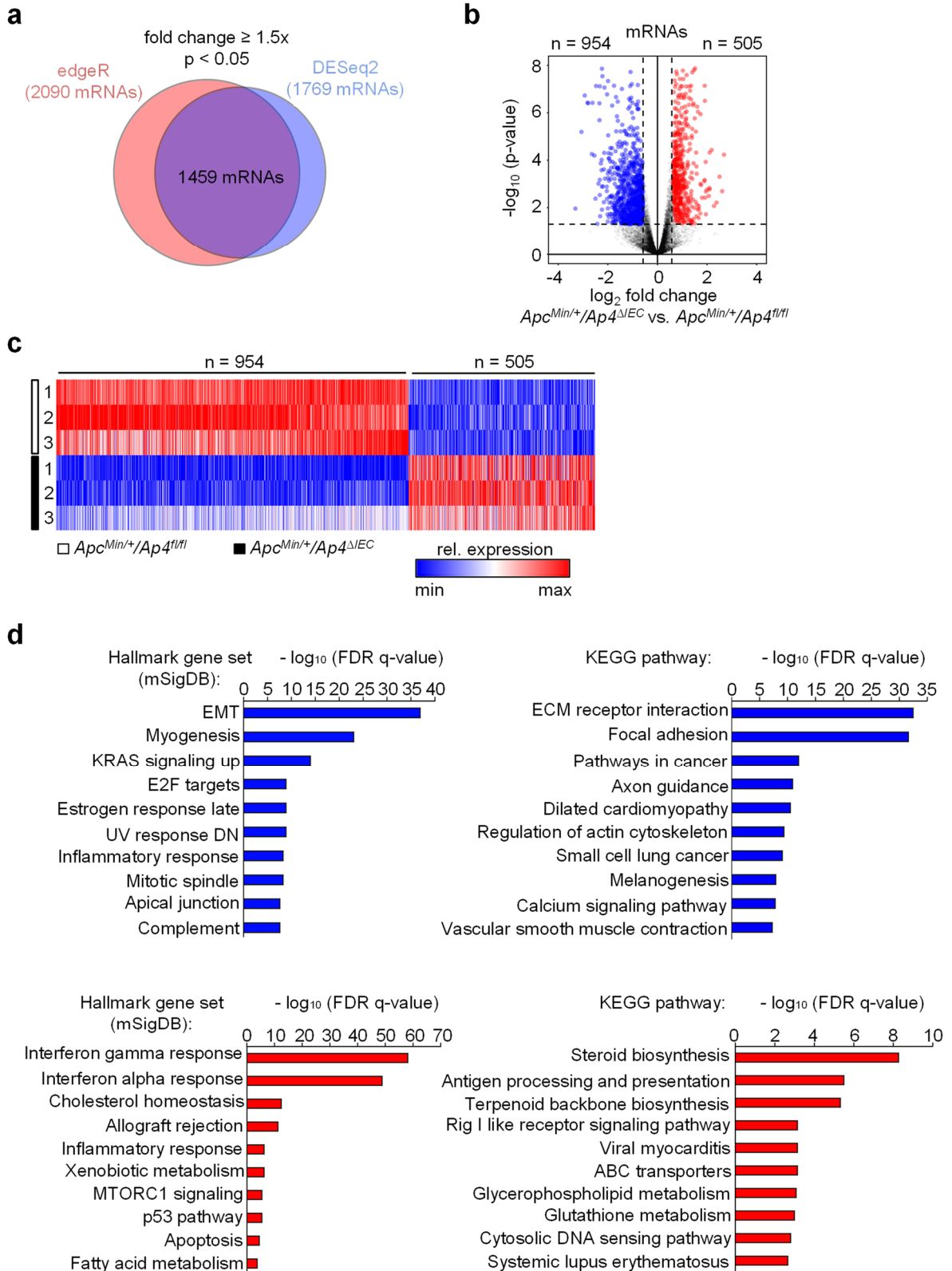


Figure 14 Expression analyses of *Ap4*-deficient adenomas from *Apc^{Min/+}* mice. **a Venn diagram displaying differentially regulated RNAs (fold change > 1.25 , $p < 0.05$) in *Ap4^{fl/fl}* and *Ap4^{ΔIEC}* *Apc^{Min/+}* adenomas as determined by edgeR and DESeq2. **b** Volcano plot depicting expression changes between *Apc^{Min/+}/Ap4^{fl/fl}* and *Apc^{Min/+}/Ap4^{ΔIEC}* tumors from 120 days old mice derived from 3 female mice (5 tumors per mouse) per genotype detected by RNA-Seq.**

Results

P-values are plotted against the \log_2 of the corresponding RNA expression changes in $Ap4^{\Delta IEC}$ versus $Ap4^{fl/fl}$ adenomas. Differentially expressed RNAs (p -value < 0.05) with a \log_2 fold change ≥ 0.58 are indicated in red, with a \log_2 fold change ≤ -0.58 are marked in blue. RNAs with $0.58 > \log_2$ fold change > -0.58 and/or with a p -value ≥ 0.05 are represented by grey dots. Dashed vertical lines indicate cut-offs for differential expression. Dashed horizontal line indicates the cut-off for adjusted p -values < 0.05 as determined with *DESeq2*. **c** Heat map depicting expression changes of differentially expressed mRNAs (fold change ≥ 1.5 and $p < 0.05$ as determined by *edgeR* and *DESeq2*) as relative expression levels normalized to the mean expression in the control, $Ap4^{Min/+}/Ap4^{fl/fl}$, samples for each indicated mRNA. Colors indicate relative expression values from minimum (blue) to maximum (red) for each RNA sample per differentially regulated mRNA. Three biological replicates per genotype were analyzed. **d** Upper panel: Hallmark gene set (mSigDB: molecular Signature Database (Liberzon et al., 2015)) and KEGG (Kyoto Encyclopedia of Genes and Genomes) analysis from down-regulated mRNAs after conditional ablation of *Ap4* in intestinal $Ap4^{Min/+}$ adenomas. The 10 most significantly enriched pathways among down-regulated mRNAs are shown. Lower panel: Hallmark gene set (mSigDB: molecular Signature Database) and KEGG (Kyoto Encyclopedia of Genes and Genomes) analysis from up-regulated mRNAs. The 10 most significantly enriched pathways among up-regulated mRNAs after conditional ablation of *Ap4* in intestinal $Ap4^{Min/+}$ adenomas are shown. See also Supplemental Data 1. All data analyses were performed by Dr. Markus Kaller.

Furthermore, Gene Set Enrichment Analysis (GSEA) showed that mRNAs characteristic for *Lgr5*-positive or *EphB2*^{high} ISCs (intestinal stem cells) (Merlos-Suarez et al., 2011; Munoz et al., 2012; van der Flier et al., 2009) were preferentially down-regulated in *Ap4*-deficient adenomas (Figure 15a, b). Moreover, mRNAs encoding for proteins involved in Wntless/Int-1(Wnt)/ β -catenin and Notch signaling, which control the homeostasis of ISCs (Beumer and Clevers, 2016; Sancho et al., 2004), were also preferentially down-regulated in *Ap4*-deficient adenomas (Figure 15a, b, Supplemental Data 2). Genes down-regulated upon deletion of *Ap4* included ISC markers induced by Wnt/ β -catenin signaling, such as *Lgr5* and *Ascl2* (Barker et al., 2007; de Lau et al., 2011; Van der Flier et al., 2007), or by Notch signaling, such as *Olfm4* (VanDussen et al., 2012), as well as additional direct Wnt/ β -catenin and/or Notch target genes with critical functions in the Wnt and Notch signaling pathways, such as *Sox4*, *Tcf7/Tcf1*, *Axin2*, *EphB3*, *Jag1*, *Jag2*, *Hes1* and *c-Myc* (Figure 15b). Furthermore, *Notch1* itself was down-regulated in *Ap4*-deficient adenomas. Taken together, these results imply that *Ap4* regulates the homeostasis of ISCs via activating Wnt/ β -catenin and/or Notch signaling pathways.

Recently, *Ap4* was shown to maintain a c-Myc-induced transcriptional program in activated T-cells (Chou et al., 2014) and germinal center B-cells (Chou et al., 2016). In line with these findings, c-Myc target genes were preferentially down-regulated in *Ap4*-deficient adenomas (Figure 15a; Supplemental Data 2). However, the changes in

Results

expression of c-Myc target genes observed after deletion of *Ap4* were rather modest compared to the regulations observed in ISC signature or Notch signaling components (Figure 15c). Likewise, E2f targets, though significantly enriched among the down-regulated RNAs (Figure 15a), displayed only modest changes in expression that were comparable to those of c-Myc targets (Figure 15c). These modest regulations of c-Myc and E2f targets may explain the lacking influence of *Ap4*-deletion on cell proliferation within adenomas. Also mRNAs involved in EMT were preferentially down-regulated in *Ap4*-deficient adenomas (Figure 15a), which matches our previous study about the role of AP4 in EMT in human colorectal cancer (CRC) cell lines (Jackstadt et al., 2013c). We exemplarily confirmed the differential regulation detected by NGS using qPCR. Thereby, we validated the down-regulation of the stem cell markers *Smoc2*, *Lgr5* and *Olfm4*, as well as the repression of several genes involved in the Wnt/ β -catenin signaling and/or Notch signaling in *Ap4*-deficient adenomas (Figure 15d). Consistent with its previously reported repression by AP4 (Jung et al., 2008), *Cdkn1a/p21* was up-regulated in *Ap4*-deficient adenomas. Interestingly, we did not detect a change in mRNA or protein levels of *Ctnnb1* (β -catenin) in *Apc^{Min}* adenomas (Figure 15d, e), suggesting that Ap4 directly regulates Wnt/ β -catenin target genes.

Results

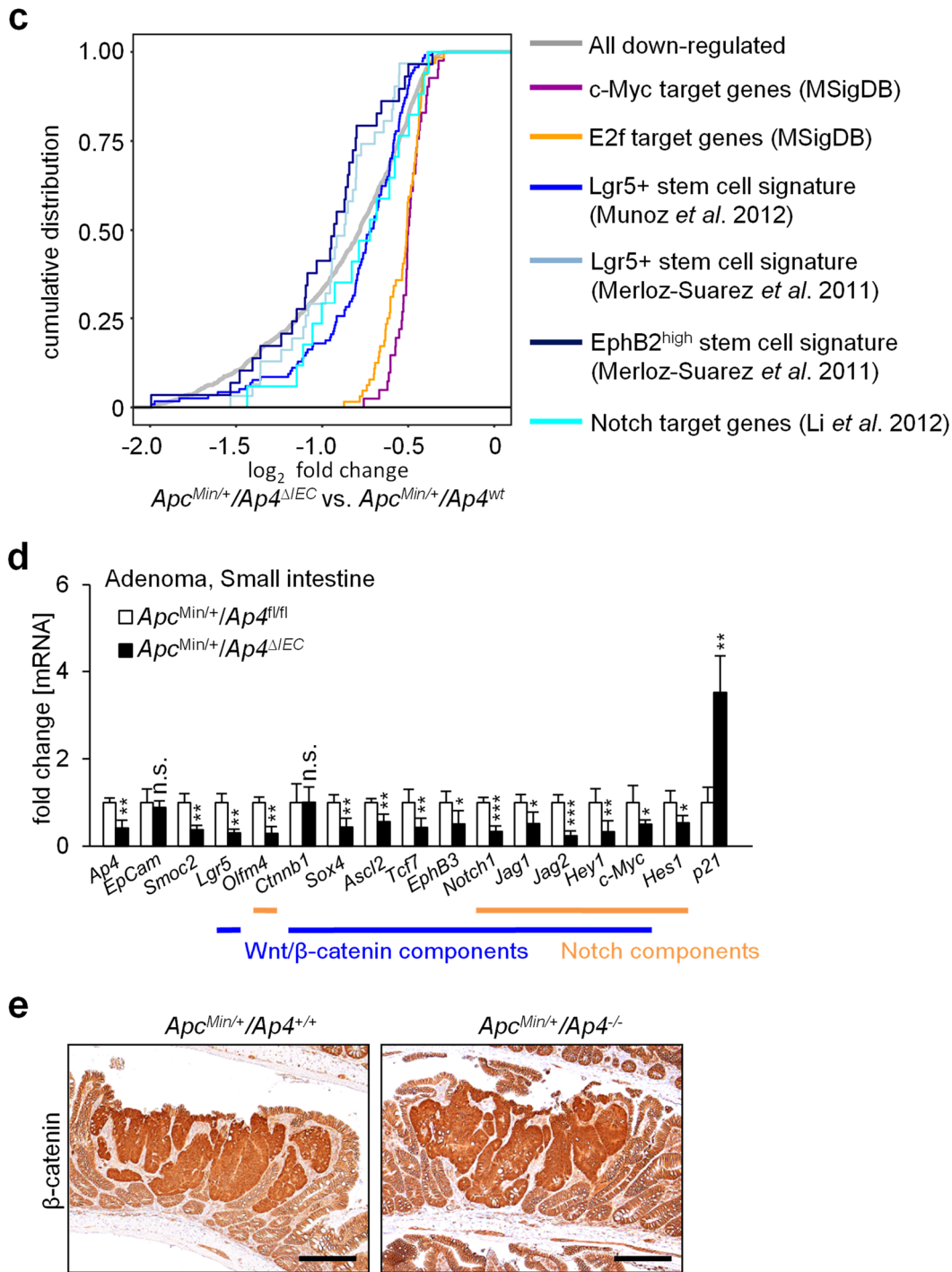


Figure 15 *Ap4*-dependent expression profiles in *Apc^{Min/+}* adenomas. **a** GSEA comparing gene expression profiles from *Apc^{Min/+}/Ap4^{fl/fl}* and *Apc^{Min/+}/Ap4^{ΔIEC}* adenomas from 120 days old mice with Lgr5-positive or EphB2^{high} stem cell signatures (Munoz *et al.*, 2012) (Merloz-Suarez *et al.*, 2011; van der Flier *et al.*, 2009), Wnt/β-catenin signaling (mSigDB: molecular Signatures Database), mRNAs significantly enriched genes down-regulated mRNAs in β-catenin-knock-out crypts which overlap with genes characteristic for other stem cell populations and intestinal tumors (Fevr *et al.*, 2007), β-catenin target genes differentially regulated after *Ctnnb1* loss (Fevr *et al.*, 2007), Notch target genes (Li *et al.*, 2012), c-Myc target genes (mSigDB), E2f target genes (mSigDB) and hallmark EMT (mSigDB). NES: Normalized Enrichment Score, Nom. P-value: Nominal p-value. **b** Heatmap of selected differentially expressed mRNAs (p-value < 0.05) from intestinal stem cell gene signatures, Wnt/β-catenin signaling and/or Notch signaling

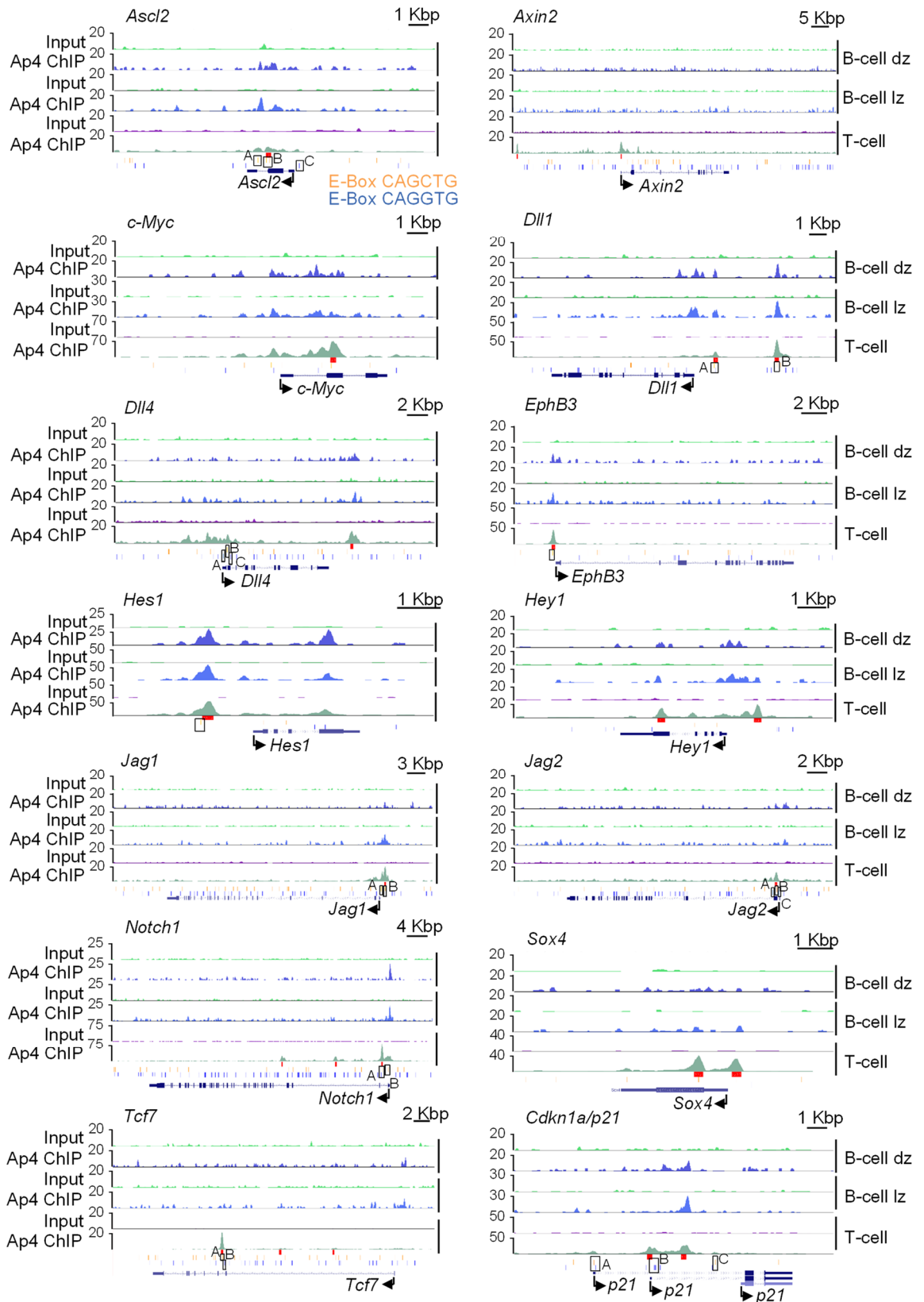
Results

gene signatures analyzed in (a). The heatmap displays relative fold changes in expression levels normalized to the mean expression in the control, *Apc^{Min/+}/Ap4^{fl/fl}*, samples for each indicated mRNA. Three biological replicates per genotype were analyzed. **c** Cumulative distribution plots comparing RNA expression changes as determined by DESeq2 of gene set members of the indicated gene signatures upon loss of AP4 in *Apc^{Min/+}* - induced adenomas. **d** qPCR analysis of the indicated *mRNA* derived from tumors from 3 female mice (5 tumors per mouse) per genotype. **e** Immunohistochemical detection of β -catenin in adenomas of 120 days old *Apc^{Min/+}* mice of the indicated genotype. Scale bar = 100 μ m. Counterstaining with hematoxylin. At least 16 adenomas from 2 male and 2 female mice per genotype were stained. d: Results represent the mean \pm SD. Results were subjected to an unpaired, two tailed Student's *t*-test with p-values * < 0.05, ** < 0.01, *** < 0.001, n.s. = not significant. a, b: See also Supplemental Data 2. a, b, c: Figures and analyses were made by Dr. Markus Kaller.

Next, we analyzed whether Ap4 directly regulates the expression of ISC markers and components of the Wnt/ β -catenin and/or Notch signaling pathways. Our analysis of Ap4 DNA binding patterns in murine T and B cells (Chou et al., 2014; Chou et al., 2016) revealed Ap4 occupancy within the promoter regions of *Ascl2*, *Axin2*, *c-Myc*, *Dll1*, *Dll4*, *EphB3*, *Hes1*, *Hey1*, *Jag1*, *Jag2*, *Notch1*, *Sox4*, and *Tcf7* (Figure 16a). We performed quantitative chromatin-immunoprecipitation (qChIP) analysis to confirm Ap4 occupancy in the murine CRC cell line CT26 at the promoters of the following genes: *Ascl2*, *Dll1*, *Dll4*, *EphB3*, *Hes1*, *Jag1*, *Jag2*, *Notch1*, *Sox4*, and *Tcf7* (Figure 16b). Similar to the promoter of human *CDKN1A/P21*, the murine *Cdkn1a/p21* promoter also contains Ap4 binding sites that showed occupancy by Ap4 (Figure 16b). Therefore, *Cdkn1a/p21* is a conserved, direct Ap4 target. Taken together, these results suggest that the differential regulation of genes involved in Wnt/ β -catenin and/or Notch signaling observed in Ap4-deficient *Apc^{Min}* adenomas is a direct consequence of the absence of Ap4 at the respective promoters.

Results

a



Results

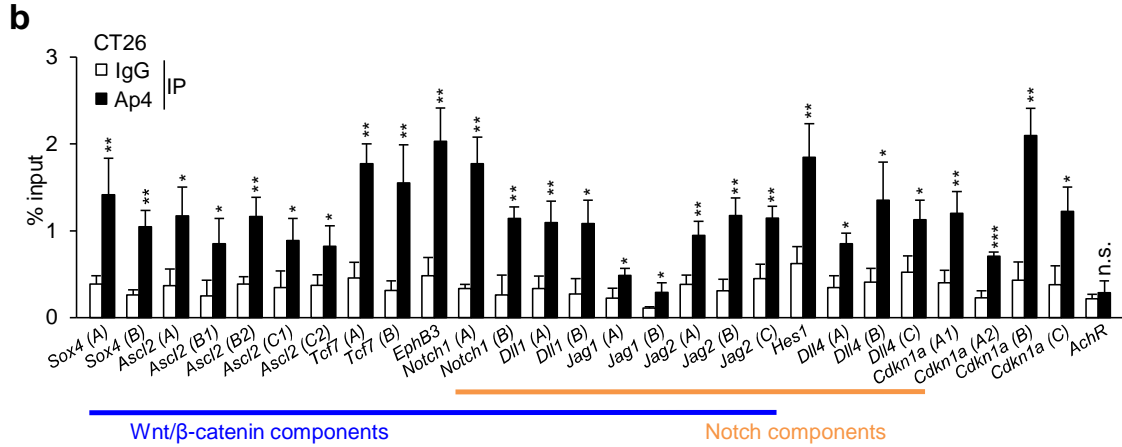


Figure 16 Ap4 binding to promoters of selected genes. **a** BedGraph histogram plots showing examples of occupancy by Ap4 within promoters of genes involved in Wnt/β-catenin and/or Notch pathways in murine T-cells and/or B-cells according to previously published ChIP-Seq analysis (Chou et al., 2014; Chou et al., 2016). The following datasets deposited at <https://www.ncbi.nlm.nih.gov/geo/> were used: GSM1400434, GSM1400430 (T-cells) and GSM2132680, GSM2132681, GSM2132682, GSM2132683 (B cells). Orange and blue vertical bars denote the genomic positions of CAGCTG and CAGGTG E-boxes, respectively. Red boxes indicate genomic coordinates of high confidence Ap4 peaks ($p < 1e-10$) identified with Homer (Hypergeometric Optimization of Motif EnRichment) (Heinz et al., 2010). Numbers on the y-axis indicate read-numbers as determined by ChIP-Seq analysis. Gene structures are indicated schematically with exons represented by thick rectangles. E-Boxes used for qChIP analysis in (b) are marked. Lz: light zone, dz: dark zone. **b** The murine CRC cells CT26 were subjected to qChIP analysis with Ap4 or IgG specific antibodies for ChIP. The mouse *acetylcholine receptor* (*AchR*) promoter, which lacks Ap4-binding motifs, served as a negative control. E-Boxes used for qChIP analysis are marked in (a). **b**: Results were subjected to an unpaired, two tailed Student's *t*-test with p-values * < 0.05 , ** < 0.01 , *** < 0.001 , n.s. = not significant. **a**: Figures and analyses were made by Dr. Markus Kaller.

5.3 Analysis of tumor organoids from *Ap4*-deficient *Apc^{Min}* mice

Our NGS results suggested that Ap4 is involved in maintaining a stem cell like expression pattern in tumor cells. This was confirmed by *in situ* hybridization with a probe detecting the mRNA expression of *Lgr5* or *Smoc2* in small intestinal adenomas of *Apc^{Min}* mice (Figure 17a). Indeed, *Ap4*-deficient adenomas displayed less cells positive for *Lgr5* or *Smoc2* mRNA expression when compared to adenomas expressing *Ap4*. Therefore, the number of tumor stem cells is presumably decreased in the absence of Ap4. Next, we generated tumor organoids using single cells derived from adenomas of *Apc^{Min}* mice. Indeed, cells directly isolated from *Ap4*-deficient adenomas formed tumor organoids *ex vivo* with a significantly lower frequency than those derived from *Ap4* wild-type adenomas (Figure 17b). However, after the first passage *ex vivo* the *Ap4*-deficient and proficient tumoroids re-built new tumor organoids with a comparable frequency and growth rate (Figure 17b). Therefore, Ap4

Results

appears to be required for the initiation, but not for the maintenance of *ex vivo* cultured intestinal tumoroids. The deletion of *Ap4* in these tumor organoids was accompanied by lower levels of the ISC markers *Smoc2*, *Lgr5* and *Olfm4* when compared to *Ap4* wild-type adenomas (Figure 17c). Additional genes involved in Wnt/ β -catenin signaling and/or Notch signaling, including *Notch1* itself, were also down-regulated in *Ap4*-deficient tumor organoids (Figure 17d). Also, at the protein level the cleaved, active form of Notch1 (Ncd1) and Hes1, which is encoded by a Notch target gene, were decreased in *Ap4*-deficient tumor organoids indicating a decrease in Notch signaling (Figure 17e). Therefore, the reduced *de novo* tumor organoid formation capacity may be caused by the down-regulation of genes required for *in vivo* ISC function upon *Ap4* loss.

Results

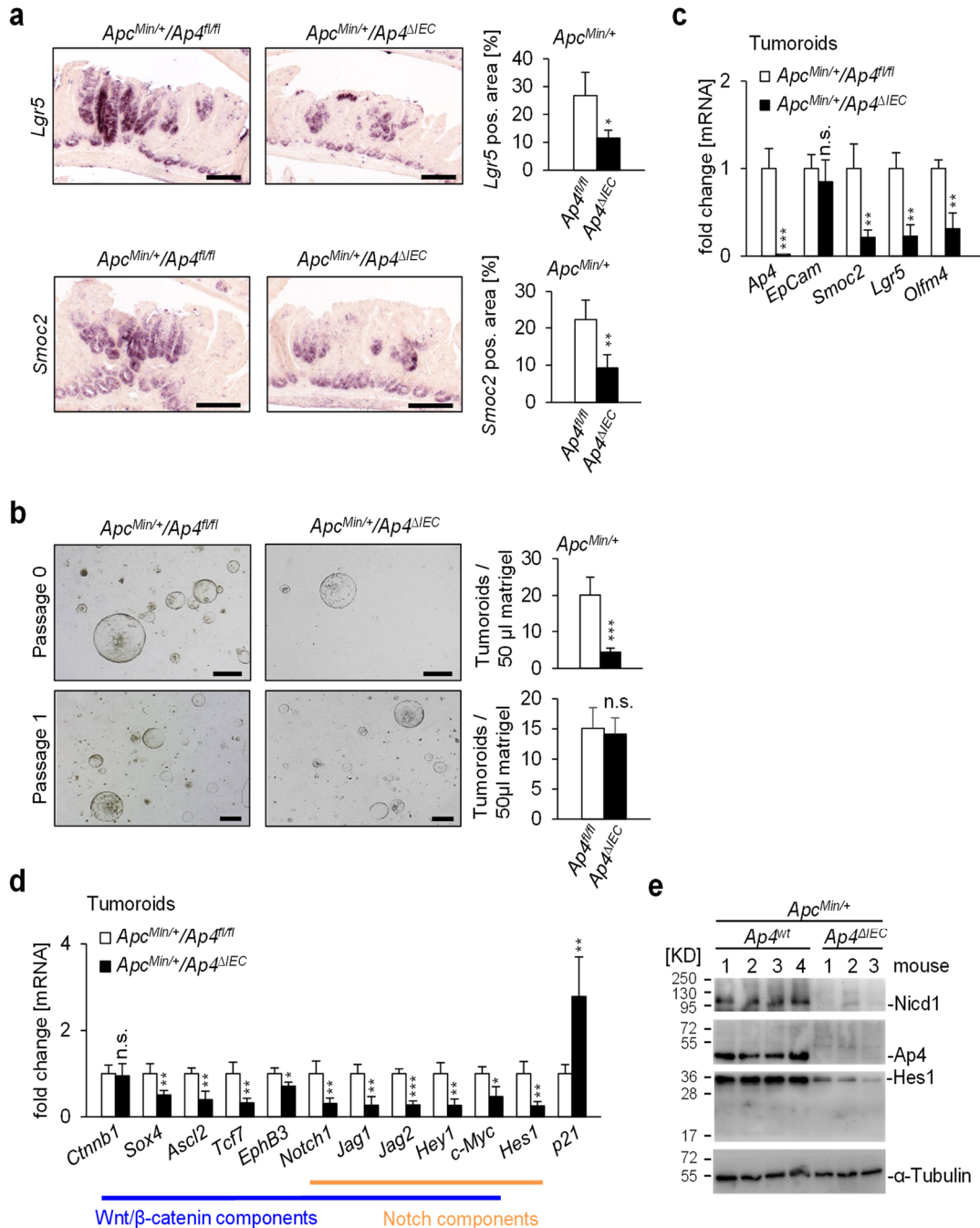


Figure 17 Deletion of *Ap4* decreases stemness in adenomas and tumor organoids. **a** Left panel: *In situ* hybridization of *Lgr5* or *Smoc2* mRNA. Scale bars represent 100 μ m. Right panel: Quantification of *Lgr5*-positive or *Smoc2*-positive area in percent (%) in the adenomas from 2 male and 1 female mice in at least 6 adenomas per genotype. **b** Left panel: representative pictures of small intestinal tumor organoids 6 days after isolation (passage 0), upper pictures, or 4 days after passaging (passage 1), lower pictures. Organoids were isolated from 3 tumors per mouse from 2 female and 2 male mice per genotype. Scale bars represent 500 μ m. right panels: number of tumor organoids per drop of 50 μ l matrigel. A total of 24 drops (passage 0) or 15 drops (passage 1) was analyzed per genotype. **c**, **d** qPCR analysis of the indicated mRNA derived from tumor organoids. **e** Western blot analysis of the indicated proteins. Uncropped Western blot membranes are shown in Supplemental Data 3. a, b, c, d: Results represent the mean \pm SD. Results were subjected to an unpaired, two tailed Student's *t*-test with p-values * < 0.05, ** < 0.01, *** < 0.001, n.s. = not significant.

Results

Subsequently, we isolated small intestinal crypts from *Lgr5-Cre^{ERT2}/Apc^{fl/fl}* and *Lgr5-Cre^{ERT2}/Apc^{fl/fl}/Ap4^{fl/fl}* mice. After plating of crypts in matrigel overlaid with ENR media (containing EGF, Noggin and RSPO1) we acutely deleted *Apc* or *Apc* in combination with *Ap4* in *Lgr5*-positive stem cells of newly formed intestinal organoids by addition of 4-hydroxy-tamoxifen (4-OHT). After passaging (passage 1) and seeding the same amount of cells per drop of matrigel we switched culture conditions to EN media devoid of RSPO1, in which only *Apc*-deficient tumoroids can grow. We obtained less *de novo* formed tumoroids after *Ap4* deletion when compared to *Ap4*-proficient tumoroids (Figure 18a, b). This supports the notion that *Ap4* has an important role during tumor initiation and confirms the result we previously obtained *in vivo*. Reassuringly, tumoroids did not form in the absence of RSPO1 and 4-OHT (Figure 18a). During serial passaging the amount and size of tumoroids was not influenced by the deletion of *Ap4* (Figure 18a, b, c). To exclude the possibility that *Ap4*-deficient tumoroids grew due to incomplete deletion of *Ap4*, the complete deletion of *Ap4* was confirmed by genomic PCR (Figure 18d). Taken together, these results confirm a critical role of *Ap4* in the initiation, but not for the maintenance of the tumoroids. These results are in line with the observations initially obtained with *Apc^{Min}* mice, where *Ap4* loss decreased the number of adenomas but not their size.

Results

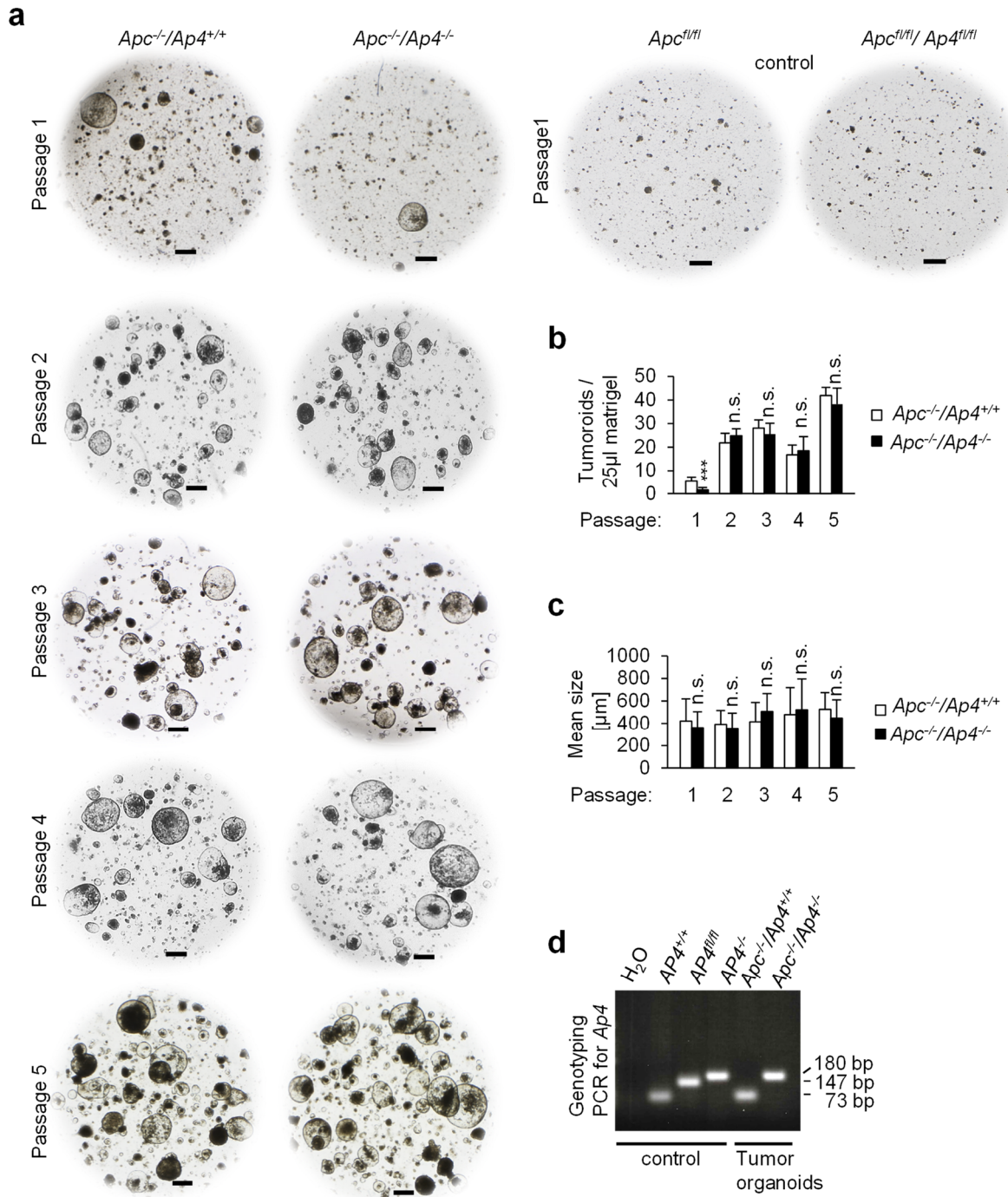


Figure 18 Deletion of *Ap4* is not important for the maintenance of tumors.

a Representative pictures of tumor organoids derived from small intestinal epithelial cells obtained from *Lgr5-CreERT2*^{+/+}/*Apc*^{fl/fl} and *Lgr5-CreERT2*^{+/+}/*Apc*^{fl/fl}/*Ap4*^{fl/fl} mice after treatment with 4-OHT. After isolation organoids were kept in ENR Media (contains EGF, Noggin and RSPO1). 48 hours after isolation organoids were treated with 4-OHT in a concentration of 100 nM for 48 hours to delete *Apc* or *Apc* in addition to *Ap4* in *Lgr5*-positive intestinal stem cells (ISC). Additional 48 hours later organoids were passaged and EN media (containing EGF and Noggin, but without RSPO-1) was used, which selectively allowed *Apc*-deficient tumoroids to expand (passage 1-5). Pictures were taken 7 days after passaging in case of passage 1, 4 days after passaging for passage 2 and 6 days after passaging for both passage 3, 4, and 5. **b** Mean tumor organoid number per drop of 25 µl matrigel calculated as a mean of a total of 20

Results

drops for passage 1 and passage 3-5 or a total of 11 drops (*Ap4* wt) and 6 drops (*Ap4* ko) for passage 2. **c** Mean tumor organoid size was measured and calculated from matrigel drops as depicted exemplarily in (b). **d** Analysis of *Ap4* status of tumoroids by genomic PCR at passage 4. b, c: Results were subjected to an unpaired, two tailed Student's *t*-test with p-values * < 0.05, ** < 0.01, *** < 0.001, n.s. = not significant.

5.4 *Ap4* regulates the homeostasis of intestinal stem cells

Next, we analyzed the expression of *Ap4* and the effect of *Ap4* deletion in the normal, murine intestine. *Ap4* protein was detected at the crypt base and in transient amplifying (TA) cells located above the crypt base in the small intestine (Figure 19a, left panel). As expected, *Ap4* expression was not detectable in the intestinal epithelia of *Ap4* knock-out mice, indicating that the antibody used here is specific for *Ap4* (Figure 19a, right panel). In mice expressing enhanced green fluorescent protein (eGFP) from an *Lgr5*-promoter *Ap4* expression was detected in eGFP-positive ISCs and TA cells, but not in the adjacent Lysozyme-positive Paneth cells (Figure 19b). In *Ap4*-deficient mice the number of eGFP-positive ISCs was significantly decreased, indicating that *Ap4* is necessary for ISC maintenance (Figure 19c). Notably, *Ap4*-deficient mice displayed a significant decrease in the number of ISCs positive for *Olfm4* mRNA expression (Figure 19d).

Results

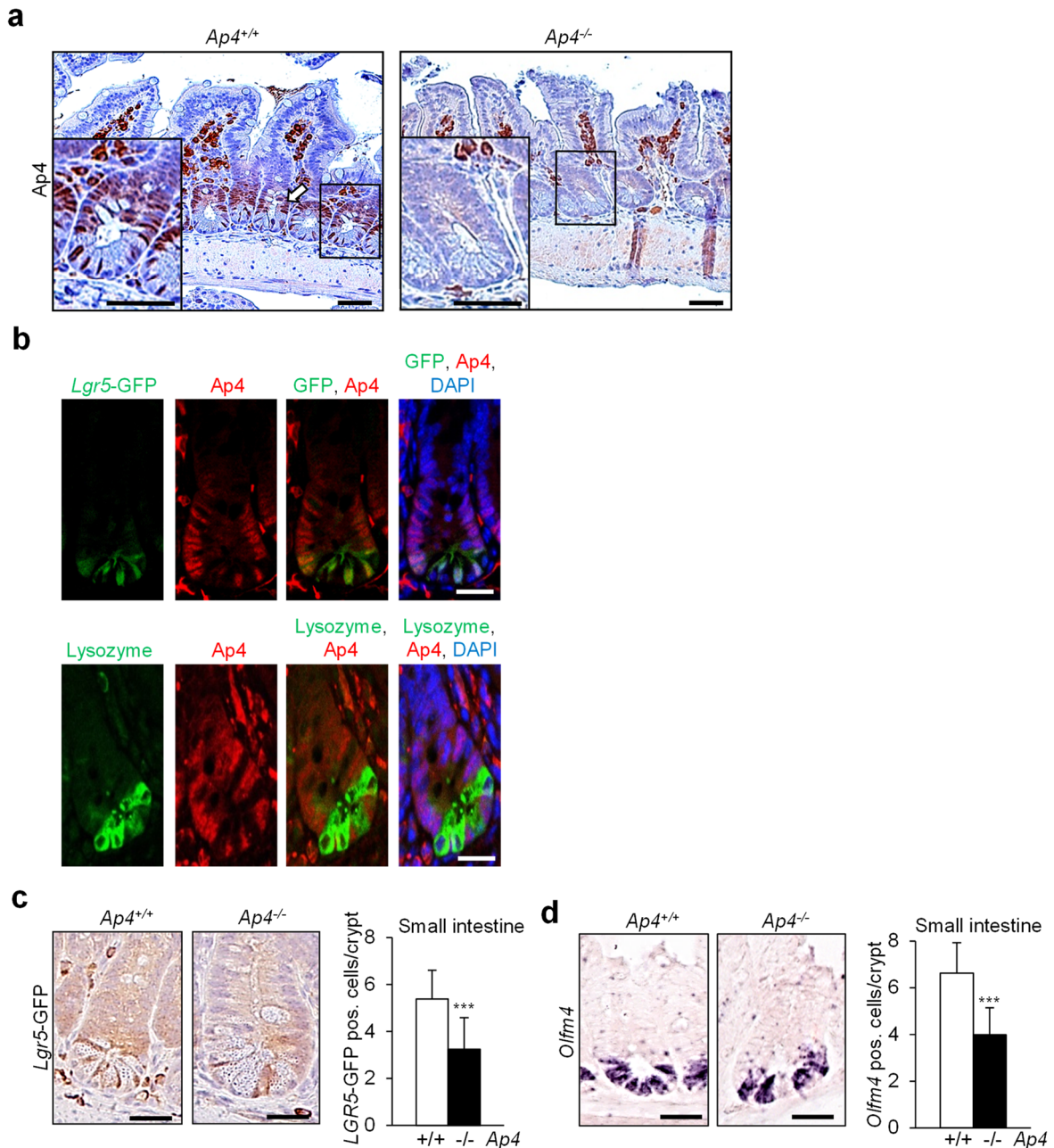
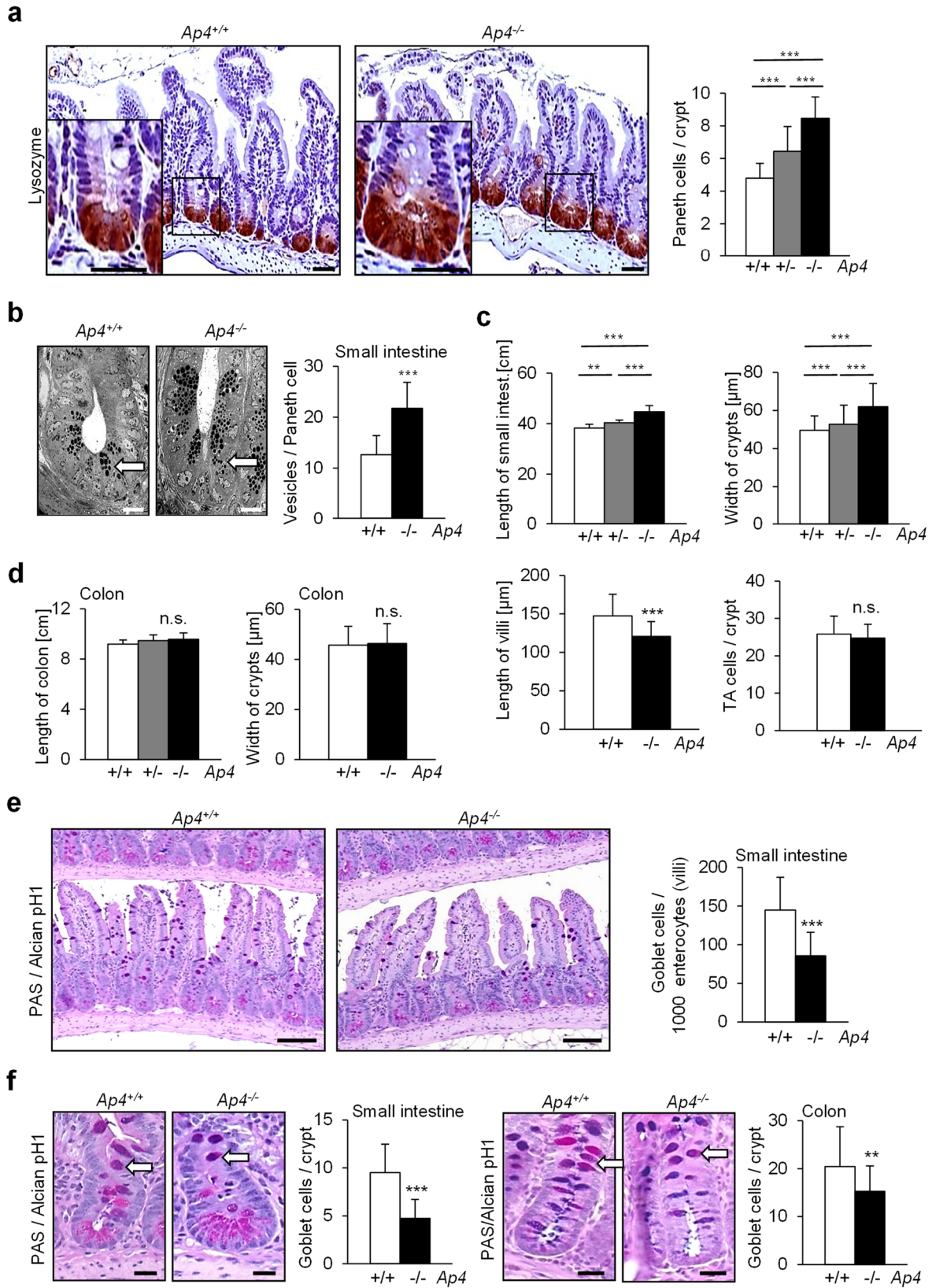


Figure 19 Inactivation of *Ap4* causes decrease of ISC numbers. **a** Immunohistochemical detection of Ap4 (brown) in small intestinal tissue, ileum of 1 male and 1 female mouse per genotype. Scale bar = 50 μ m (25 μ m insert), white arrow: site of specific Ap4 expression. Mast cells in the villi display an unspecific staining. Counterstaining with hematoxylin. **b** Confocal immunofluorescence analysis of Ap4, GFP = *Lgr5* (top panel) and Ap4, Lysozyme (bottom panel) expression in intestinal (ileum) mucosa of 63 days old *Lgr5-eGFP* mice (Barker et al., 2007). Nuclear DNA was stained with DAPI. Scale bars represent 25 μ m. **c** Left panel: Immuno-histochemical analyses of *Lgr5-eGFP* in intestinal sections of 63 days old *Lgr5-eGFP* mice. Scale bars represent 25 μ m. Right panel: *Lgr5-eGFP* positive cells in the crypt base of the ileum from 2 male and 2 female mice (130 crypts) per genotype. **d** Left panel: *In situ* hybridization of *Olfm4* mRNA. Scale bars represent 25 μ m. Right panel: *Olfm4* positive cells in the crypt base from 2 male and 2 female mice (316 crypts) per genotype. **c, d**: Results were subjected to an unpaired, two tailed Student's *t*-test with p-values * < 0.05, ** < 0.01, *** < 0.001, n.s. = not significant. **b**: Stainings were performed by Ursula Götze; pictures were taken by Dr. Rene Jackstadt.

Results

Furthermore, they showed an increased number of Paneth cells in all regions of the small intestine (Figure 20a): in the ileum each crypt section contained ~8 Paneth cells compared to ~5 Paneth cells in wild-type mice. As determined by electron microscopy, Paneth cells of *Ap4*-deficient mice also displayed an increased number of vesicles, which contain antimicrobial proteins, such as Lysozyme and Cryptdin (Figure 20b). The length of the small intestine was increased in *Ap4*-deficient mice, presumably as a result of widened crypt bases (Figure 20c). The length of the villi in the ileum was slightly decreased when compared to wild-type mice (Figure 20c). However, the number of TA cells in small intestinal crypts (Figure 20c), the length of the colon and the width of colonic crypts remained unchanged (Figure 20d). The latter presumably due to the absence of classical Paneth cells in the colon. *Ap4*-deficiency also resulted in a decreased number of secretory goblet cells in villi of the small intestine (Figure 20e) and in crypts of the small intestine and colon (Figure 20f). Accordingly, mRNA expression of stem cell markers (*Smoc2*, *Lgr5*, *Olfm4*) and the goblet cell markers (*Gob5*, *Muc2*) was significantly decreased, whereas Paneth cell markers (*Lysozyme*, *Cryptdin*) were significantly increased in the epithelia of the small intestine of *Ap4*-deficient mice (Figure 20g). We did not detect an effect of *Ap4*-deletion on the rate of apoptosis or proliferation in the small intestine (Figure 20h, i). Therefore, these processes did presumably not cause the changes in the numbers of Paneth cells, goblet cells and ISCs observed in *Ap4*-deficient mice. In addition, the effects of *Ap4* deletion described here were independent of the gender of the mice (Figure 20j, k).

Results



Results

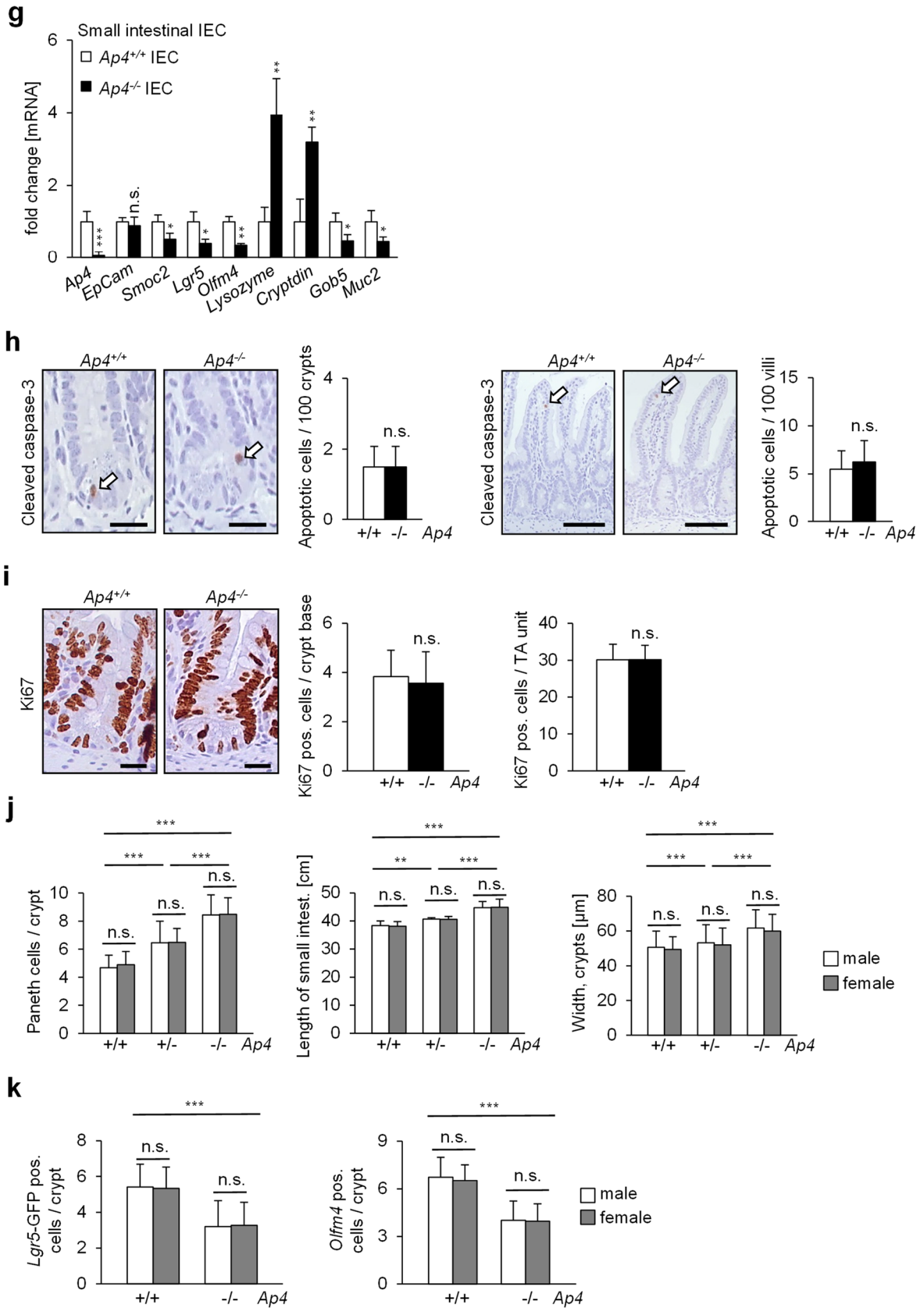


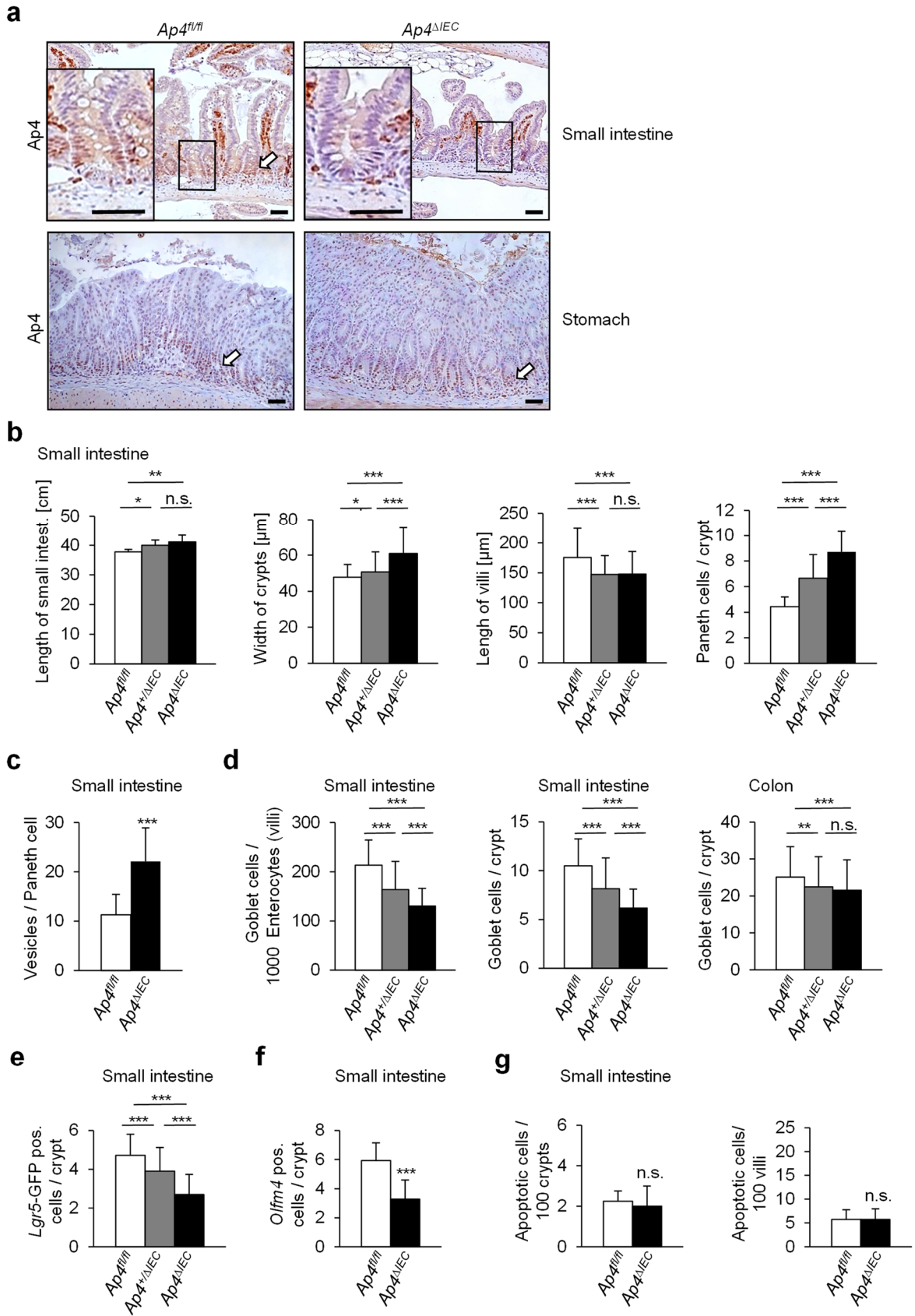
Figure 20 Effects of *Ap4*-deletion on the small intestine and the colon. a Left: Immunohistochemical detection of Lysozyme (brown) expressed in Paneth cells. Counterstaining with hematoxylin. Scale bar: 50 µm (25 µm insert). **Right:** The small

Results

intestine/ileum from 2 male and 2 female mice (100 crypts) per genotype was analyzed for Paneth cells per crypt. **b** Electron microscopic analysis of small intestinal crypt base; white arrow: Paneth cells. Scale bar: 25 μ m. **c** Analysis of small intestine/ileum for length of small intestine from 4 male and 4 female mice per genotype, width of crypts of the ileum from 2 male and 2 female mice (260 crypts) per genotype, length of villi from 2 male and 2 female mice (100 villi) per genotype and the number of TA cells per crypt from 2 male and 2 female mice (160 crypts) per genotype. **d** The colon was analyzed for the length of colon from 4 male and 4 female mice per genotype or for the width of crypts from 2 male and 2 female mice in a total of 200 crypts per genotype. **e** Left panel: The ileum of 63 days old mice was stained with periodic acid-Schiff (PAS)/Alcian Blue (pH1.0) and counterstained with hematoxylin. Scale bar = 100 μ m. Right panel: Goblet cells were counted in ileum of 2 male and 2 female mice (225 villi) per genotype. **f** Goblet cells in the ileum or colon were detected by PAS/Alcian Blue (pH1) staining. Counterstaining with hematoxylin. Goblet cells in the crypts (indicated by a white arrow) were counted from 2 male and 2 female mice (125 crypts) per genotype. Scale bar: 25 μ m. **g** qPCR analysis of the indicated *mRNAs* in IECs of the ileum of 2 male and 1 female mice per genotype. **h** Immunohistochemical detection of cleaved caspase-3 in small intestinal (ileum) crypts or villi from mice of the indicated genotype. Left panel: scale bar = 25 μ m. Right panel: scale bar = 100 μ m. Counterstaining with hematoxylin. 200 crypts or villi of the ileum from 2 male and 2 female mice per genotype were analyzed for cleaved caspase-3 positive cells. **i** Left panel: Immunohistochemical detection of Ki67 of the ileum of mice of the indicated genotype, scale bar = 25 μ m. Counterstaining with hematoxylin. Right panel: Quantification of Ki67-positive cells per crypt base or TA unit in 2 male and 2 female mice and a total of 102 crypts per genotype. **j** Left panel: Number of Paneth cells in the ileum divided into gender: 2 male and 2 female mice per genotype (50 crypts per gender and genotype). Central panel: length of small intestine divided into gender: 4 male and 4 female mice per genotype. Right panel: width of crypts of the ileum divided into gender: 2 male and 2 female mice per genotype (140 crypts per gender and genotype). **k** Left panel: Quantification of *Lgr5*-eGFP-positive cells in the crypt base of the ileum detected in 2 male and 2 female mice per genotype (65 crypts per gender and genotype). Right panel: Quantification of *Olfm4*-positive cells in the crypt base of the ileum in 2 male and 2 female mice per genotype (158 crypts per gender and genotype). a, b, c, d, e, f, g, h, i, j, k: Results represent the mean \pm SD. Results were subjected to an unpaired, two tailed Student's *t*-test with p-values * < 0.05, ** < 0.01, *** < 0.001, n.s. = not significant. b: Pictures were taken by Dr. Susanna Müller.

Furthermore, IEC (intestinal epithelial cell)-specific deletion of *Ap4* had the same effects on the small intestinal and colonic architecture as the germ-line deletion of *Ap4* (Figure 21a-h). Therefore, the effects of *Ap4* loss on ISCs and their derivatives were intestinal epithelial cell-autonomous. Interestingly, *Ap4*-deficiency also decreased the number of stem cells in the colon (Figure 21i, j).

Results



Results

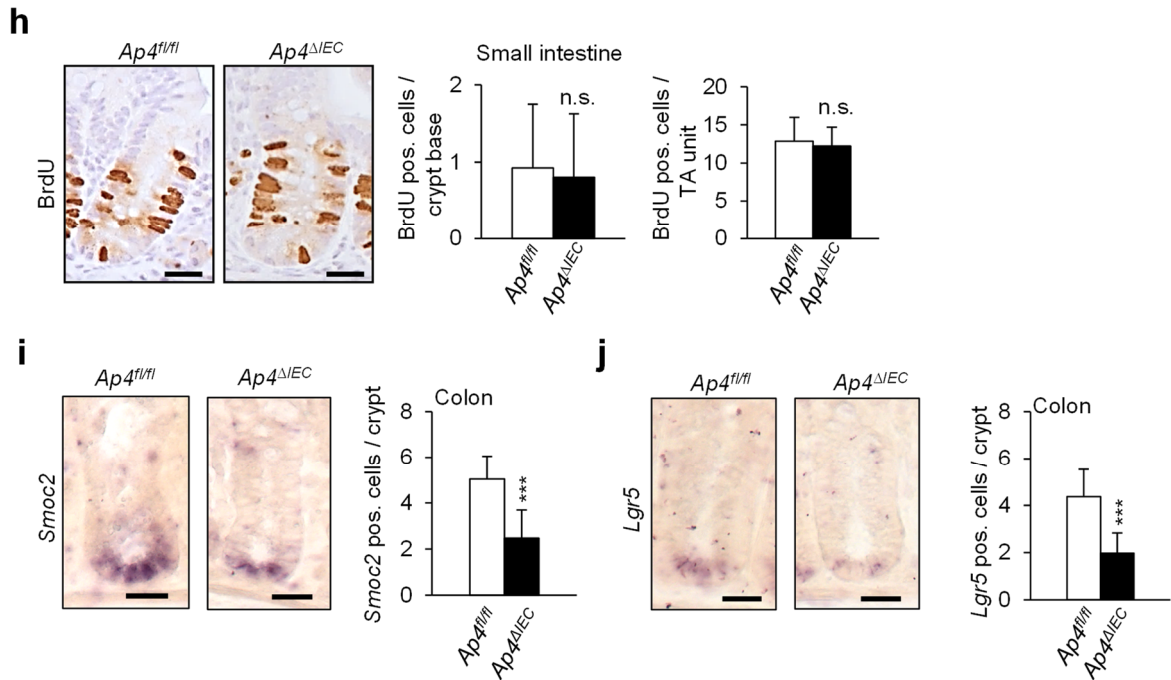


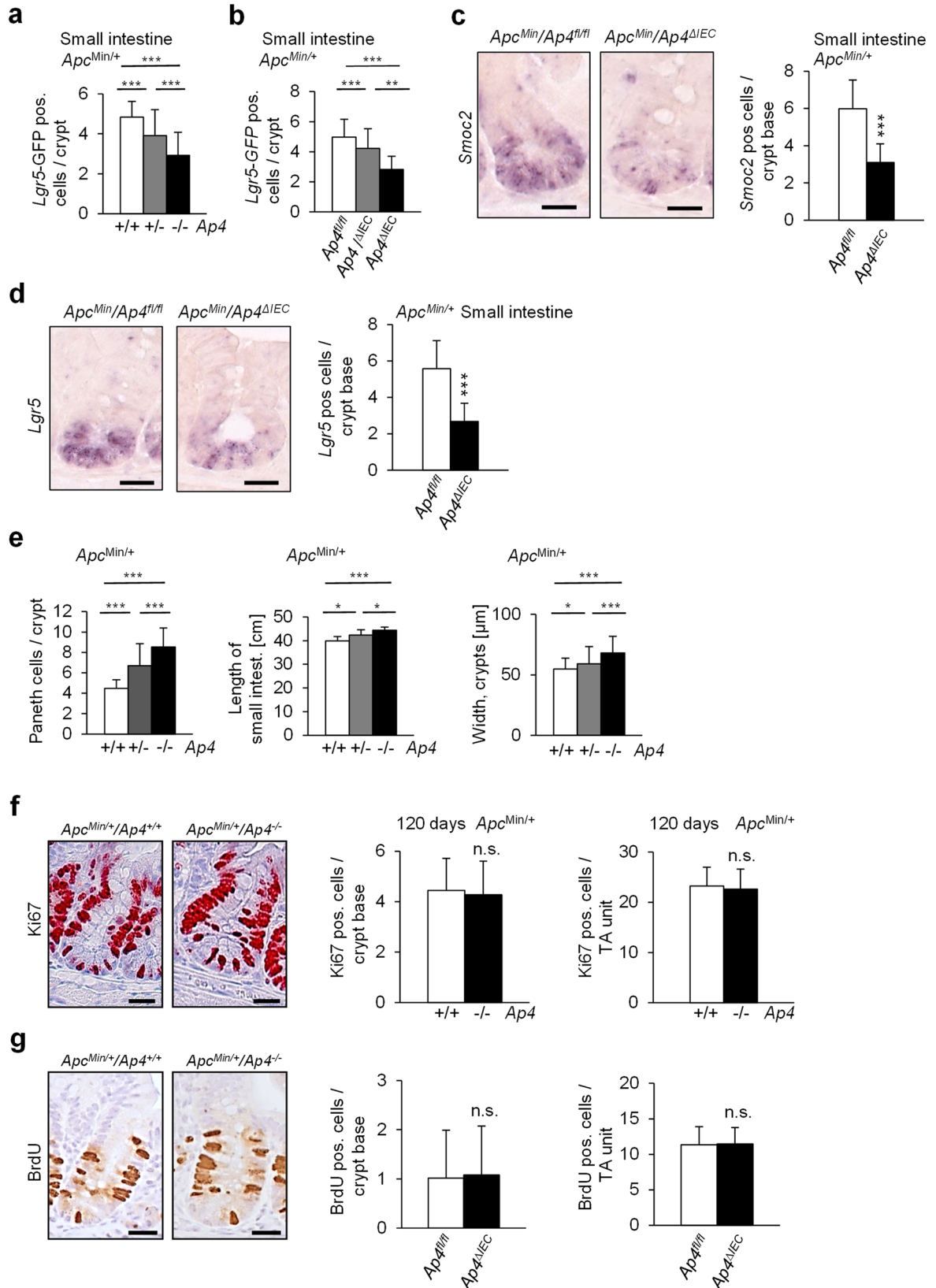
Figure 21 Effects of conditional deletion of *Ap4* on the small intestine and colon.

a Immunohistochemical detection of *Ap4* (brown) in small intestinal tissue, ileum (upper panel) or in the stomach (lower panel) of 1 male and 1 female 63 days old mouse per genotype. Scale bar = 50 μ m, white arrow: site of specific *Ap4* expression. Mast cells in the villi display an unspecific staining. Counterstaining with hematoxylin. **b** The small intestine, ileum, was analyzed for the indicated parameters by analyzing the intestine from 4 male and 4 female mice per genotype for length of small intestine, 2 male and 2 female mice and a total of 200 crypts per genotype for width of crypts, 2 male and 2 female mice and a total of 120 villi per genotype for length of villi, 2 male and 2 female mice and a total of 120 crypts per genotype for Paneth cells per crypt. **c** 2 male and 1 female mice and a total of 30 Paneth cells per genotype were analyzed for the number of vesicles per Paneth cell. **d** 2 male and 2 female mice and a total of 130 villi per genotype were analyzed for goblet cells per villi in small intestine (ileum). 2 male and 2 female mice and a total of 120 crypts per genotype were analyzed for goblet cells per small intestinal crypts. 2 male and 2 female mice and a total of 115 crypts per genotype were analyzed for goblet cells per colonic crypts. **e** The small intestine (ileum) was analyzed for the *Lgr5*-GFP positive cells in 3 male and 3 female mice and a total of 160 crypts per genotype (*Ap4^{fl/fl}* and *Ap4^{ΔIEC}*) or from 2 male and 3 female mice and a total of 130 crypts per genotype (*Ap4^{+/ΔIEC}*). **f** Quantification of *Olfm4* positive cells in the crypt base of the ileum. 280 crypts were evaluated from 2 male and 2 female mice per genotype. **g** 200 crypts or villi from the ileum of 2 male and 2 female mice were analyzed for cleaved caspase-3 positive cells. **h** Left panel: Immunohistochemical detection of BrdU in the ileum of mice with the indicated genotype, scale bar = 25 μ m. Counterstaining with hematoxylin. Right panel: BrdU-positive cells per crypt base or TA unit were counted by analyzing 2 male and 2 female mice and a total of 100 crypts. **i** Left panel: Detection of *Smoc2* mRNA by *in situ* hybridization. Scale bars represent 25 μ m. Right panel: Quantification of *Smoc2*-positive cells in the crypt base from 1 male and 2 female mice (150 crypts) per genotype. **j** Left panel: Detection of *Lgr5* mRNA by *in situ* hybridization. Scale bars represent 25 μ m. Right panel: Quantification of *Lgr5*-positive cells in the crypt base from 1 male and 2 female mice (80 crypts) per genotype. **b, c, d, e, f, g, h, i, j**: Results represent the mean \pm SD. Results were subjected to an unpaired, two tailed Student's *t*-test with *p*-values * < 0.05, ** < 0.01, *** < 0.001, n.s. = not significant

Results

Age-matched *Apc^{Min}* mice deficient for *Ap4* also displayed a decreased number of *Lgr5*- and *Smoc2*-positive ISCs per crypt, an increase in Paneth cells, increased length of the small intestine and enlargement of the crypt base of normal intestine, without any change in proliferation or apoptosis in normal epithelium (Figure 22a-h) independent of the gender (Figure 22i). Notably, ISCs have been shown to efficiently form intestinal tumors upon deletion of *Apc* (Barker et al., 2009) and play a critical role in adenoma and cancer cell self-renewal (de Sousa e Melo et al., 2017; Schepers et al., 2012). Taken together, these results suggest that the decreased rate of tumor formation in *Ap4*-deficient *Apc^{Min}* mice is due to the lower number of functional ISCs in the intestinal crypts.

Results



Results

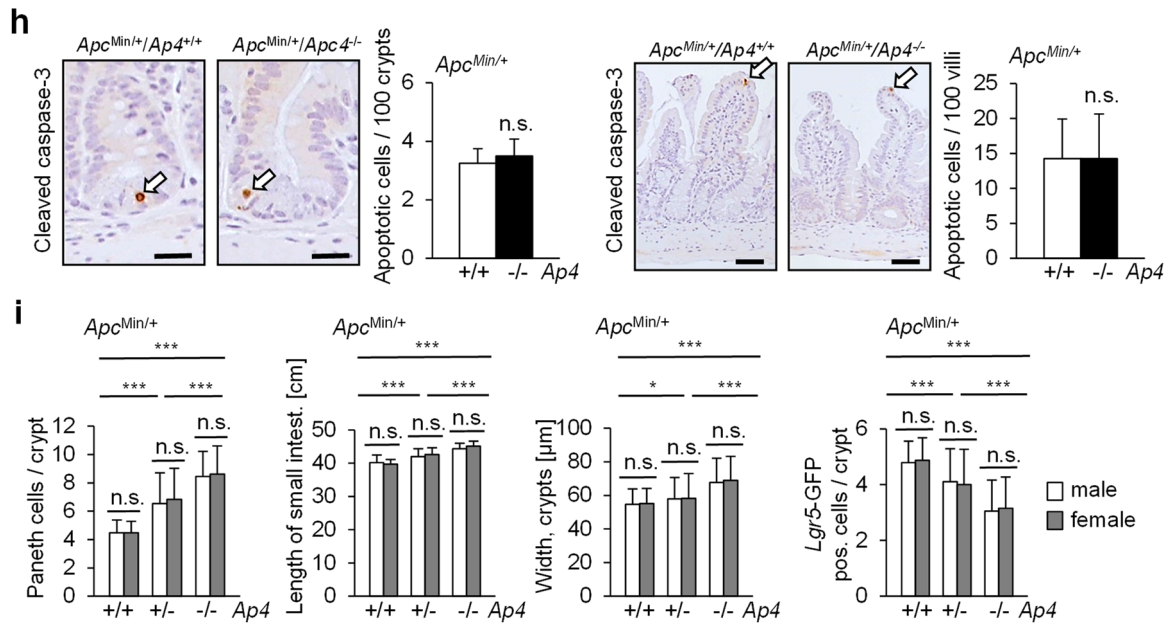


Figure 22 Effects of *Ap4* loss on the small intestine and colon in *Apc^{Min/+}* mice. **a** The amount of *Lgr5*-positive stem cells per crypt within the ileum was determined in 2 male and 2 female mice and a total of 150 crypts per genotype. **b** The small intestine (ileum) was analyzed for *Lgr5*-GFP positive cells in 2 male and 2 female mice in a total of 85 crypts per genotype. **c** Left panel: *In situ* hybridization of *Smoc2* mRNA. Scale bars represent 25 μ m. Right panel: Detection of *Smoc2* positive cells in the crypt base from 2 male and 1 female mice (90 crypts) per genotype. **d** Left panel: *In situ* hybridization of *Lgr5* mRNA. Scale bars represent 25 μ m. Right panel: Detection of *Lgr5*-positive cells in the crypt base from 2 male and 1 female mice (75 crypts) per genotype. **e** The ileum was analyzed for the indicated parameters by analyzing the intestine from 2 male and 2 female mice and a total of 100 crypts per genotype for Paneth cells per crypt, 4 male and 4 female mice per genotype for length of small intestine and 2 male and 2 female mice and a total of 310 crypts per genotype for width of crypt. **f** Left panel: Immunohistochemical detection of Ki67 of the ileum of mice of the indicated genotype, scale bar = 25 μ m. Counterstaining with hematoxylin. Right panel: Ki67 positive cells per crypt base or TA unit were counted within 140 crypts of 2 male and 2 female mice. **g** Left panel: Immunohistochemical detection of BrdU incorporation in crypts of 120 days old *Apc^{Min/+}* mice of the indicated genotype. Counterstaining with hematoxylin. Scale bar = 25 μ m. Right Panel: Quantification of BrdU-positive cells in crypts of the small intestine from 1 male and 2 female mice and a total of 76 crypts per genotype. **h** Immunohistochemical detection of cleaved caspase-3 in normal ileum from mice of the indicated genotype. Left panel: scale bar = 25 μ m. Right panel: scale bar = 50 μ m. Counterstaining with hematoxylin. 200 crypts or villi of the ileum from 2 male and 2 female mice were analyzed for cleaved caspase-3 positive cells. **i** Quantification of Paneth cells per crypt in the ileum in 2 male and 2 female mice per genotype (50 crypts per gender and genotype), length of small intestine of 4 male and 4 female mice per genotype, width of crypts of the ileum of 2 male and 2 female mice per genotype (155 crypts per gender and genotype) or the amount of *Lgr5*-eGFP positive cells in the crypt base of the ileum divided into gender: 2 male and 2 female mice per genotype (75 crypts per gender and genotype). **a, b, c, d, e, f, g, h, i:** Results represent the mean \pm SD. Results were subjected to an unpaired, two tailed Student's *t*-test with *p*-values * < 0.05, ** < 0.01, *** < 0.001, n.s. = not significant.

Results

5.5 Analysis of *Ap4* function in intestinal organoids

To further analyze the functional relevance of *Ap4* for ISCs, we generated small intestinal organoids by *ex vivo* culture of small intestinal crypts derived from *Villin-Cre-ERT2/Ap4^{fl/fl}* mice. After addition of 4-OHT to established organoids, *Ap4* expression was decreased by ~90% within three days, which demonstrates efficient, Cre-mediated deletion of the floxed *Ap4* allele in these organoids (Figure 23a). Upon acute *Ap4* inactivation, organoids showed a pronounced decrease of ISC markers, an increase of Paneth cell markers, as well as a decrease of goblet cell markers within 3 days after exposure to 4-OHT, whereas organoids derived from *Villin-Cre-ERT2/Ap4* wild-type mice exposed to 4-OHT did not display significant changes in the expression of these markers (Figure 23a). Importantly, *Ap4*-deficient organoids formed less protrusions (crypt-like-structures), when compared to the *Ap4*-expressing organoids (Figure 23b). Since the number of protrusions corresponds to the number of self-renewing ISCs within organoids (Wolfe et al., 2017), the decrease in the number of protrusions in *Ap4*-deficient organoids is presumably caused by a decrease in functional ISCs. Taken together, these results suggest that *Ap4* is essential for maintaining ISCs in their undifferentiated state and plays an important role in the homeostasis of ISCs and Paneth cells.

Results

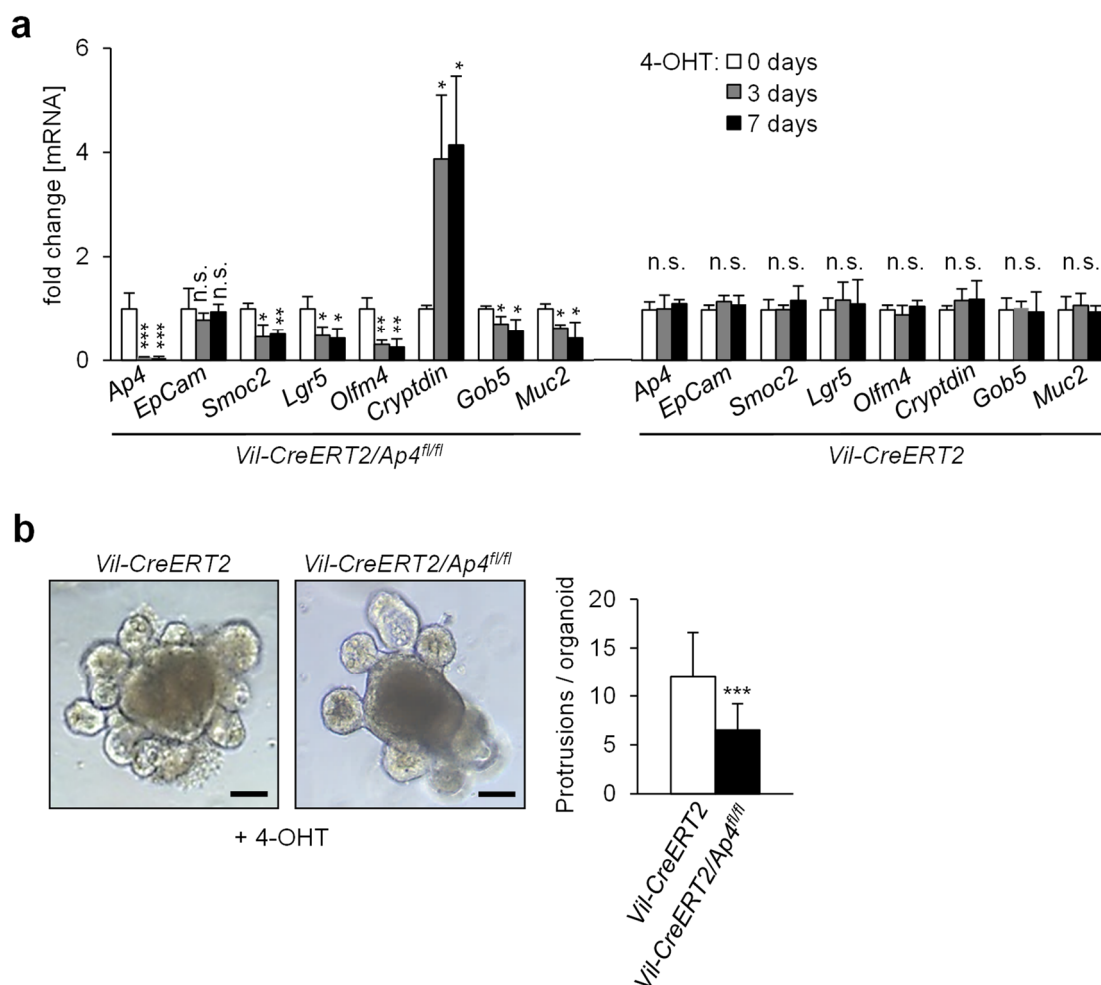


Figure 23 Effects of *Ap4* deletion in intestinal organoids. **a** qPCR analysis of the indicated *mRNA* from organoids isolated from 3 female mice per genotype after passaging and 7 days after Cre activation by 4-OHT. **b** Left panel: representative pictures of small intestinal organoids 7 days after passaging and Cre activation by 4-OHT. Scale bars represent 20 μ m. Right panel: Quantification of protrusions (crypt-like structures) per organoid derived from 3 female mice per genotype. A total of 81 organoids were evaluated per genotype. **a, b:** Results represent the mean \pm SD. Results were subjected to an unpaired, two tailed Student's t-test with p-values * < 0.05, ** < 0.01, *** < 0.001, n.s. = not significant.

5.6 Gene expression profiling of *Ap4*-deficient organoids

Next, we obtained RNA expression profiles of *Ap4*-deficient and *Ap4* wild-type organoids 7 days after 4-OHT treatment using NGS. Changes in gene expression observed after deletion of *Ap4* were considerably less pronounced in organoids when compared to adenomas. By setting the cut-off for differential expression to a fold-change ≥ 1.5 ($p < 0.05$) we identified 693 mRNAs as differentially regulated as a consequence to deletion of *Ap4* (Figure 24a), with 319 mRNAs being significantly down-regulated, and 374 showing up-regulation (Figure 24b, c). Remarkably, factors

Results

involved in Notch signaling and Wnt/ β -catenin signaling were significantly over-represented among the down-regulated mRNAs (Figure 24d, Supplemental Data 1).

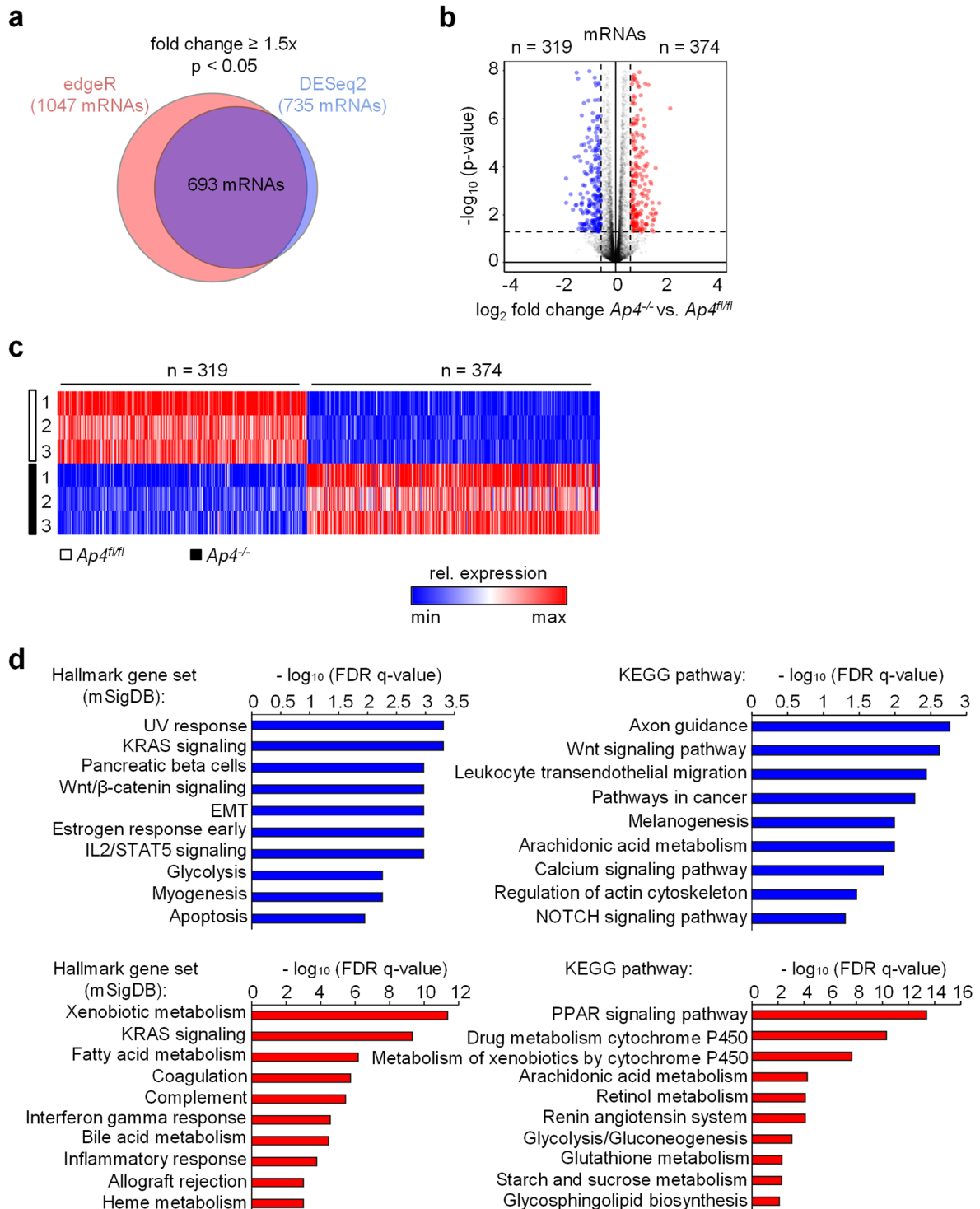


Figure 24 Expression analyses of $Ap4$ -deficient organoids. **a** Venn diagram displaying differentially regulated mRNAs (fold change $> 1.5x$, $p < 0.05$) in $Ap4^{fl/fl}$ and $Ap4^{\Delta IEC}$ organoids as determined by edgeR and DESeq2. **b**, **c** Volcano plot (**b**) and heat map (**c**) depicting expression changes of differentially expressed mRNAs between Vil -Cre-ERT2 and Vil -Cre-

Results

ERT2/Ap4^{fl/fl} organoids, 7 days after Cre activation by 4-OHT, detected by RNA-Seq. **b:** Volcano plot depicting expression changes of differentially expressed mRNAs (fold change > 1.5) from *Ap4^{fl/fl}* and *Ap4^{ΔIEC}* organoids. Down-regulated mRNAs are depicted in blue, up-regulated mRNAs are depicted in red. RNAs with fold changes < 1.5 and/or statistically non-significant changes in expression are indicated in black. Dashed vertical lines indicate 1.5 fold change cutoff. Dashed horizontal line indicates the cutoff for adjusted p-values < 0.05 as determined with *DESeq2*. **c:** Heat-map depicting expression changes of differentially expressed mRNAs (fold change > 1.5 p < 0.05 as determined by *edgeR* and *DESeq2*) from *Ap4^{fl/fl}* and *Ap4^{ΔIEC}* organoids. Colors indicate relative expression values from minimum (blue) to maximum (red) for each RNA sample per differentially regulated mRNA. **d** Upper panel: Hallmark gene set (mSigDB: molecular Signature Database (Liberzon et al., 2015)) and KEGG (Kyoto Encyclopedia of Genes and Genomes) analysis from down-regulated mRNAs after conditional ablation of *Ap4* in intestinal organoids. The 10 most significantly enriched pathways among down-regulated mRNAs are shown. Lower Panel: Hallmark gene set (mSigDB: molecular Signature Database) and KEGG (Kyoto Encyclopedia of Genes and Genomes) analysis from up-regulated mRNAs. The 10 most significantly enriched pathways among up-regulated mRNAs after conditional ablation of *AP4* in intestinal organoids are shown. See also Supplemental Data 1. All data analyses were performed by Dr. Markus Kaller.

In line with the effect of *Ap4* deletion in adenomas GSEA indicated that mRNAs characteristic for *Lgr5*-positive or *EphB2^{high}* ISCs and several factors involved in Wnt/ β -catenin and Notch signaling pathways were preferentially down-regulated upon deletion of *Ap4* (Figure 25a, Supplemental Data 2): For example *Sox4*, *Axin2*, *EphB3* were down-regulated (Figure 25b, Supplemental Data 2). Down-regulated components of the Notch signaling pathway included *Notch1*, and the Notch target gene *Hes1*, as well as the Notch activating ligands *Dll1*, *Dll3*, *Dll4* and *Jag2* (Figure 25b, Supplemental Data 2). Exemplary confirmations of mRNA down-regulations of genes important in Wnt/ β -catenin signaling and/or Notch signaling upon acute deletion of *Ap4* in intestinal epithelial cell derived organoids are shown in Figure 25c. The decreased activity of the Notch pathway after *Ap4* loss was confirmed by immunohistochemical detection of *Nicd1* (Notch intracellular domain 1) in normal crypts in the small intestine (Figure 25d, e). Not only was the frequency of *Nicd1*-positive cells per crypt lower, but also the intensity of the *Nicd1* signal was decreased, which indicates a lower activity of the Notch signaling pathway in these cells. Taken together, these results show that *Ap4* contributes to the Wnt/ β -catenin and Notch transcriptional program in normal intestinal tissue.

Interestingly, the transcription factor *Spdef* (SAM pointed domain containing ETS factor) was down-regulated in *Ap4*-deficient organoids according to NGS analysis and validated by qPCR (Figure 25b, c). *Spdef* regulates the differentiation and maturation

Results

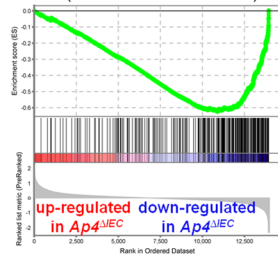
of goblet cells (Noah et al., 2010). Down-regulation of *Spdef* may therefore contribute to the decreased number of goblet cells observed in *Ap4*-deficient mice.

As observed in adenomas, *c-Myc* and *E2f* target genes were significantly enriched among the down-regulated RNAs in *Ap4*-deficient organoids (Figure 25a, Supplemental Data 2) albeit with rather modest fold changes in expression that were considerably less pronounced compared to those of ISC signature and Notch target genes (Figure 25f, Supplemental Data 2). Interestingly, the differential mRNA expression caused by deletion of *Ap4* was similar in organoids and adenomas as determined by correlation analysis (Figure 25g). As the organoid derived expression profiles were obtained in the absence of non-epithelial cells or stroma, these findings indicate that gene expression changes resulting from the inactivation of *Ap4* are largely epithelial cell autonomous. These results suggest that the differential regulation of factors involved in *Wnt*/ β -catenin and/or Notch signaling observed after deletion of *Ap4* in *Apc*^{Min} mice occur in normal intestinal epithelial stem cells prior to adenoma development.

Results

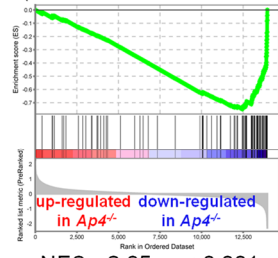
a

Lgr5+ stem cell signature
(Munoz *et al.* 2012)



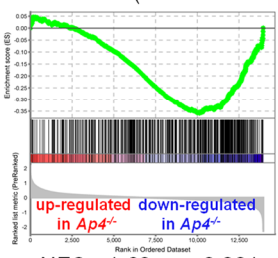
NES: -2.70; $p < 0.001$

Lgr5+ stem cell signature
(Merlos-Suarez *et al.* 2011)



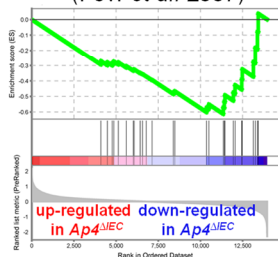
NES: -2.85; $p < 0.001$

mRNAs down-regulated after
Ctnnb1 loss (Fevr *et al.* 2007)



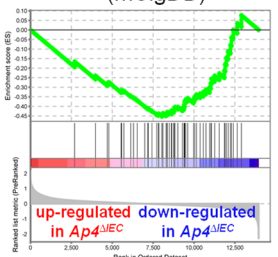
NES: -1.63; $p < 0.001$

Wnt/β-cat./ISC markers
(Fevr *et al.* 2007)



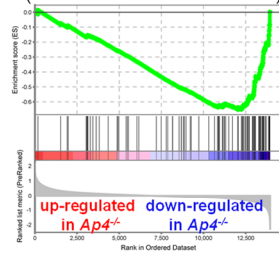
NES: -1.79; $p = 0.002$

c-Myc targets
(mSigDB)



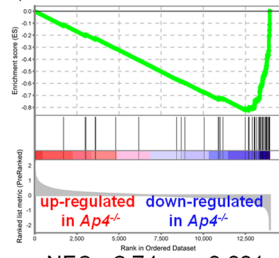
NES: -1.53; $p = 0.014$

Lgr5+ stem cell signature
(Van der Flier *et al.* 2009)



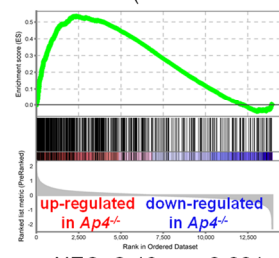
NES: -2.47; $p < 0.001$

EphB2^{high} stem cell signature
(Merlos-Suarez *et al.* 2011)



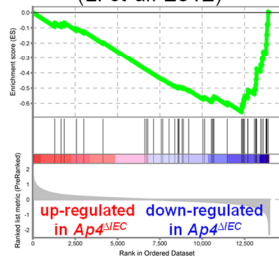
NES: -2.74; $p < 0.001$

mRNAs up-regulated after
Ctnnb1 loss (Fevr *et al.* 2007)



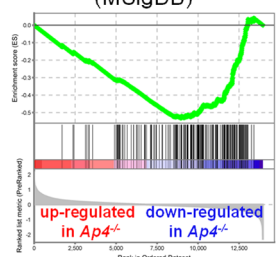
NES: 2.46; $p < 0.001$

Direct Notch targets
(Li *et al.* 2012)



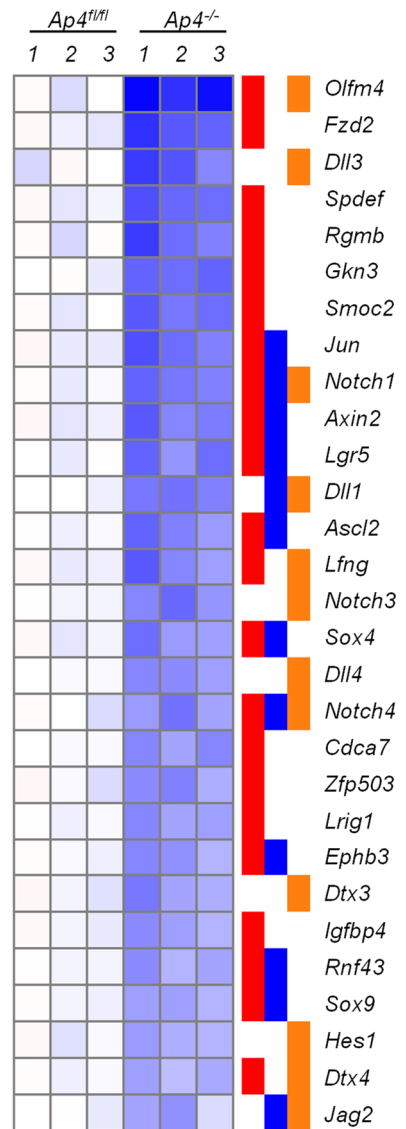
NES: -2.17; $p < 0.001$

E2f target genes
(MSigDB)



NES: -2.21; $p < 0.001$

b

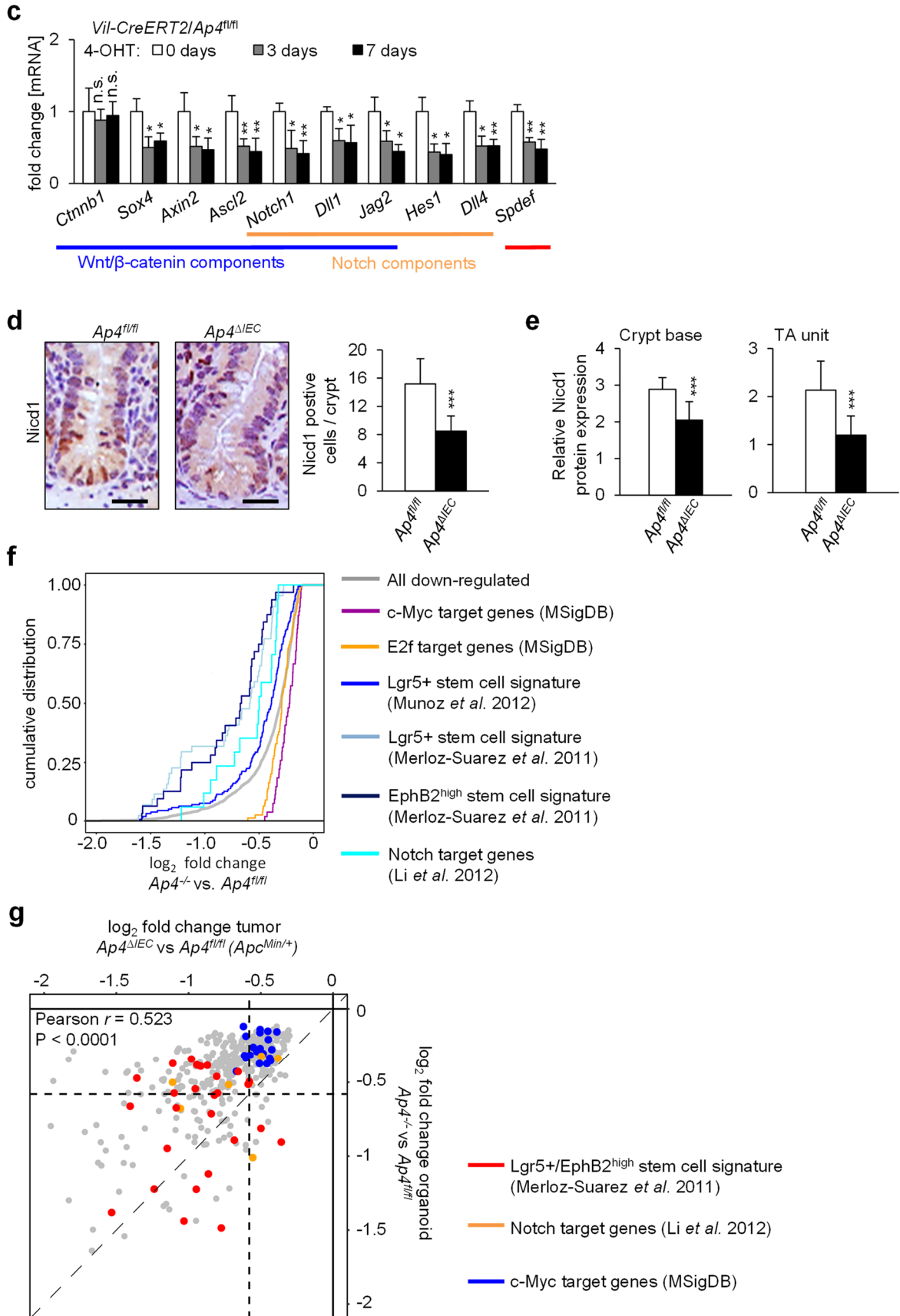


fold change
Ap4^{ΔIEC} vs. *Ap4*^{wt}

0.25 1 4

- █ Stem cell signature
- █ Wnt/β-cat. components
- █ Notch components

Results



Results

Figure 25 NGS analysis of intestinal organoids after deletion of *Ap4*. **a** GSEA comparing gene expression profiles from *Vil-Cre-ERT2* and *Vil-Cre-ERT2/Ap4^{f/f}* organoids 7 days after Cre activation (change in GSEA Curves to *Ap4* ΔIEC in a and to *Ap4* wt and *Ap4* IEC in b) by 4-OHT with *Lgr5*-positive or *EphB2^{high}* stem cell signatures (Munoz et al., 2012) (Merlos-Suarez et al., 2011; van der Flier et al., 2009), mRNAs differentially regulated after *Ctnnb1* loss (Fevr et al., 2007), β -catenin regulated / ISC specific genes (Fevr et al., 2007), Notch targets genes (Li et al., 2012), c-Myc target genes (mSigDB: molecular Signatures Database) or E2f target genes (mSigDB). NES: Normalized Enrichment Score, Nom. p-value: Nominal p-value. **b** Heat-map depicting expression changes of selected differentially expressed mRNAs (p-value < 0.05) from stem cell gene signatures, Wnt signaling and/or Notch signaling gene signatures analyzed in (a). The heatmap displays relative expression levels normalized to the mean expression in the control (*Vil-CreERT2*) samples for each mRNA. Three biological replicates per genotype were analyzed. **c** qPCR analysis of the indicated *mRNA* of organoids with the indicated genotypes 3 days and 7 days after 4-OHT induction. **d** Left panel: Immunohistochemical detection of *Nicd1* of the ileum from mice of the indicated genotype, scale bar = 25 μ m. Counterstaining with hematoxylin. Right panel: Quantification of *Nicd1*-positive cells per crypt in 2 male and 2 female mice and a total of 120 crypts per genotype. **e** Relative *Nicd1* protein expression was measured as the intensity of staining in *Nicd1*-positive cells in the crypt base (left panel) and the TA unit (right panel). For the intensity, a score from 1-3 was used (1 = weak, 2 = moderate, 3 = strong staining). **f** Cumulative distribution plots comparing RNA expression changes as determined by DESeq2 of gene set members of the indicated gene signatures upon loss of *Ap4* in organoids. **g** Scatter plot displaying the correlation of expression changes of the 424 mRNAs significantly (p < 0.05) downregulated in both adenomas and organoids (shown in grey). The mRNAs from stem cell gene signatures, Notch target gene signatures and c-Myc target genes analyzed in Figure 15a and 25a in both adenomas and organoids are highlighted with the indicated colors. The Pearson correlation coefficient of all 424 mRNAs down-regulated in both adenomas and organoids and statistical significance are indicated. c, d, e: Results represent the mean \pm SD. Results were subjected to an unpaired, two tailed Student's t-test with p-values * < 0.05, ** < 0.01, *** < 0.001, n.s. = not significant. a, b: See also Supplemental Data 2. a, b, f, g: Figures and analyses were made by Dr. Markus Kaller.

5.7 Regulation of the NOTCH pathway by AP4 in human CRC cells

In order to determine whether the connection between *Ap4* and Notch detected here is conserved between species and relevant to human CRCs, we performed expression and functional analyses in human CRC cell lines. In line with the results described above, the expression of AP4 and NICD1 proteins positively correlated in a panel of 5 CRC cell lines (Figure 26a). After ectopic AP4 expression in DLD-1 cells *NOTCH1/NICD1* and the NOTCH-target genes *HES1* and *NRARP* were induced at the protein and mRNA levels (Figure 26b, c). Down-regulation of AP4 by RNA interference decreased NICD1 protein expression in Colo320 cells (Figure 26d). Furthermore, a NOTCH activity reporter plasmid was induced by ectopic AP4 expression, but not by a mutant AP4 protein, which lacks the basic DNA-binding region (Figure 26e). In addition, analysis of public ChIP-Seq data showed open and active chromatin

Results

surrounding the sites of AP4 occupancy at the *NOTCH1* promoter, since histone H3K4me1 and H3K27Ac modifications were increased in their vicinity (Figure 26f).

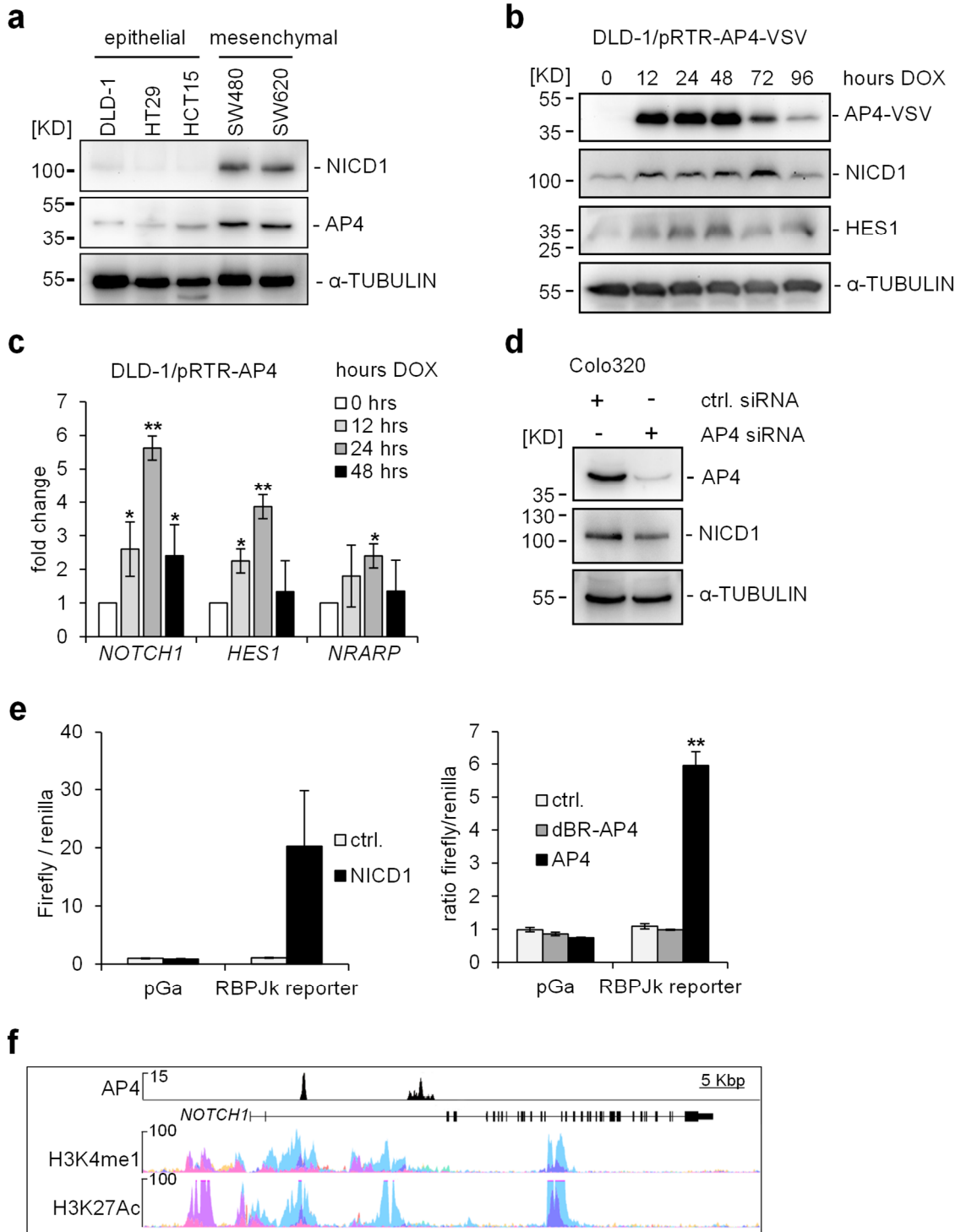


Figure 26 AP4 regulates *NOTCH1* in human CRC cell lines. **a** Western blot analysis of AP4 and NICD1 protein expression in CRC lines. Detection of α -TUBULIN served as a loading control. **b** Western blot analysis of the indicated proteins after ectopic expression of AP4 in DLD-1 cells for the indicated periods. **c** qPCR analysis of the indicated mRNAs after activation of ectopic AP4 expression in DLD-1 CRC cells by addition of doxycycline (DOX) for the indicated periods. Gene expression changes after DOX treatment for the indicated time points

Results

(fold change) were normalized to untreated cells (0h DOX) and β -actin. Results are given as mean \pm s.d. (n=3) **d** Colo320 cells were transfected with an *AP4*-specific siRNA. 72 h later, protein lysates were subjected to immunoblot analysis of the indicated proteins. **e** *RBPJk* reporter activity was determined in HEK293T cells 24 hours after transfection with the indicated vectors. **f** Representative AP4 ChIP-seq result for the *NOTCH1* promoter in DLD-1 cells. H3K4me1 and H3K27Ac ChIP-seq results were obtained from the ENCODE Consortium of the UCSC Genome Browser. a, b, d: Uncropped western blot membranes are shown in Supplemental Data 3. c, e: $n = 3$, results represent the mean \pm SD. Results were subjected to an unpaired, two-tailed Student's *t*-test with p-values * < 0.05 , ** < 0.01 , *** < 0.001 , n.s. = not significant. All analyses were performed by Dr. Rene Jackstadt.

When we analyzed ChIP-Seq data, which we had previously obtained after ectopic AP4 expression in the CRC cell line DLD-1 (Jackstadt et al., 2013c), we detected AP4 occupancy at the *ASCL2*, *DLL1*, *DLL4*, *EPHB3*, *HES1*, *JAG1*, *JAG2*, *NOTCH1*, *SOX4* and *TCF7* promoters in human DLD-1 CRC cells (Figure 27). Therefore, AP4 regulates genes involved in WNT/ β -CATENIN and/or NOTCH signaling directly by binding to their promoters in CRC cells.

Results

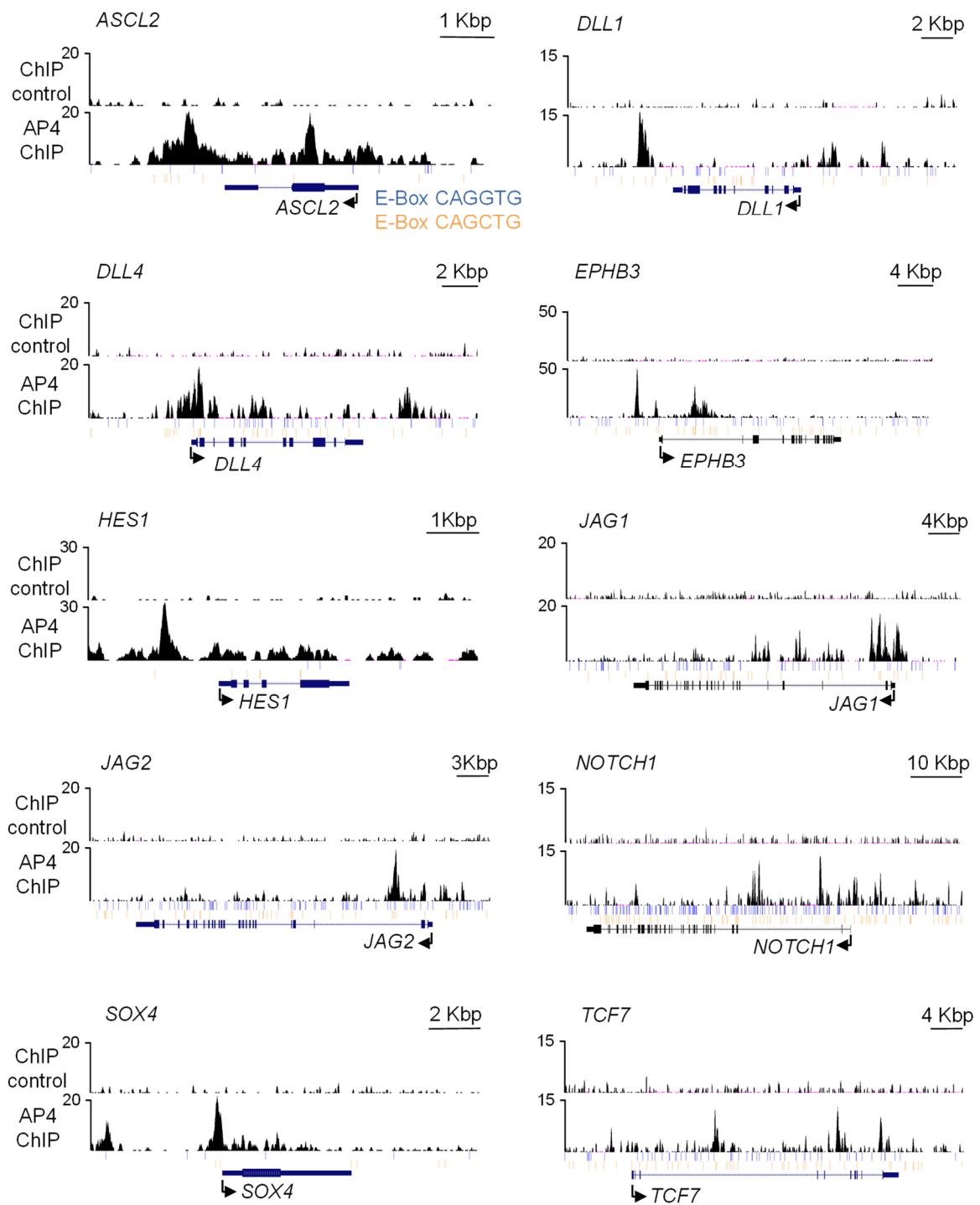
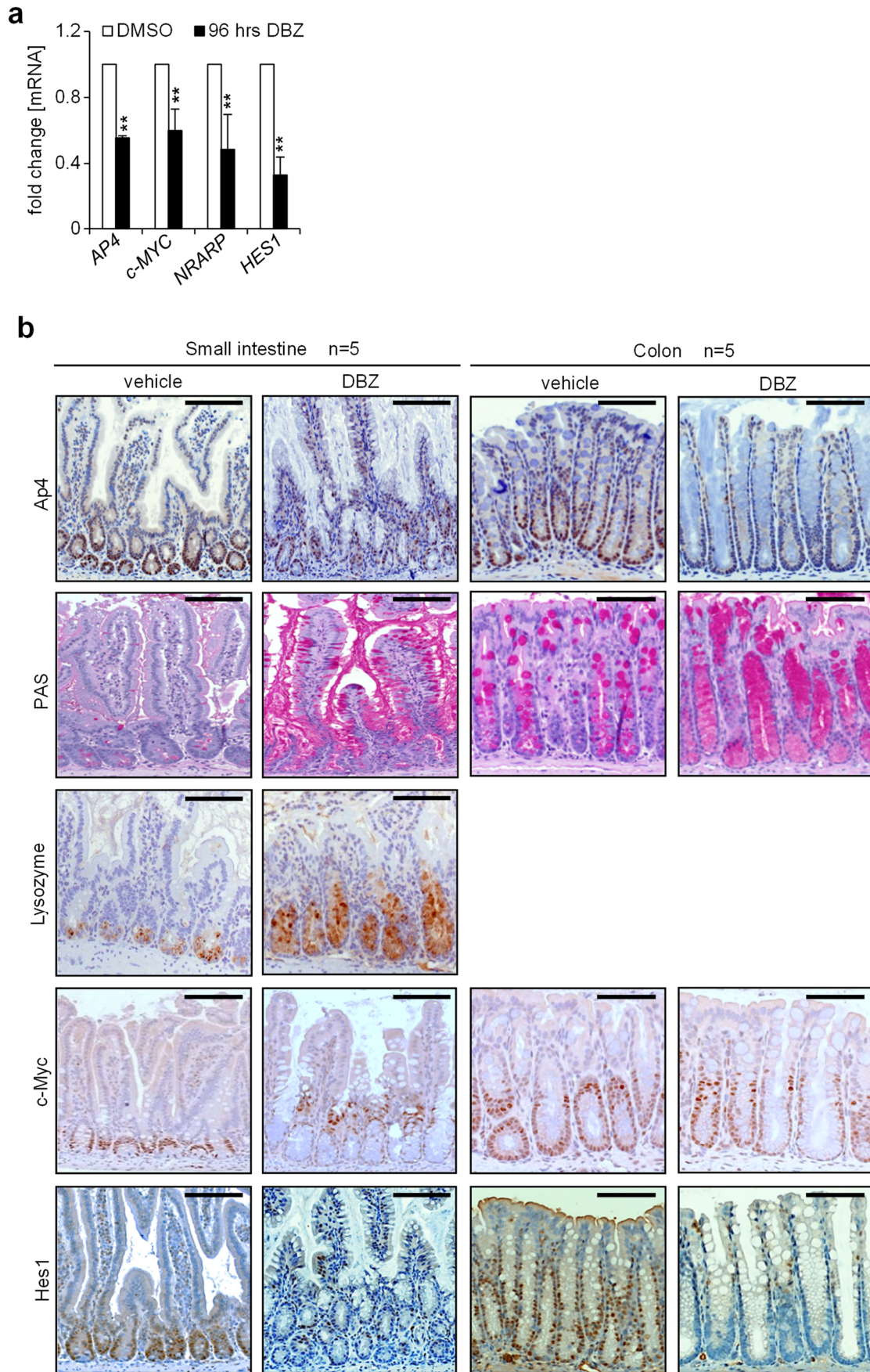


Figure 27 AP4 regulates directly WNT/ β -CATENIN and/or NOTCH pathway components in human CRC cell lines. Histogram plots showing examples of occupancy by AP4 within promoters of genes involved in WNT/ β -CATENIN and/or NOTCH pathways in the human DLD-1 cell line upon ectopic expression of AP4 or vector control. ChIP-seq data were adapted from our NGS analysis published in (Jackstadt et al., 2013c). Orange and blue vertical bars denote the genomic positions of CAGCTG and CAGGTG E-boxes, respectively. Figures and analyses were made by Dr. Markus Kaller.

Results

In addition, inhibition of NOTCH signaling by exposure to the γ -secretase inhibitor Dibenazepine (DBZ) resulted in a decrease of *AP4* and *c-MYC* expression in SW620 CRC cells (Figure 28a). As expected, the NOTCH-target genes *NRARP* and *HES1* were also repressed. Notably, DBZ suppressed Ap4 protein expression in the small and large intestine of mice (Figure 28b). As expected, inhibition of Notch signaling led to an increase in the number of Paneth cells and goblet cells as well as to a decrease of Hes1 and c-Myc expression. Since we could not obtain experimental evidence for a direct regulation of *AP4* by NICD1 (data not shown), the regulation of *AP4* by the NOTCH pathway is presumably mediated by c-MYC, which represents a known target of the NOTCH pathway (Palomero et al., 2006; Weng et al., 2006). Therefore, AP4, the NOTCH pathway and c-MYC form a positive feed-back loop.

Results



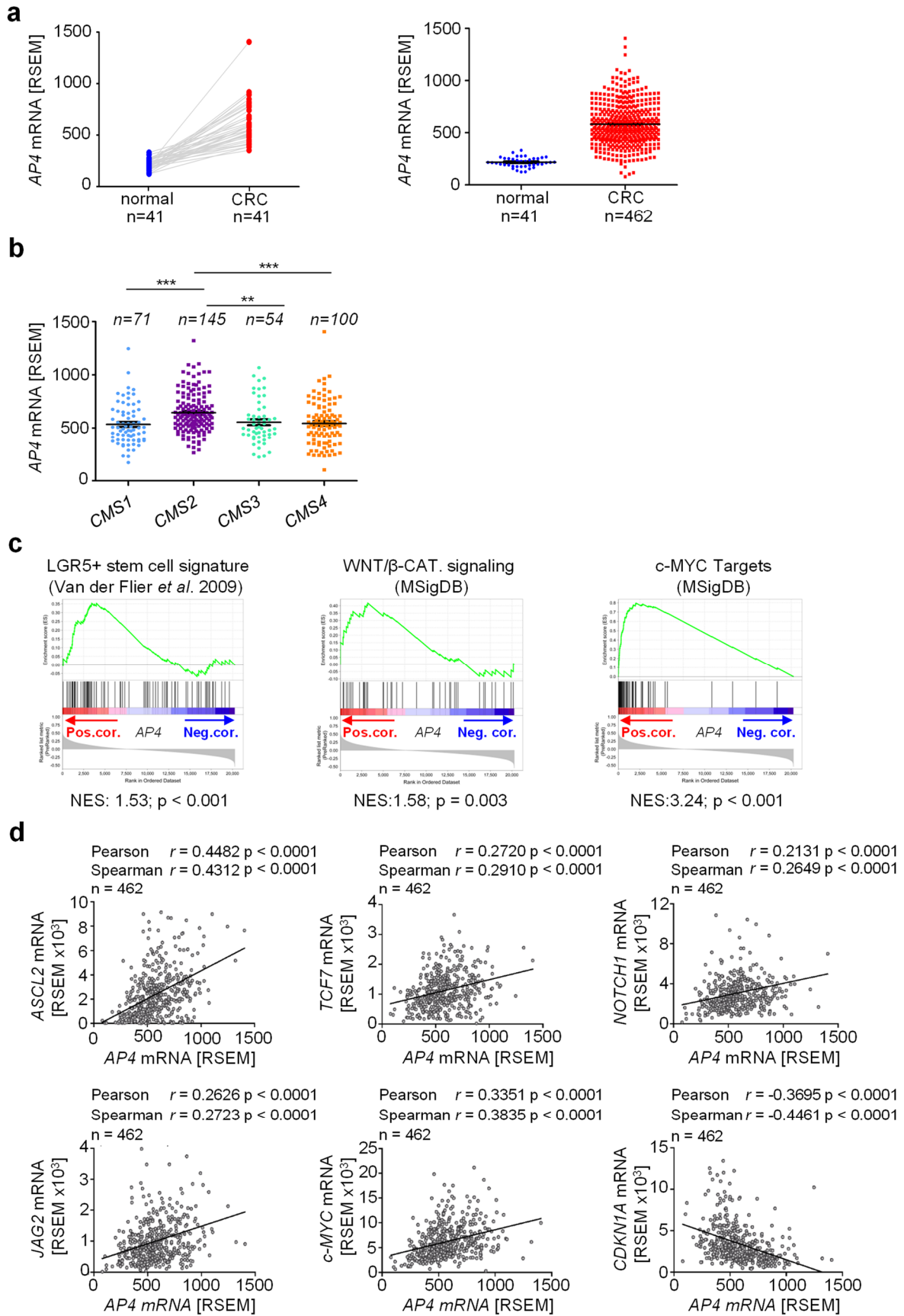
Results

Figure 28 Inhibition of Notch signaling leads to down-regulation of Ap4. **a** qPCR analysis of the indicated mRNAs in SW620 cells 96 hours after DBZ (5 mM) treatment. Results represent the mean +/- SD. **b** Immunohistochemical analysis of small intestine (Ileum) and colon from ~ 6 months old mice treated with vehicle (DMSO) or DBZ for 5 consecutive days with the indicated antibodies or PAS staining; scale bar indicates 100 μ m. *n* represents the number of mice analyzed per genotype. *a*: *n* = 3, results represent the mean +/- SD. Results were subjected to an unpaired, two-tailed Student's *t*-test with p-values * < 0.05, ** < 0.01, *** < 0.001, n.s. = not significant. *a*: Figure and analysis was made by Dr. Rene Jackstadt. *b*: DBZ treatment of mice was performed by Prof. Dr. David Horst, stainings of Ap4, c-Myc and Hes1 were performed by Ursula Götz, pictures (except the pictures of Lysozyme) were taken by Dr. Rene Jackstadt.

5.8 Role of AP4 in human CRCs

To obtain further evidence for a clinical relevance of AP4 in CRC initiation and progression we analyzed patient-derived expression data that were generated by the TCGA consortium (Cancer Genome Atlas, 2012). Indeed, *AP4* mRNA expression was significantly increased in primary CRCs when compared to normal mucosa in 41 matched normal versus CRC patient samples, as well as in unmatched patient samples representing normal mucosa (*n*=41) and primary CRCs (*n*=462) (Figure 29a). Recently, CRCs were shown to belong to four different molecular sub-groups, the so-called consensus molecular subtypes (CMS) 1-4 (Guinney et al., 2015). In line with the results obtained here, CRCs belonging to the CMS2 subtype, which is characterized by high WNT and c-MYC activity, showed significantly elevated expression of *AP4* when compared to the three other CMS subtypes (Figure 29b). Moreover, in CRCs from the TCGA cohort *AP4* expression showed a positive correlation with the expression of mRNAs characteristic for Lgr5-positive intestinal stem cells (van der Flier et al., 2009), as well as with mRNAs encoding factors involved in WNT/ β -CATENIN signaling and c-MYC target genes (mSigDB, molecular Signature Database: (Liberzon et al., 2015)) (Figure 29c). Furthermore, *AP4* expression showed a significant positive correlation with *ASCL2*, *TCF7*, *NOTCH1* and *JAG2* expression in 462 primary CRCs in the TCGA cohort (Figure 29d). As expected, *AP4* expression was also positively associated with c-MYC and negatively associated with *CDKN1A/p21* expression.

Results



Results

Figure 29 *Ap4* expression and associations in human CRCs deposited within TCGA.

a *Ap4* RNA expression levels from matched patient samples from normal mucosa and tumor tissue (left), or unmatched normal mucosa and tumor tissues (right). RNA expression data were obtained from publically available TCGA colorectal adenocarcinoma (COAD) datasets (Cancer Genome Atlas, 2012). Left panel: matched samples, 41 normal mucosa and 41 tumor tissue samples. Right panel: 41 normal mucosa samples and 462 tumor tissue samples were used. **b** Box plots showing *Ap4* RNA expression levels in 462 COAD samples from (a) associated with the different CRC consensus molecular subtypes (CMS) as defined in (Guinney et al., 2015). **c** Expression of human homologues of the LGR5-positive stem cell signature (van der Flier et al., 2009), members of the HALLMARK WNT signaling gene set (Liberzon et al., 2015) or c-MYC target genes (Liberzon et al., 2015) are strongly linked with AP4 expression in human tumors. All genes within the TCGA datasets from human colorectal tumors were pre-ranked by expression correlation coefficient (Pearson r) with *Ap4* in descending order from left (positive correlation) to right (negative correlation) and analyzed by GSEA. **d** Scatter plots displaying pairwise comparisons of mRNA expression levels [RSEM] of the indicated genes for 462 TCGA COAD samples. The correlation coefficients and p-values of Pearson's and Spearman's correlations, as well as the linear regression trend line are indicated. a, left panel: Results were subjected to a paired, two tailed Student's t -test with p-values * < 0.05, ** < 0.01, *** < 0.001. a, right panel and c: Results represent the mean +/- SD. Results were subjected to an unpaired, two tailed Student's t -test with p-values * < 0.05, ** < 0.01, *** < 0.001, n.s. = not significant. All analyses were made by Dr. Markus Kaller.

In order to determine whether the positive correlation between AP4 and NOTCH1/NICD1/HES1 also exists on the level of protein expression in human CRCs, we determined AP4, NICD1 and HES1 expression levels by immunohistochemical analysis of 220 primary CRC samples. For the evaluation of AP4, NICD1 and HES1 expression we established a 4-stage scoring scheme (Figure 30a). AP4 expression was highly concordant with both NICD1 and HES1 expression (Figure 30b) indicating that the reciprocal regulation between AP4 and the NOTCH pathway also occurs in primary, human CRCs.

Results

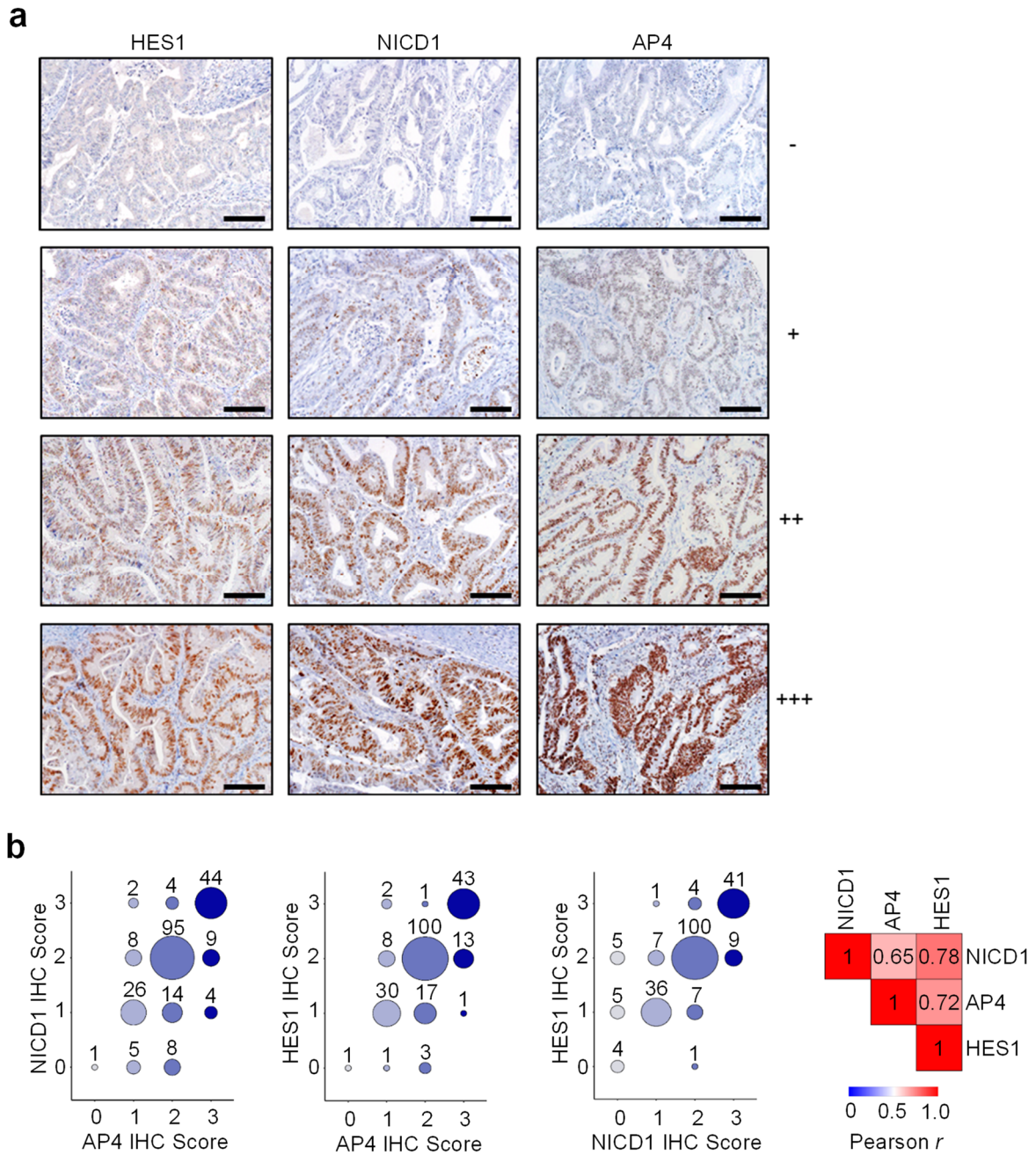


Figure 30 Correlative analysis of AP4, NICD1 and HES1 protein expression in human CRCs. **a** The intensity of nuclear AP4, NICD1 and HES1 staining in human CRC TMA (Tumor Microarray) samples was assigned the following scores: none = -, weak = +, moderate = ++, and strong = +++ expression. Examples of representative immunohistochemistry results were shown. Scale bar: 100 μ m. **b** Left: Dot plots displaying pairwise comparisons of IHC staining scores explained in (a) for AP4, NICD and HES1 from 220 human CRC TMA samples. Dot sizes represent tumor sample numbers. Right: Heatmap displaying Pearson r correlation coefficients of IHC scores obtained from 220 tumor samples stained for AP4, NICD1 and HES1 expression. **b:** Figures were made by Dr. Markus Kaller.

Discussion

6. Discussion

This study identified Ap4 as an important, rate limiting mediator of intestinal adenoma initiation (Jaeckel et al., 2018; summarizing model in Figure 31): Deletion of *Ap4* in the germ-line and in intestinal epithelial cells resulted in a reduced number of Lgr5+ intestinal stem cells (ISCs) and a reciprocal increase in Paneth cells. Ap4 loss decreased intestinal adenoma formation in *Apc^{Min}* mice, presumably due to the reduced number of functional ISCs amenable for adenoma initiating mutational events. The Wnt- and Notch-pathways were identified as important mediators of Ap4 function in the healthy intestine and during adenoma formation.

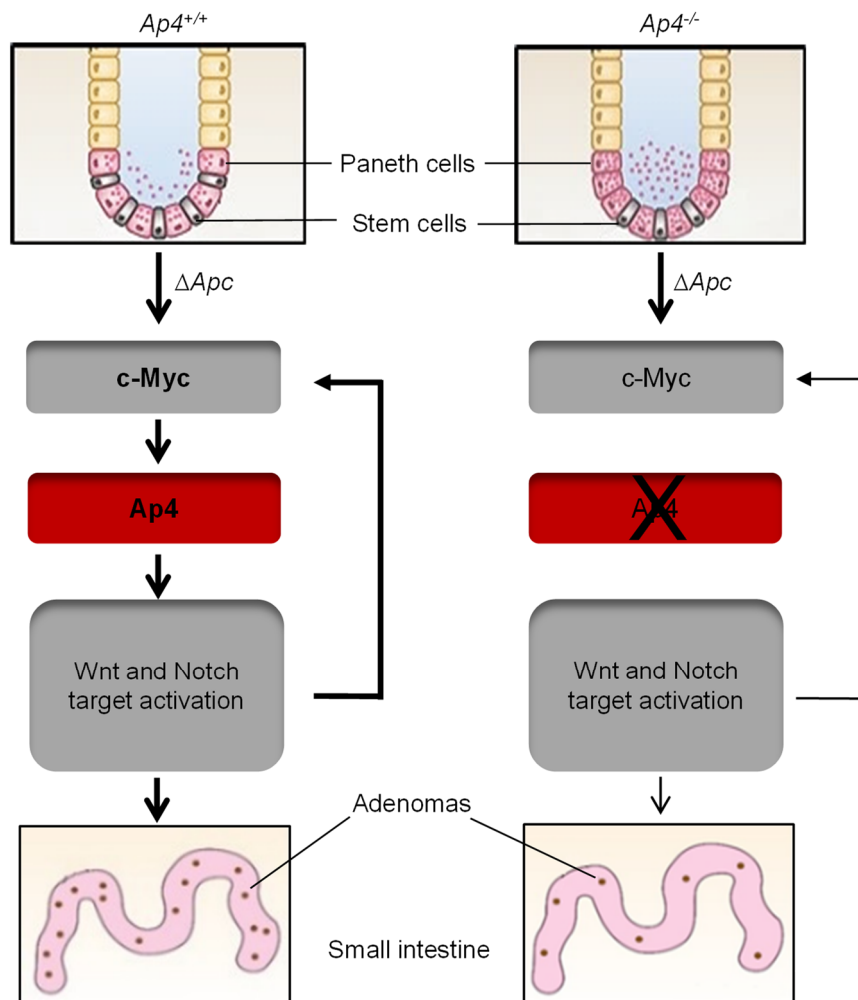


Figure 31 Model summarizing the results of this study. Schematic model summarizing the results of this study. The dots in the Paneth cells represent vesicles containing antimicrobial proteins such as Lysozyme and Cryptdin. The dots in the lumen represent antimicrobial proteins excreted by Paneth cells.

Discussion

Since inactivation of *Ap4* led to a decrease in the number of ISCs and an increase in Paneth cells, it is conceivable that the decreased formation of adenomas in the absence of *Ap4* is due to the smaller number of bona-fide ISCs that are able to initiate adenomas after acquiring genetic and epigenetic alterations. This hypothesis is in accordance with the observation that tumor-promoting mutations in ISCs are more efficient in generating tumors than mutations in other, more differentiated intestinal epithelial cells. This may be because ISCs are long-lived and self-renewing (e.g. have a high proliferation rate), which results in a high probability to accumulate mutations (Barker et al., 2009; Powell et al., 2012). In addition, recent analyses have provided further support for a direct role of stem cell abundance in the determination of tumor frequencies (Tomasetti and Vogelstein, 2015): i.e. a strong correlation was found between the tissue-specific stem cell number and the risk to develop a tumor for this particular tissue. Furthermore, cancer cells with stem cell characteristics are present in tumors of human colorectal cancer (CRC). Human CRC cells expressing the stem cell markers CD133 (O'Brien et al., 2007; Ricci-Vitiani et al., 2007) or CD44/CD166 (Dalerba et al., 2007) are able to induce tumors when injected into mice. These results show that tumors may have their origin in the stem cells of the intestinal crypt or at least in cells with stem cell like characteristics. Indeed, mutations in progenitor cells in the transit amplifying unit of the intestinal crypt are much less effective in tumor initiation than the stem cells in the crypt base, since *Apc* deletion in the transit amplifying (TA) cells are only causing microadenomas and very rarely macroadenomas (Barker et al., 2009). However, also differentiated cells may function as the origin of intestinal cancer as soon as they dedifferentiate into a stem-cell-like phenotype (Schwitalla et al., 2013).

Unexpectedly, deletion of *Ap4* in intestinal epithelial cells (IECs) had no effect on cellular proliferation. In contrast, acute deletion of *c-Myc* using *Ah-Cre* or *Villin-CreER* alleles in post-natal IECs resulted in defects in proliferation and biosynthetic activity in the small intestine (Bettess et al., 2005; Muncan et al., 2006). These divergent results may be due to the different timing of gene inactivation. Here we used either germ-line or *Villin-Cre* mediated deletion of *Ap4*. The latter leads to deletion of *Ap4* at embryonic day E12.5. However, the two studies on *c-Myc* employed deletion at least 7 days after birth and later which was necessary since *c-Myc* is essential during embryogenesis. They observed that IEC proliferation is at least in part independent of *c-Myc*. Therefore,

Discussion

IECs may rely on alternative pathways for promoting cell proliferation. In addition, these differences indicate that *Ap4* is responsible for mediating a distinct aspect of *c-Myc* function and does not simply perform all functions of *c-Myc*. *c-Myc* is a target gene of both the Wnt pathway (He et al., 1998) and the Notch pathway (Klinakis et al., 2006; Palomero et al., 2006; Sharma et al., 2006; Weng et al., 2006). Direct activation of *c-Myc* gene expression by using tamoxifen in *Villin-MycER^{TAM}* mice induces loss of Paneth and goblet cells (Finch et al., 2009). Since we showed that *Ap4*-deficiency leads to an increased Paneth cell number and *AP4* represents a direct target of *c-MYC* (Jung et al., 2008), the decrease of Paneth cells after *c-Myc* activation may be due to activation of *Ap4*. However, further analysis are necessary to support this hypothesis.

Notably, the deletion of *Ap4* resulted in decreased expression of Notch pathway components including Notch1 itself. Interestingly, Notch pathway inactivation promotes differentiation of intestinal stem cells into Paneth cells (VanDussen et al., 2012), leading to Paneth cell hyperplasia and a decrease in ISCs (Carulli et al., 2015; VanDussen et al., 2012). However, the number of goblet cells increases after Notch inhibition, whereas it decreased after *Ap4* inactivation in our study. Therefore, *Ap4* loss does not simply recapitulate inhibition of the Notch pathway suggesting that *Ap4* regulates additional pathways/genes, which contribute to the differentiation of goblet cells. For example, *Ap4*-deficiency resulted in a decrease in expression of the transcription factor *Spdef* (SAM pointed domain-containing Ets transcription factor). Interestingly, ectopic expression of *Spdef* in the murine intestine promotes the differentiation of goblet cells, while it decreases the number of Paneth cells (Noah et al., 2010). Accordingly, the decrease of *Spdef* observed in *Ap4*-deficient organoids could potentially also contribute to the decreased number of goblet cells detected after *Ap4* deletion. Alternatively, the decrease in goblet cells may have been a compensatory response to the increase in Paneth cells caused by *Ap4* deletion.

Additionally, a controlled balance of the Notch and Wnt pathway activity is important for the homeostasis of stem cells and cell fate decisions in the intestine and these two pathways regulate each other at multiple points (Tian et al., 2015). For example, activated Notch signaling does not lead to the expected cell proliferation after inhibition of Wnt signaling in *Tcf4* knock-out mice (Fre et al., 2009), showing the dependence on Wnt signaling for the effect of activated Notch signaling. The Notch and the Wnt signaling are linked to each other, since the expression of the Notch ligand *Jag1*

Discussion

(Rodilla et al., 2009) and other genes involved in Notch signaling (Ungerback et al., 2011) are regulated by Wnt signaling. Thereby, Wnt signaling can indirectly activate Notch signaling. Specifically, inhibition of Notch1/2 receptors induces Wnt-signaling, which then promotes goblet cell differentiation (Tian et al., 2015). The decrease of Wnt-pathway component expression after *Ap4* deletion may therefore alter the expected outcome of a Notch inhibition (i.e. increase of all secretory cell numbers) unto the decrease of goblet cell differentiation observed here.

In addition, the increased number of Paneth cells in *Ap4*-deficient mice might result from an increased propensity of *Ap4*-deficient ISCs to generate Paneth cell precursors during asymmetric stem cell division. Interestingly, *LGR5* represents an AP4 target gene in human CRC cell lines (Jackstadt et al., 2013c) and *Lgr5*-deficiency promotes Paneth cell differentiation in mice (Garcia et al., 2009).

Recently, it was shown that ablation of Lgr5-positive cells does not affect the tumor growth upon orthotopic transplantation of syngeneic tumor cells to the colon mucosal wall (de Sousa e Melo et al., 2017). Hence, Lgr5-positive cells seem to be dispensable after the initiation of adenomas. The tumor TA cells or, hypothetically, Lgr5-negative tumor stem cells, seem to be sufficient to maintain adenoma growth in the colon. Lgr5-positive cells are only indispensable to establish and maintain liver metastasis in this model. This is in agreement with the effects of *Ap4* inactivation observed here: a decreased number of ISCs and adenomas, whereas tumor cell proliferation and tumor size was not affected by *Ap4* deletion. In accordance, the results obtained in tumoroids derived from *Apc^{Min}* mice and in tumoroids generated by acute deletion of *Apc* imply that Ap4 is important for the initiation but not required for the maintenance of tumoroids. Interestingly, *Lgr5* gene expression has been reported previously to be dispensable for *ex vivo* tumor organoid maintenance (Sato et al., 2011a).

NOTCH signaling is involved in many different types of tumors including colon cancer (Akiyoshi et al., 2008; Sureban et al., 2008), pancreatic cancer (Kimura et al., 2007; Miyamoto et al., 2003; Terris et al., 2002; Wang et al., 2006), breast cancer (Reedijk et al., 2005; Stylianou et al., 2006), liver cancer (Gao et al., 2007; Qi et al., 2003) and lung cancer (Konishi et al., 2007). This may be due to regulation of important cancer-specific pathways, such as the Akt pathway (Efferson et al., 2010; Meurette et al., 2009), the Ras pathway (Fitzgerald et al., 2000) as well as the NF- κ B pathway (Cheng et al., 2001; Espinosa et al., 2002; Oswald et al., 1998; Wang et al., 2001). In CRC

Discussion

Notch signaling is important for intestinal tumor initiation, but not for tumor progression (Fre et al., 2009). A 20-fold increase in the number of adenomas was observed in mice with *Apc* mutation combined with *Notch* activation compared to *Apc* mutation alone. The acceleration of adenoma growth due to *Notch* activation may also be the case in human CRC, since *NOTCH* activation occurs in most adenomas in humans (Fre et al., 2009). Inhibition of NOTCH signaling leads to mitotic arrest and apoptosis in human colon cancer cells (Akiyoshi et al., 2008) as well as less tumor growth through inhibition of the formation of blood vessels by angiogenesis (Li et al., 2007; Noguera-Troise et al., 2006; Ridgway et al., 2006). Taken all these results in consideration, the Notch pathway may represent a route via which Ap4 promotes intestinal adenoma initiation.

Ectopic AP4 expression is sufficient to activate the WNT pathway in human CRC cell lines (Jackstadt et al., 2013c). Our NGS analysis presented here further supports these findings with *in vivo* evidence, since numerous components of the Wnt/ β -catenin signaling pathway were down-regulated in *Ap4*-deficient adenomas and derived organoids. In support of this conjecture, a comprehensive study has recently shown that Ap4 is an important component of Wnt signaling during *X. laevis* development and acts down-stream of the β -catenin destruction complex to regulate expression of Wnt/ β -catenin target genes (Lebensohn et al., 2016). Furthermore, AP4 is upregulated in human hepatocellular carcinoma (HCC), where it activates WNT/ β -CATENIN signaling to promote tumor growth and by this decreasing survival time (Song et al., 2018). Therefore, Ap4 presumably represents an integral component of the Wnt pathway and its activities during development and tumorigenesis. The down-regulation of genes involved in Wnt signaling observed here may critically contribute to the decreased number of ISCs observed in *Ap4*-deficient mice, since an activated Wnt pathway is necessary for the maintenance of stemness and suppression of differentiation in ISCs (Andreu et al., 2005; Pinto et al., 2003; van Es et al., 2005a).

Furthermore, Notch and Wnt signaling cooperate in tumorigenesis. Activation of Notch signaling works together with *Apc* mutation to induce adenoma formation in *Apc^{Min}* mice by maintenance of highly proliferative undifferentiated cells (van Es et al., 2005b). In addition, activation of Notch signaling increases the tumor load of Wnt-induced tumors and shortens the survival time in mice heterozygous for mutated *Apc* allele. This may be a result of the increased proliferation after *Notch* activation increasing the possibility of cancer promoting mutations in cancer initiating precursor

Discussion

cells as well as higher proliferation rate of already transformed cancer cells (Fre et al., 2009). Also, in human tumorigenesis, active WNT and NOTCH signaling cooperate in the initiation of CRC (Fre et al., 2009). The regulation of both pathways by Ap4 may contribute to the effects of *Ap4*-deletion in this study.

Recent studies identified Ap4 as important for maintaining a c-Myc-induced transcriptional program, which is critical for the function of activated B- and T-cells (Chou et al., 2014; Chou et al., 2016). Interestingly, we found that Ap4 may act upstream of c-Myc, as c-Myc expression in adenomas was decreased after deletion of *Ap4*. This effect is most likely due to a decrease in Wnt and/or Notch activity that resulted from the inactivation of *Ap4*, since *c-Myc* is a target gene of both pathways. c-Myc is known to be necessary for adenoma formation caused by deletion of *Apc* (Sansom et al., 2007; Sur et al., 2012). Furthermore, moderately reduced expression of c-Myc is sufficient to decrease the tumor load in *Apc^{Min}* mice without affecting adenoma size (Sur et al., 2012). Interestingly, this phenotype is reminiscent to the effect of *Ap4* deletion on adenoma formation described here. Therefore, the effects of *Ap4* deletion on adenoma formation in *Apc^{Min}* mice may at least in part result from a decrease in c-Myc expression.

AP4 has been shown to induce EMT (epithelial-mesenchymal-transition) in human CRC cells by regulating genes controlling this process and to promote metastasis in a xenograft model (Jackstadt et al., 2013c). The next-generation sequencing (NGS) results in this study show a tendency towards a decreased expression of genes involved in EMT in *Ap4*-deficient adenomas derived from *Apc^{Min}* mice. In addition, our results indicate a decrease of tumor stem cells in these adenomas. Interestingly, passage through an EMT is associated with the acquisition of stem cell traits (Mani et al., 2008). In line with this, cancer stem cells (CSCs) of the primary tumor may be the precursor for metastasis in different cancer types (Lawson et al., 2015; Odoux et al., 2008). These results suggest that Ap4 may promote EMT and metastasis by the maintenance of the stem cell-like characteristics of cancer cells. However, *Apc^{Min}* mice in a C57BL/6 background are not the adequate mouse model to analyze metastasis, since these mice do not develop metastasis (Halberg et al., 2009). In future, it will be necessary to analyse the role of Ap4 in the initiation of metastasis and the underlying mechanism.

Discussion

In addition, the *Ap4^{Min}* mouse model has the limitation that most tumors are located in the small intestine rather than in the colon. We assume that the decrease in the number of colonic stem cells in the absence of Ap4 would also translate into a decreased number of colorectal cancers if studied in a suitable mouse model. Similarly, in humans AP4 may also have a critical function in the control of colonic stem cell number and thereby influence the incidence of colorectal cancer. Since many mechanisms and pathways are conserved between small intestinal and colonic tumors, the results obtained in the mouse model used here may also provide insights into the biology of human CRCs and FAP, the inherited syndrome associated with germ-line *APC* mutations. Since the up-regulation of *AP4* in human CRC samples was associated with activation of the same signaling pathways that we identified in the mouse model, the findings presented here are likely to play a role in human CRC.

In conclusion, our study demonstrates an unexpected, central role of *Ap4* in ISC and Paneth cell homeostasis and reveals, that Ap4 function is critical for adenoma initiation in a preclinical model of inherited colon cancer. Besides illuminating an important aspect of CRC biology our results indicate that Ap4 represents a candidate therapeutic target for the treatment of CRCs.

Summary

7. Summary

The gene encoding the transcription factor TFAP4/AP4 represents a direct target of the c-MYC oncoprotein. AP4 contributes to the progression of colorectal cancer by regulating genes involved in proliferation and EMT (epithelial-mesenchymal transition). Previously we reported that AP4 is expressed in proliferating cells in human colonic crypts in a pattern similar to c-MYC. Also in human colorectal cancer, AP4 is highly expressed in proliferating cells. Taken together, these results suggested that AP4 may have an important function in intestinal homeostasis and carcinogenesis. In this study we deleted *Ap4* in *Apc^{Min}* mice, a preclinical model of inherited colorectal cancer. *Ap4*-deficiency extended their average survival by 110 days and decreased the formation of intestinal adenomas and tumor-derived organoids. Deletion of *Ap4* in the germ-line and in intestinal epithelial cells resulted in a reduced number of intestinal stem cells and a reciprocal increase in Paneth cells. The effects of *Ap4* deletion in *Apc^{Min}* mice are presumably due to the reduced number of functional intestinal stem cells amenable to adenoma initiating mutational events. Deletion of *Ap4* also decreased the number of colonic stem cells leading to a decrease of adenomas also in the colon. Expression profiling revealed that intestinal stem cell signatures, as well as the Wnt/ β -catenin and Notch signaling pathways are down-regulated in *Ap4*-deficient adenomas and intestinal organoids. Both the Wnt/ β -catenin and Notch signaling pathway are important for the maintenance of intestinal stem cells. The down-regulation of these pathways may be the cause of the lower number of intestinal stem cells in the crypt base in *Ap4*-deficient mice. *Ap4*-associated gene expression signatures are conserved between murine adenomas and human colorectal cancer samples. Our results establish *Ap4* as a rate limiting mediator of adenoma initiation as well as a regulator of intestinal stem cell and Paneth cell homeostasis.

8. Zusammenfassung

Das für den Transkriptionsfaktor TFAP4/AP4 kodierende Gen stellt ein direktes Ziel des c-MYC-Onkoproteins dar. AP4 trägt zur Progression von kolorektalem Krebs bei, indem es Gene reguliert, welche Proliferation und EMT (Epithial-mesenchymale-Transition) steuern. Zuvor berichteten wir, dass AP4 in proliferierenden Zellen in humanen Kolonkrypten ein ähnliches Expressionsmuster wie c-MYC hat. Auch beim kolorektalen Krebs im Menschen wird AP4 in proliferierenden Zellen stark exprimiert. Zusammenfassend legen diese Ergebnisse nahe, dass AP4 eine wichtige Funktion in der intestinalen Homöostase und Karzinogenese haben könnte. In der vorliegenden Studie haben wir *Ap4* in *Apc^{Min}*-Mäusen, einem präklinischen Modell des erblichen Kolorektalkarzinoms, deletiert. Der Verlust von *Ap4* verlängerte das durchschnittliche Überleben um 110 Tage und verringerte die Bildung von Adenomen im Darm und von Tumorzellen abgeleiteten Organoiden. Die Deletion von *Ap4* in der Keimbahn und in Darmepithelzellen führte zu einer verminderten Anzahl an intestinalen Stammzellen und einem reziproken Anstieg der Paneth-Zellen. Die Auswirkungen der *Ap4*-Deletion in *Apc^{Min}* Mäusen sind vermutlich auf die verringerte Anzahl von funktionellen intestinalen Stammzellen zurückzuführen, die für Adenom-initiiierende Mutationsereignisse zugänglich sind. Die Deletion von *Ap4* verringerte auch die Anzahl von Kolonstammzellen, was auch im Dickdarm zu einer Abnahme von Adenomen führte. Die Erstellung von Expressionsprofilen zeigte, dass intestinale Stammzell-Signaturen, sowie die Wnt/ β -Catenin- und Notch-Signalwege, in *Ap4*-defizienten Adenomen und intestinalen Organoiden herabreguliert sind. Sowohl der Wnt/ β -Catenin- als auch der Notch-Signalweg ist wichtig für den Erhalt von intestinalen Stammzellen. Die Herunterregulierung dieser Signalwege könnte die Ursache für die geringere Anzahl von intestinalen Stammzellen an der Kryptenbase in *Ap4*-defizienten Mäusen sein. *Ap4*-assoziierte Gen-Expressions-Signaturen sind zwischen murinen Adenomen und humanen kolorektalen Krebsproben konserviert. Unsere Ergebnisse etablieren *Ap4* als limitierenden Mediator der Adenom-Initiation, sowie als Regulator der Homöostase von intestinalen Stammzellen und Paneth-Zellen.

Acknowledgements

9. Acknowledgements

My deepest gratitude goes to my supervisor Prof. Dr. Heiko Hermeking for the interesting project and his advice, support and scientific input during my doctoral study.

Many thanks go to Dr. Markus Kaller for the bioinformatics analyses and associated figures as well as for advices and discussions about my project.

I would like to thank Ursula Götz for her technical support in the laboratory and her support in breeding of mice as well as for her help in the establishment of primary antibodies for immunohistochemistry and in performing immunohistochemical stainings.

I also would like to thank Dr. Peter Jung for the organoid culture protocols, the advices and supports for organoid experiments as well as for discussions about my results.

In addition, I would like to acknowledge all the other people supporting my doctoral work:

Prof. Dr. med. David Horst for the paraffin slides from human CRC cohorts and the DBZ treatment of mice.

Dr. Rene Jackstadt for the human CRC cell culture work and the associated figures.

People working in the pathological entrance laboratory for the dehydration of the mouse tissues, help with histological staining, performing immunohistochemistry on slides from human CRC cohorts and for allowing me to cut my paraffin blocks at their microtomes.

Andrea Sendelhofert and Anja Heier for their help in immunohistochemistry in establishment primary antibodies.

Dr. med. Susanna Müller and Sabine Schäfer for electron microscopic analysis and preparation of intestinal tissue for electron microscopy, respectively.

Additionally, I would like to thank all colleagues from AG Hermeking and all other people from the institute for a good time during my doctoral work. Many thanks to my mother and grandmother always motivating me during my doctoral time.

References

10. References

- Akiyoshi, T., Nakamura, M., Yanai, K., Nagai, S., Wada, J., Koga, K., Nakashima, H., Sato, N., Tanaka, M., and Katano, M. (2008). Gamma-secretase inhibitors enhance taxane-induced mitotic arrest and apoptosis in colon cancer cells. *Gastroenterology* *134*, 131-144.
- Andreu, P., Colnot, S., Godard, C., Gad, S., Chafey, P., Niwa-Kawakita, M., Laurent-Puig, P., Kahn, A., Robine, S., Perret, C., *et al.* (2005). Crypt-restricted proliferation and commitment to the Paneth cell lineage following Apc loss in the mouse intestine. *Development* *132*, 1443-1451.
- Barker, N. (2014). Adult intestinal stem cells: critical drivers of epithelial homeostasis and regeneration. *Nat Rev Mol Cell Biol* *15*, 19-33.
- Barker, N., and Clevers, H. (2007). Tracking down the stem cells of the intestine: strategies to identify adult stem cells. *Gastroenterology* *133*, 1755-1760.
- Barker, N., Ridgway, R.A., van Es, J.H., van de Wetering, M., Begthel, H., van den Born, M., Danenberg, E., Clarke, A.R., Sansom, O.J., and Clevers, H. (2009). Crypt stem cells as the cells-of-origin of intestinal cancer. *Nature* *457*, 608-611.
- Barker, N., van Es, J.H., Kuipers, J., Kujala, P., van den Born, M., Cozijnsen, M., Haegebarth, A., Korving, J., Begthel, H., Peters, P.J., *et al.* (2007). Identification of stem cells in small intestine and colon by marker gene Lgr5. *Nature* *449*, 1003-1007.
- Batlle, E., Henderson, J.T., Beghtel, H., van den Born, M.M., Sancho, E., Huls, G., Meeldijk, J., Robertson, J., van de Wetering, M., Pawson, T., *et al.* (2002). Beta-catenin and TCF mediate cell positioning in the intestinal epithelium by controlling the expression of EphB/ephrinB. *Cell* *111*, 251-263.
- Bettesse, M.D., Dubois, N., Murphy, M.J., Dubey, C., Roger, C., Robine, S., and Trumpp, A. (2005). c-Myc is required for the formation of intestinal crypts but dispensable for homeostasis of the adult intestinal epithelium. *Mol Cell Biol* *25*, 7868-7878.
- Beumer, J., and Clevers, H. (2016). Regulation and plasticity of intestinal stem cells during homeostasis and regeneration. *Development* *143*, 3639-3649.
- Buczacki, S.J., Zecchini, H.I., Nicholson, A.M., Russell, R., Vermeulen, L., Kemp, R., and Winton, D.J. (2013). Intestinal label-retaining cells are secretory precursors expressing Lgr5. *Nature* *495*, 65-69.
- Cancer Genome Atlas, N. (2012). Comprehensive molecular characterization of human colon and rectal cancer. *Nature* *487*, 330-337.
- Carulli, A.J., Keeley, T.M., Demitrack, E.S., Chung, J., Maillard, I., and Samuelson, L.C. (2015). Notch receptor regulation of intestinal stem cell homeostasis and crypt regeneration. *Dev Biol* *402*, 98-108.

References

- Cheng, P., Zlobin, A., Volgina, V., Gottipati, S., Osborne, B., Simel, E.J., Miele, L., and Gabrilovich, D.I. (2001). Notch-1 regulates NF-kappaB activity in hemopoietic progenitor cells. *J Immunol* *167*, 4458-4467.
- Chou, C., Pinto, A.K., Curtis, J.D., Persaud, S.P., Cella, M., Lin, C.C., Edelson, B.T., Allen, P.M., Colonna, M., Pearce, E.L., *et al.* (2014). c-Myc-induced transcription factor AP4 is required for host protection mediated by CD8+ T cells. *Nat Immunol* *15*, 884-893.
- Chou, C., Verbaro, D.J., Tonc, E., Holmgren, M., Cella, M., Colonna, M., Bhattacharya, D., and Egawa, T. (2016). The Transcription Factor AP4 Mediates Resolution of Chronic Viral Infection through Amplification of Germinal Center B Cell Responses. *Immunity* *45*, 570-582.
- Chu, D., Zhang, Z., Zhou, Y., Wang, W., Li, Y., Zhang, H., Dong, G., Zhao, Q., and Ji, G. (2011). Notch1 and Notch2 have opposite prognostic effects on patients with colorectal cancer. *Ann Oncol* *22*, 2440-2447.
- Clevers, H. (2006). Wnt/beta-catenin signaling in development and disease. *Cell* *127*, 469-480.
- Clevers, H., Loh, K.M., and Nusse, R. (2014). Stem cell signaling. An integral program for tissue renewal and regeneration: Wnt signaling and stem cell control. *Science* *346*, 1248012.
- Clevers, H., and Nusse, R. (2012). Wnt/beta-catenin signaling and disease. *Cell* *149*, 1192-1205.
- Clevers, H.C., and Bevins, C.L. (2013). Paneth cells: maestros of the small intestinal crypts. *Annu Rev Physiol* *75*, 289-311.
- D'Annibale, S., Kim, J., Magliozzi, R., Low, T.Y., Mohammed, S., Heck, A.J., and Guardavaccaro, D. (2014). Proteasome-dependent Degradation of Transcription Factor Activating Enhancer-binding Protein 4 (TFAP4) Controls Mitotic Division. *J Biol Chem* *289*, 7730-7737.
- Dalerba, P., Dylla, S.J., Park, I.K., Liu, R., Wang, X., Cho, R.W., Hoey, T., Gurney, A., Huang, E.H., Simeone, D.M., *et al.* (2007). Phenotypic characterization of human colorectal cancer stem cells. *Proc Natl Acad Sci U S A* *104*, 10158-10163.
- de Lau, W., Barker, N., Low, T.Y., Koo, B.K., Li, V.S., Teunissen, H., Kujala, P., Haegebarth, A., Peters, P.J., van de Wetering, M., *et al.* (2011). Lgr5 homologues associate with Wnt receptors and mediate R-spondin signalling. *Nature* *476*, 293-297.
- de Sousa e Melo, F., Kurtova, A.V., Harnoss, J.M., Kljavin, N., Hoeck, J.D., Hung, J., Anderson, J.E., Storm, E.E., Modrusan, Z., Koeppen, H., *et al.* (2017). A distinct role for Lgr5(+) stem cells in primary and metastatic colon cancer. *Nature* *543*, 676-680.

References

- Efferson, C.L., Winkelmann, C.T., Ware, C., Sullivan, T., Giampaoli, S., Tammam, J., Patel, S., Mesiti, G., Reilly, J.F., Gibson, R.E., *et al.* (2010). Downregulation of Notch pathway by a gamma-secretase inhibitor attenuates AKT/mammalian target of rapamycin signaling and glucose uptake in an ERBB2 transgenic breast cancer model. *Cancer Res* 70, 2476-2484.
- el Marjou, F., Janssen, K.P., Chang, B.H., Li, M., Hindie, V., Chan, L., Louvard, D., Chambon, P., Metzger, D., and Robine, S. (2004). Tissue-specific and inducible Cre-mediated recombination in the gut epithelium. *Genesis* 39, 186-193.
- Espinosa, L., Santos, S., Ingles-Esteve, J., Munoz-Canoves, P., and Bigas, A. (2002). p65-NFkappaB synergizes with Notch to activate transcription by triggering cytoplasmic translocation of the nuclear receptor corepressor N-CoR. *J Cell Sci* 115, 1295-1303.
- Fearon, E.R., and Vogelstein, B. (1990). A genetic model for colorectal tumorigenesis. *Cell* 61, 759-767.
- Fevr, T., Robine, S., Louvard, D., and Huelsken, J. (2007). Wnt/beta-catenin is essential for intestinal homeostasis and maintenance of intestinal stem cells. *Mol Cell Biol* 27, 7551-7559.
- Finch, A.J., Soucek, L., Junttila, M.R., Swigart, L.B., and Evan, G.I. (2009). Acute overexpression of Myc in intestinal epithelium recapitulates some but not all the changes elicited by Wnt/beta-catenin pathway activation. *Mol Cell Biol* 29, 5306-5315.
- Fitzgerald, K., Harrington, A., and Leder, P. (2000). Ras pathway signals are required for notch-mediated oncogenesis. *Oncogene* 19, 4191-4198.
- Frank, S.R., Schroeder, M., Fernandez, P., Taubert, S., and Amati, B. (2001). Binding of c-Myc to chromatin mediates mitogen-induced acetylation of histone H4 and gene activation. *Genes Dev* 15, 2069-2082.
- Fre, S., Huyghe, M., Mourikis, P., Robine, S., Louvard, D., and Artavanis-Tsakonas, S. (2005). Notch signals control the fate of immature progenitor cells in the intestine. *Nature* 435, 964-968.
- Fre, S., Pallavi, S.K., Huyghe, M., Lae, M., Janssen, K.P., Robine, S., Artavanis-Tsakonas, S., and Louvard, D. (2009). Notch and Wnt signals cooperatively control cell proliferation and tumorigenesis in the intestine. *Proc Natl Acad Sci U S A* 106, 6309-6314.
- Gao, J., Chen, C., Hong, L., Wang, J., Du, Y., Song, J., Shao, X., Zhang, J., Han, H., Liu, J., *et al.* (2007). Expression of Jagged1 and its association with hepatitis B virus X protein in hepatocellular carcinoma. *Biochem Biophys Res Commun* 356, 341-347.
- Garcia, M.I., Ghiani, M., Lefort, A., Libert, F., Strollo, S., and Vassart, G. (2009). LGR5 deficiency deregulates Wnt signaling and leads to precocious Paneth cell differentiation in the fetal intestine. *Dev Biol* 331, 58-67.

References

- Gong, H., Han, S., Yao, H., Zhao, H., and Wang, Y. (2014). AP4 predicts poor prognosis in nonsmall cell lung cancer. *Mol Med Rep* 10, 336-340.
- Gregorieff, A., and Clevers, H. (2005). Wnt signaling in the intestinal epithelium: from endoderm to cancer. *Genes Dev* 19, 877-890.
- Gregorieff, A., and Clevers, H. (2010). In situ hybridization to identify gut stem cells. *Curr Protoc Stem Cell Biol Chapter 2, Unit 2F 1*.
- Gronostajski, R.M., and Sadowski, P.D. (1985). The FLP recombinase of the *Saccharomyces cerevisiae* 2 microns plasmid attaches covalently to DNA via a phosphotyrosyl linkage. *Mol Cell Biol* 5, 3274-3279.
- Guillen-Ahlers, H., Suckow, M.A., Castellino, F.J., and Ploplis, V.A. (2010). Fas/CD95 deficiency in *ApcMin/+* mice increases intestinal tumor burden. *PLoS One* 5, e9070.
- Guinney, J., Dienstmann, R., Wang, X., de Reynies, A., Schlicker, A., Song, C., Marisa, L., Roepman, P., Nyamundanda, G., Angelino, P., *et al.* (2015). The consensus molecular subtypes of colorectal cancer. *Nat Med* 21, 1350-1356.
- Halberg, R.B., Waggoner, J., Rasmussen, K., White, A., Clipson, L., Prunuske, A.J., Bacher, J.W., Sullivan, R., Washington, M.K., Pitot, H.C., *et al.* (2009). Long-lived *Min* mice develop advanced intestinal cancers through a genetically conservative pathway. *Cancer Res* 69, 5768-5775.
- Hanahan, D., and Weinberg, R.A. (2000). The hallmarks of cancer. *Cell* 100, 57-70.
- Hanahan, D., and Weinberg, R.A. (2011). Hallmarks of cancer: the next generation. *Cell* 144, 646-674.
- He, T.C., Sparks, A.B., Rago, C., Hermeking, H., Zawel, L., da Costa, L.T., Morin, P.J., Vogelstein, B., and Kinzler, K.W. (1998). Identification of c-MYC as a target of the APC pathway. *Science* 281, 1509-1512.
- Heinz, S., Benner, C., Spann, N., Bertolino, E., Lin, Y.C., Laslo, P., Cheng, J.X., Murre, C., Singh, H., and Glass, C.K. (2010). Simple combinations of lineage-determining transcription factors prime cis-regulatory elements required for macrophage and B cell identities. *Mol Cell* 38, 576-589.
- Hoshiko, S., Kawaguchi, M., Fukushima, T., Haruyama, Y., Yorita, K., Tanaka, H., Seiki, M., Inatsu, H., Kitamura, K., and Kataoka, H. (2013). Hepatocyte growth factor activator inhibitor type 1 is a suppressor of intestinal tumorigenesis. *Cancer Res* 73, 2659-2670.
- Hu, B.S., Zhao, G., Yu, H.F., Chen, K., Dong, J.H., and Tan, J.W. (2013). High expression of AP-4 predicts poor prognosis for hepatocellular carcinoma after curative hepatectomy. *Tumour Biol* 34, 271-276.

References

- Huels, D.J., Bruens, L., Hodder, M.C., Cammareri, P., Campbell, A.D., Ridgway, R.A., Gay, D.M., Solar-Abboud, M., Faller, W.J., Nixon, C., *et al.* (2018). Wnt ligands influence tumour initiation by controlling the number of intestinal stem cells. *Nat Commun* 9, 1132.
- Jackstadt, R., Jung, P., and Hermeking, H. (2013a). AP4 directly downregulates p16 and p21 to suppress senescence and mediate transformation. *Cell Death Dis* 4, e775.
- Jackstadt, R., Menssen, A., and Hermeking, H. (2013b). Genome-wide analysis of c-MYC-regulated mRNAs and miRNAs, and c-MYC DNA binding by next-generation sequencing. *Methods Mol Biol* 1012, 145-185.
- Jackstadt, R., Roh, S., Neumann, J., Jung, P., Hoffmann, R., Horst, D., Berens, C., Bornkamm, G.W., Kirchner, T., Menssen, A., *et al.* (2013c). AP4 is a mediator of epithelial-mesenchymal transition and metastasis in colorectal cancer. *J Exp Med* 210, 1331-1350.
- Jaeckel, S., Kaller, M., Jackstadt, R., Gotz, U., Muller, S., Boos, S., Horst, D., Jung, P., and Hermeking, H. (2018). Ap4 is rate limiting for intestinal tumor formation by controlling the homeostasis of intestinal stem cells. *Nat Commun* 9, 3573.
- Jarriault, S., Brou, C., Logeat, F., Schroeter, E.H., Kopan, R., and Israel, A. (1995). Signalling downstream of activated mammalian Notch. *Nature* 377, 355-358.
- Jarriault, S., Le Bail, O., Hirsinger, E., Pourquie, O., Logeat, F., Strong, C.F., Brou, C., Seidah, N.G., and Israel, A. (1998). Delta-1 activation of notch-1 signaling results in HES-1 transactivation. *Mol Cell Biol* 18, 7423-7431.
- Jensen, J., Pedersen, E.E., Galante, P., Hald, J., Heller, R.S., Ishibashi, M., Kageyama, R., Guillemot, F., Serup, P., and Madsen, O.D. (2000). Control of endodermal endocrine development by Hes-1. *Nat Genet* 24, 36-44.
- Jung, P., and Hermeking, H. (2009). The c-MYC-AP4-p21 cascade. *Cell Cycle* 8, 982-989.
- Jung, P., Menssen, A., Mayr, D., and Hermeking, H. (2008). AP4 encodes a c-MYC-inducible repressor of p21. *Proc Natl Acad Sci U S A* 105, 15046-15051.
- Kayahara, T., Sawada, M., Takaishi, S., Fukui, H., Seno, H., Fukuzawa, H., Suzuki, K., Hiai, H., Kageyama, R., Okano, H., *et al.* (2003). Candidate markers for stem and early progenitor cells, Musashi-1 and Hes1, are expressed in crypt base columnar cells of mouse small intestine. *FEBS Lett* 535, 131-135.
- Kent, W.J., Sugnet, C.W., Furey, T.S., Roskin, K.M., Pringle, T.H., Zahler, A.M., and Haussler, D. (2002). The human genome browser at UCSC. *Genome Res* 12, 996-1006.

References

- Kimura, K., Satoh, K., Kanno, A., Hamada, S., Hirota, M., Endoh, M., Masamune, A., and Shimosegawa, T. (2007). Activation of Notch signaling in tumorigenesis of experimental pancreatic cancer induced by dimethylbenzanthracene in mice. *Cancer Sci* 98, 155-162.
- Kinzler, K.W., and Vogelstein, B. (1996). Lessons from hereditary colorectal cancer. *Cell* 87, 159-170.
- Klinakis, A., Szabolcs, M., Politi, K., Kiaris, H., Artavanis-Tsakonas, S., and Efstratiadis, A. (2006). Myc is a Notch1 transcriptional target and a requisite for Notch1-induced mammary tumorigenesis in mice. *Proc Natl Acad Sci U S A* 103, 9262-9267.
- Konishi, J., Kawaguchi, K.S., Vo, H., Haruki, N., Gonzalez, A., Carbone, D.P., and Dang, T.P. (2007). Gamma-secretase inhibitor prevents Notch3 activation and reduces proliferation in human lung cancers. *Cancer Res* 67, 8051-8057.
- Korinek, V., Barker, N., Moerer, P., van Donselaar, E., Huls, G., Peters, P.J., and Clevers, H. (1998). Depletion of epithelial stem-cell compartments in the small intestine of mice lacking Tcf-4. *Nat Genet* 19, 379-383.
- Kuhnert, F., Davis, C.R., Wang, H.T., Chu, P., Lee, M., Yuan, J., Nusse, R., and Kuo, C.J. (2004). Essential requirement for Wnt signaling in proliferation of adult small intestine and colon revealed by adenoviral expression of Dickkopf-1. *Proc Natl Acad Sci U S A* 101, 266-271.
- Lawson, D.A., Bhakta, N.R., Kessenbrock, K., Prummel, K.D., Yu, Y., Takai, K., Zhou, A., Eyob, H., Balakrishnan, S., Wang, C.Y., *et al.* (2015). Single-cell analysis reveals a stem-cell program in human metastatic breast cancer cells. *Nature* 526, 131-135.
- Lebensohn, A.M., Dubey, R., Neitzel, L.R., Tacchelly-Benites, O., Yang, E., Marceau, C.D., Davis, E.M., Patel, B.B., Bahrami-Nejad, Z., Travaglini, K.J., *et al.* (2016). Comparative genetic screens in human cells reveal new regulatory mechanisms in WNT signaling. *Elife* 5.
- Li, J.L., Sainson, R.C., Shi, W., Leek, R., Harrington, L.S., Preusser, M., Biswas, S., Turley, H., Heikamp, E., Hainfellner, J.A., *et al.* (2007). Delta-like 4 Notch ligand regulates tumor angiogenesis, improves tumor vascular function, and promotes tumor growth in vivo. *Cancer Res* 67, 11244-11253.
- Li, Y., Hibbs, M.A., Gard, A.L., Shylo, N.A., and Yun, K. (2012). Genome-wide analysis of N1ICD/RBPJ targets in vivo reveals direct transcriptional regulation of Wnt, SHH, and hippo pathway effectors by Notch1. *Stem Cells* 30, 741-752.
- Li, Y., Yang, Y., Li, J., Liu, H., Chen, F., Li, B., Cui, B., and Liu, Y. (2017). USP22 drives colorectal cancer invasion and metastasis via epithelial-mesenchymal transition by activating AP4. *Oncotarget* 8, 32683-32695.

References

- Liberzon, A., Birger, C., Thorvaldsdottir, H., Ghandi, M., Mesirov, J.P., and Tamayo, P. (2015). The Molecular Signatures Database (MSigDB) hallmark gene set collection. *Cell Syst* 1, 417-425.
- Love, M.I., Huber, W., and Anders, S. (2014). Moderated estimation of fold change and dispersion for RNA-seq data with DESeq2. *Genome Biol* 15, 550.
- Ma, W., Liu, B., Li, J., Jiang, J., Zhou, R., Huang, L., Li, X., He, X., and Zhou, Q. (2018). MicroRNA-302c represses epithelial-mesenchymal transition and metastasis by targeting transcription factor AP-4 in colorectal cancer. *Biomed Pharmacother* 105, 670-676.
- Mani, S.A., Guo, W., Liao, M.J., Eaton, E.N., Ayyanan, A., Zhou, A.Y., Brooks, M., Reinhard, F., Zhang, C.C., Shipitsin, M., *et al.* (2008). The epithelial-mesenchymal transition generates cells with properties of stem cells. *Cell* 133, 704-715.
- McCarthy, D.J., Chen, Y., and Smyth, G.K. (2012). Differential expression analysis of multifactor RNA-Seq experiments with respect to biological variation. *Nucleic Acids Res* 40, 4288-4297.
- Menssen, A., Epanchintsev, A., Lodygin, D., Rezaei, N., Jung, P., Verdoodt, B., Diebold, J., and Hermeking, H. (2007). c-MYC delays prometaphase by direct transactivation of MAD2 and BubR1: identification of mechanisms underlying c-MYC-induced DNA damage and chromosomal instability. *Cell Cycle* 6, 339-352.
- Merlos-Suarez, A., Barriga, F.M., Jung, P., Iglesias, M., Cespedes, M.V., Rossell, D., Sevillano, M., Hernando-Mombona, X., da Silva-Diz, V., Munoz, P., *et al.* (2011). The intestinal stem cell signature identifies colorectal cancer stem cells and predicts disease relapse. *Cell Stem Cell* 8, 511-524.
- Meurette, O., Stylianou, S., Rock, R., Collu, G.M., Gilmore, A.P., and Brennan, K. (2009). Notch activation induces Akt signaling via an autocrine loop to prevent apoptosis in breast epithelial cells. *Cancer Res* 69, 5015-5022.
- Miyamoto, Y., Maitra, A., Ghosh, B., Zechner, U., Argani, P., Iacobuzio-Donahue, C.A., Sriuranpong, V., Iso, T., Meszoely, I.M., Wolfe, M.S., *et al.* (2003). Notch mediates TGF alpha-induced changes in epithelial differentiation during pancreatic tumorigenesis. *Cancer Cell* 3, 565-576.
- Moser, A.R., Pitot, H.C., and Dove, W.F. (1990). A dominant mutation that predisposes to multiple intestinal neoplasia in the mouse. *Science* 247, 322-324.
- Muncan, V., Sansom, O.J., Tertoolen, L., Phesse, T.J., Begthel, H., Sancho, E., Cole, A.M., Gregorieff, A., de Alboran, I.M., Clevers, H., *et al.* (2006). Rapid loss of intestinal crypts upon conditional deletion of the Wnt/Tcf-4 target gene c-Myc. *Mol Cell Biol* 26, 8418-8426.

References

- Munoz, J., Stange, D.E., Schepers, A.G., van de Wetering, M., Koo, B.K., Itzkovitz, S., Volckmann, R., Kung, K.S., Koster, J., Radulescu, S., *et al.* (2012). The Lgr5 intestinal stem cell signature: robust expression of proposed quiescent '+4' cell markers. *EMBO J* 31, 3079-3091.
- Noah, T.K., Kazanjian, A., Whitsett, J., and Shroyer, N.F. (2010). SAM pointed domain ETS factor (SPDEF) regulates terminal differentiation and maturation of intestinal goblet cells. *Experimental Cell Research* 316, 452-465.
- Noah, T.K., and Shroyer, N.F. (2013). Notch in the intestine: regulation of homeostasis and pathogenesis. *Annu Rev Physiol* 75, 263-288.
- Noguera-Troise, I., Daly, C., Papadopoulos, N.J., Coetzee, S., Boland, P., Gale, N.W., Lin, H.C., Yancopoulos, G.D., and Thurston, G. (2006). Blockade of Dll4 inhibits tumour growth by promoting non-productive angiogenesis. *Nature* 444, 1032-1037.
- O'Brien, C.A., Pollett, A., Gallinger, S., and Dick, J.E. (2007). A human colon cancer cell capable of initiating tumour growth in immunodeficient mice. *Nature* 445, 106-110.
- Odoux, C., Fohrer, H., Hoppo, T., Guzik, L., Stolz, D.B., Lewis, D.W., Gollin, S.M., Gamblin, T.C., Geller, D.A., and Lagasse, E. (2008). A stochastic model for cancer stem cell origin in metastatic colon cancer. *Cancer Res* 68, 6932-6941.
- Oswald, F., Liptay, S., Adler, G., and Schmid, R.M. (1998). NF-kappaB2 is a putative target gene of activated Notch-1 via RBP-Jkappa. *Mol Cell Biol* 18, 2077-2088.
- Oswald, F., Tauber, B., Dobner, T., Bourteele, S., Kostezka, U., Adler, G., Liptay, S., and Schmid, R.M. (2001). p300 acts as a transcriptional coactivator for mammalian Notch-1. *Mol Cell Biol* 21, 7761-7774.
- Palomero, T., Lim, W.K., Odom, D.T., Sulis, M.L., Real, P.J., Margolin, A., Barnes, K.C., O'Neil, J., Neuberg, D., Weng, A.P., *et al.* (2006). NOTCH1 directly regulates c-MYC and activates a feed-forward-loop transcriptional network promoting leukemic cell growth. *Proc Natl Acad Sci U S A* 103, 18261-18266.
- Payne, J.E. (1990). Colorectal carcinogenesis. *Aust N Z J Surg* 60, 11-18.
- Pellegrinet, L., Rodilla, V., Liu, Z., Chen, S., Koch, U., Espinosa, L., Kaestner, K.H., Kopan, R., Lewis, J., and Radtke, F. (2011). Dll1- and dll4-mediated notch signaling are required for homeostasis of intestinal stem cells. *Gastroenterology* 140, 1230-1240 e1231-1237.
- Pinto, D., Gregorieff, A., Begthel, H., and Clevers, H. (2003). Canonical Wnt signals are essential for homeostasis of the intestinal epithelium. *Genes Dev* 17, 1709-1713.

References

- Powell, A.E., Wang, Y., Li, Y., Poulin, E.J., Means, A.L., Washington, M.K., Higginbotham, J.N., Juchheim, A., Prasad, N., Levy, S.E., *et al.* (2012). The pan-ErbB negative regulator Lrig1 is an intestinal stem cell marker that functions as a tumor suppressor. *Cell* 149, 146-158.
- Powell, S.M., Petersen, G.M., Krush, A.J., Booker, S., Jen, J., Giardiello, F.M., Hamilton, S.R., Vogelstein, B., and Kinzler, K.W. (1993). Molecular diagnosis of familial adenomatous polyposis. *N Engl J Med* 329, 1982-1987.
- Qi, R., An, H., Yu, Y., Zhang, M., Liu, S., Xu, H., Guo, Z., Cheng, T., and Cao, X. (2003). Notch1 signaling inhibits growth of human hepatocellular carcinoma through induction of cell cycle arrest and apoptosis. *Cancer Res* 63, 8323-8329.
- Reedijk, M., Odorcic, S., Chang, L., Zhang, H., Miller, N., McCreedy, D.R., Lockwood, G., and Egan, S.E. (2005). High-level coexpression of JAG1 and NOTCH1 is observed in human breast cancer and is associated with poor overall survival. *Cancer Res* 65, 8530-8537.
- Ricci-Vitiani, L., Lombardi, D.G., Pilozzi, E., Biffoni, M., Todaro, M., Peschle, C., and De Maria, R. (2007). Identification and expansion of human colon-cancer-initiating cells. *Nature* 445, 111-115.
- Riccio, O., van Gijn, M.E., Bezdek, A.C., Pellegrinet, L., van Es, J.H., Zimmer-Strobl, U., Strobl, L.J., Honjo, T., Clevers, H., and Radtke, F. (2008). Loss of intestinal crypt progenitor cells owing to inactivation of both Notch1 and Notch2 is accompanied by derepression of CDK inhibitors p27Kip1 and p57Kip2. *EMBO Rep* 9, 377-383.
- Ridgway, J., Zhang, G., Wu, Y., Stawicki, S., Liang, W.C., Chantry, Y., Kowalski, J., Watts, R.J., Callahan, C., Kasman, I., *et al.* (2006). Inhibition of Dll4 signalling inhibits tumour growth by deregulating angiogenesis. *Nature* 444, 1083-1087.
- Risso, D., Ngai, J., Speed, T.P., and Dudoit, S. (2014). Normalization of RNA-seq data using factor analysis of control genes or samples. *Nature biotechnology* 32, 896-902.
- Robinson, M.D., McCarthy, D.J., and Smyth, G.K. (2010). edgeR: a Bioconductor package for differential expression analysis of digital gene expression data. *Bioinformatics* 26, 139-140.
- Rodilla, V., Villanueva, A., Obrador-Hevia, A., Robert-Moreno, A., Fernandez-Majada, V., Grilli, A., Lopez-Bigas, N., Bellora, N., Alba, M.M., Torres, F., *et al.* (2009). Jagged1 is the pathological link between Wnt and Notch pathways in colorectal cancer. *Proc Natl Acad Sci U S A* 106, 6315-6320.
- Sancho, E., Batlle, E., and Clevers, H. (2004). Signaling pathways in intestinal development and cancer. *Annu Rev Cell Dev Biol* 20, 695-723.
- Sangiorgi, E., and Capecchi, M.R. (2008). Bmi1 is expressed in vivo in intestinal stem cells. *Nat Genet* 40, 915-920.

References

- Sansom, O.J., Meniel, V.S., Muncan, V., Pheese, T.J., Wilkins, J.A., Reed, K.R., Vass, J.K., Athineos, D., Clevers, H., and Clarke, A.R. (2007). Myc deletion rescues Apc deficiency in the small intestine. *Nature* **446**, 676-679.
- Sasaki, N., Sachs, N., Wiebrands, K., Ellenbroek, S.I., Fumagalli, A., Lyubimova, A., Begthel, H., van den Born, M., van Es, J.H., Karthaus, W.R., *et al.* (2016). Reg4+ deep crypt secretory cells function as epithelial niche for Lgr5+ stem cells in colon. *Proc Natl Acad Sci U S A* **113**, E5399-5407.
- Sato, T., and Clevers, H. (2013). Growing self-organizing mini-guts from a single intestinal stem cell: mechanism and applications. *Science* **340**, 1190-1194.
- Sato, T., Stange, D.E., Ferrante, M., Vries, R.G., Van Es, J.H., Van den Brink, S., Van Houdt, W.J., Pronk, A., Van Gorp, J., Siersema, P.D., *et al.* (2011a). Long-term expansion of epithelial organoids from human colon, adenoma, adenocarcinoma, and Barrett's epithelium. *Gastroenterology* **141**, 1762-1772.
- Sato, T., van Es, J.H., Snippert, H.J., Stange, D.E., Vries, R.G., van den Born, M., Barker, N., Shroyer, N.F., van de Wetering, M., and Clevers, H. (2011b). Paneth cells constitute the niche for Lgr5 stem cells in intestinal crypts. *Nature* **469**, 415-418.
- Sato, T., Vries, R.G., Snippert, H.J., van de Wetering, M., Barker, N., Stange, D.E., van Es, J.H., Abo, A., Kujala, P., Peters, P.J., *et al.* (2009). Single Lgr5 stem cells build crypt-villus structures in vitro without a mesenchymal niche. *Nature* **459**, 262-265.
- Schepers, A.G., Snippert, H.J., Stange, D.E., van den Born, M., van Es, J.H., van de Wetering, M., and Clevers, H. (2012). Lineage tracing reveals Lgr5+ stem cell activity in mouse intestinal adenomas. *Science* **337**, 730-735.
- Schwenk, F., Baron, U., and Rajewsky, K. (1995). A cre-transgenic mouse strain for the ubiquitous deletion of loxP-flanked gene segments including deletion in germ cells. *Nucleic Acids Res* **23**, 5080-5081.
- Schwitalla, S., Fingerle, A.A., Cammareri, P., Nebelsiek, T., Goktuna, S.I., Ziegler, P.K., Canli, O., Heijmans, J., Huels, D.J., Moreaux, G., *et al.* (2013). Intestinal tumorigenesis initiated by dedifferentiation and acquisition of stem-cell-like properties. *Cell* **152**, 25-38.
- Serafin, V., Persano, L., Moserle, L., Esposito, G., Ghisi, M., Curtarello, M., Bonanno, L., Masiero, M., Ribatti, D., Sturzl, M., *et al.* (2011). Notch3 signalling promotes tumour growth in colorectal cancer. *J Pathol* **224**, 448-460.
- Sharma, V.M., Calvo, J.A., Draheim, K.M., Cunningham, L.A., Hermance, N., Beverly, L., Krishnamoorthy, V., Bhasin, M., Capobianco, A.J., and Kelliher, M.A. (2006). Notch1 contributes to mouse T-cell leukemia by directly inducing the expression of c-myc. *Mol Cell Biol* **26**, 8022-8031.

References

- Shi, L., Jackstadt, R., Siemens, H., Li, H., Kirchner, T., and Hermeking, H. (2014). p53-induced miR-15a/16-1 and AP4 form a double-negative feedback loop to regulate epithelial-mesenchymal transition and metastasis in colorectal cancer. *Cancer Res* 74, 532-542.
- Siemens, H., Jackstadt, R., Hunten, S., Kaller, M., Menssen, A., Gotz, U., and Hermeking, H. (2011). miR-34 and SNAIL form a double-negative feedback loop to regulate epithelial-mesenchymal transitions. *Cell Cycle* 10.
- Song, J., Xie, C., Jiang, L., Wu, G., Zhu, J., Zhang, S., Tang, M., Song, L., and Li, J. (2018). Transcription factor AP-4 promotes tumorigenic capability and activates the Wnt/beta-catenin pathway in hepatocellular carcinoma. *Theranostics* 8, 3571-3583.
- Stylianou, S., Clarke, R.B., and Brennan, K. (2006). Aberrant activation of notch signaling in human breast cancer. *Cancer Res* 66, 1517-1525.
- Su, L.K., Kinzler, K.W., Vogelstein, B., Preisinger, A.C., Moser, A.R., Luongo, C., Gould, K.A., and Dove, W.F. (1992). Multiple intestinal neoplasia caused by a mutation in the murine homolog of the APC gene. *Science* 256, 668-670.
- Subramanian, A., Tamayo, P., Mootha, V.K., Mukherjee, S., Ebert, B.L., Gillette, M.A., Paulovich, A., Pomeroy, S.L., Golub, T.R., Lander, E.S., *et al.* (2005). Gene set enrichment analysis: a knowledge-based approach for interpreting genome-wide expression profiles. *Proc Natl Acad Sci U S A* 102, 15545-15550.
- Sur, I.K., Hallikas, O., Vaharautio, A., Yan, J., Turunen, M., Enge, M., Taipale, M., Karhu, A., Aaltonen, L.A., and Taipale, J. (2012). Mice lacking a Myc enhancer that includes human SNP rs6983267 are resistant to intestinal tumors. *Science* 338, 1360-1363.
- Sureban, S.M., May, R., George, R.J., Dieckgraefe, B.K., McLeod, H.L., Ramalingam, S., Bishnupuri, K.S., Natarajan, G., Anant, S., and Houchen, C.W. (2008). Knockdown of RNA binding protein musashi-1 leads to tumor regression in vivo. *Gastroenterology* 134, 1448-1458.
- Terris, B., Blaveri, E., Crnogorac-Jurcevic, T., Jones, M., Missiaglia, E., Ruzzniewski, P., Sauvanet, A., and Lemoine, N.R. (2002). Characterization of gene expression profiles in intraductal papillary-mucinous tumors of the pancreas. *Am J Pathol* 160, 1745-1754.
- Tian, H., Biehs, B., Chiu, C., Siebel, C.W., Wu, Y., Costa, M., de Sauvage, F.J., and Klein, O.D. (2015). Opposing activities of notch and wnt signaling regulate intestinal stem cells and gut homeostasis. *Cell Rep* 11, 33-42.
- Tian, H., Biehs, B., Warming, S., Leong, K.G., Rangell, L., Klein, O.D., and de Sauvage, F.J. (2011). A reserve stem cell population in small intestine renders Lgr5-positive cells dispensable. *Nature* 478, 255-259.

References

- Tomasetti, C., and Vogelstein, B. (2015). Cancer etiology. Variation in cancer risk among tissues can be explained by the number of stem cell divisions. *Science* 347, 78-81.
- Ungerback, J., Elander, N., Grunberg, J., Sigvardsson, M., and Soderkvist, P. (2011). The Notch-2 gene is regulated by Wnt signaling in cultured colorectal cancer cells. *PLoS One* 6, e17957.
- Van der Flier, L.G., Sabates-Bellver, J., Oving, I., Haegerbarth, A., De Palo, M., Anti, M., Van Gijn, M.E., Suijkerbuijk, S., Van de Wetering, M., Marra, G., *et al.* (2007). The Intestinal Wnt/TCF Signature. *Gastroenterology* 132, 628-632.
- van der Flier, L.G., van Gijn, M.E., Hatzis, P., Kujala, P., Haegerbarth, A., Stange, D.E., Begthel, H., van den Born, M., Guryev, V., Oving, I., *et al.* (2009). Transcription factor achaete scute-like 2 controls intestinal stem cell fate. *Cell* 136, 903-912.
- van Es, J.H., de Geest, N., van de Born, M., Clevers, H., and Hassan, B.A. (2010). Intestinal stem cells lacking the Math1 tumour suppressor are refractory to Notch inhibitors. *Nat Commun* 1, 18.
- van Es, J.H., Haegerbarth, A., Kujala, P., Itzkovitz, S., Koo, B.K., Boj, S.F., Korving, J., van den Born, M., van Oudenaarden, A., Robine, S., *et al.* (2012). A critical role for the Wnt effector Tcf4 in adult intestinal homeostatic self-renewal. *Mol Cell Biol* 32, 1918-1927.
- van Es, J.H., Jay, P., Gregorieff, A., van Gijn, M.E., Jonkheer, S., Hatzis, P., Thiele, A., van den Born, M., Begthel, H., Brabletz, T., *et al.* (2005a). Wnt signalling induces maturation of Paneth cells in intestinal crypts. *Nat Cell Biol* 7, 381-386.
- van Es, J.H., van Gijn, M.E., Riccio, O., van den Born, M., Vooijs, M., Begthel, H., Cozijnsen, M., Robine, S., Winton, D.J., Radtke, F., *et al.* (2005b). Notch/gamma-secretase inhibition turns proliferative cells in intestinal crypts and adenomas into goblet cells. *Nature* 435, 959-963.
- VanDussen, K.L., Carulli, A.J., Keeley, T.M., Patel, S.R., Puthoff, B.J., Magness, S.T., Tran, I.T., Maillard, I., Siebel, C., Kolterud, A., *et al.* (2012). Notch signaling modulates proliferation and differentiation of intestinal crypt base columnar stem cells. *Development* 139, 488-497.
- Wang, J., Shelly, L., Miele, L., Boykins, R., Norcross, M.A., and Guan, E. (2001). Human Notch-1 inhibits NF-kappa B activity in the nucleus through a direct interaction involving a novel domain. *J Immunol* 167, 289-295.
- Wang, Z., Banerjee, S., Li, Y., Rahman, K.M., Zhang, Y., and Sarkar, F.H. (2006). Down-regulation of notch-1 inhibits invasion by inactivation of nuclear factor-kappaB, vascular endothelial growth factor, and matrix metalloproteinase-9 in pancreatic cancer cells. *Cancer Res* 66, 2778-2784.

References

- Weng, A.P., Millholland, J.M., Yashiro-Ohtani, Y., Arcangeli, M.L., Lau, A., Wai, C., Del Bianco, C., Rodriguez, C.G., Sai, H., Tobias, J., *et al.* (2006). c-Myc is an important direct target of Notch1 in T-cell acute lymphoblastic leukemia/lymphoma. *Genes Dev* 20, 2096-2109.
- Wolfe, A.R., Ernlund, A., McGuinness, W., Lehmann, C., Carl, K., Balmaceda, N., and Neufeld, K.L. (2017). Suppression of intestinal tumorigenesis in Apc mutant mice by Musashi-1 deletion. *J Cell Sci.*
- Wu, W.K., Wang, X.J., Cheng, A.S., Luo, M.X., Ng, S.S., To, K.F., Chan, F.K., Cho, C.H., Sung, J.J., and Yu, J. (2013). Dysregulation and crosstalk of cellular signaling pathways in colon carcinogenesis. *Crit Rev Oncol Hematol* 86, 251-277.
- Xinghua, L., Bo, Z., Yan, G., Lei, W., Changyao, W., Qi, L., Lin, Y., Kaixiong, T., Guobin, W., and Jianying, C. (2012). The overexpression of AP-4 as a prognostic indicator for gastric carcinoma. *Med Oncol* 29, 871-877.
- Zhang, Y., Li, B., Ji, Z.Z., and Zheng, P.S. (2010). Notch1 regulates the growth of human colon cancers. *Cancer* 116, 5207-5218.
- Zhang, Z., Bu, X., Yang, J., Zhu, S., He, S., Zheng, J., Wang, W., and Chu, D. (2018). NOTCH4 regulates colorectal cancer proliferation, invasiveness, and determines clinical outcome of patients. *J Cell Physiol* 233, 6975-6985.
- Zhu, L., Gibson, P., Currle, D.S., Tong, Y., Richardson, R.J., Bayazitov, I.T., Poppleton, H., Zakharenko, S., Ellison, D.W., and Gilbertson, R.J. (2009). Prominin 1 marks intestinal stem cells that are susceptible to neoplastic transformation. *Nature* 457, 603-607.

11. Supplements

11.1 Supplemental Data 1

Related to Figure 14d and 24d.

Differential gene expression resulting from *AP4* deletion was subjected to comparative analysis with mSigDB Hallmark gene sets and KEGG pathways.

Related to Figure 14d:

Functional categories (mSigDB Hallmark gene sets) overrepresented among mRNAs down-regulated in adenomas of *Apc^{Min}/Ap4^{ΔIEC}* vs *Apc^{Min}/Ap4^{fl/fl}* mice

EMT

Igfbp3, Col3a1, Col1a1, Col4a2, Tgfb1, Sparc, Col6a2, Col6a3, Adam12, Spp1, Igfbp4, Itgb3, Col5a2, Col1a2, Lamc1, Itga5, Flna, Mmp2, Myl9, Slit2, Fn1, Cd59, Igfbp2, Gas1, Postn, Fstl1, Col4a1, Dcn, Col5a1, Lox, Tnc, Lgals1, Cadm1, Serpinh1, Basp1, Fermt2, Glipr1, Col12a1, Eln, Pcolce2, Loxl2, Mgp, Col5a3, Serpine2, Pthlh, Sntb1, Thbs2, Vim

Myogenesis

Igfbp3, Col3a1, Col1a1, Col4a2, Tgfb1, Sparc, Col6a2, Col6a3, Adam12, Tnnt2, Sphk1, Aplnr, Kcnh2, Speg, Cd36, Nos1, Ckm, Stc2, Nav2, Prnp, Notch1, Tnni1, Col15a1, Itga7, Dtna, Cacna1h, Wwtr1, Cnn3, Cryab, Aebp1, Dmpk, Ephb3, Igfbp7, Fxyd1, Smtn, Casq2

KRAS signaling

Igfbp3, Col3a1, Spp1, Tnnt2, Cpe, Pcp4, Tfpi, Dcbld2, Il1b, Mmp9, Pecam1, Plat, Fcer1g, Etv4, Mmp10, Sparcl1, Ptgs2, Arg1, Eng, Etv5, F13a1, Flt4, Tmem158, Gng11, Trib2, Tmem176a, Tph1, Laptm5

E2F targets

Top2a, Cenpe, Brca2, Cdkn2c, Mcm2, Pds5b, Mybl2, Pole, Ccp110, Hmgb2, Msh2, Ung, Nap111, Cit, Psip1, Kif18b, Dnmt1, Atad2, Hells, Bub1b, Ncapd2

Estrogen response late

Igfbp4, Cpe, Pcp4, Top2a, Atp2b4, Prkar2b, Slc7a5, Celsr2, Krt13, Scarb1, Slc27a2, Slc1a4, Foxc1, Slc24a3, Kif20a, Homer2, Slc29a1, Fabp5, Plxnb1, Tpsab1, Cxcl14

UV response

Col3a1, Col1a1, Itgb3, Col5a2, Col1a2, Lamc1, Tfpi, Atp2b4, Prkar2b, Nek7, Celf2, Rbpms, Fzd2, Kit, Ltbp1, Plcb4, Ptprm, Mta1

Inflammatory response

Itgb3, Itga5, Sphk1, Aplnr, Dcbld2, Il1b, Olr1, Pik3r5, Edn1, Slc7a2, Abca1, Gpc3, Ifitm1, Calcrl, Sema4d, Ffar2, Itgb8, P2rx7, Ccl24, C5ar1

Mitotic spindle

Flna, Top2a, Cenpe, Brca2, Fscn1, Dock4, Bub1, Kif11, Kif20b, Bcl2l11, Cep250, Kif3c, Pkd2, Anln, Cep192, Arap3, Alms1, Sorbs2, Wasf1, Kntc1

Apical junction

Mmp2, Myl9, Slit2, Kcnh2, Speg, Mmp9, Pecam1, Fscn1, Gnai1, Sdc3, Dsc3, Itga9, Msn, Nrtn, Evi, Amigo1, Rac2, Actg2, Cd34

Complement

Col4a2, Fn1, Cd59, Cd36, Plat, Fcer1g, Olr1, Pik3r5, Dock4, Plek, Serping1, Csrp1, Timp2, Ctstl1, Hspa1a, Mmp12, Mmp13, Pik3cg, Zeb1

Related to Figure 14d:

Functional categories (KEGG pathways) overrepresented among mRNAs down-regulated in adenomas of *Apc^{Min}/Ap4^{ΔIEC}* vs *Apc^{Min}/Ap4^{fl/fl}* mice

ECM receptor interaction

Itga2b, Fn1, Lamc1, Col4a1, Col4a2, Lama4, Lama5, Lamb1, Lamb2, Itga1, Itga5, Itgb3, Itga9, Itgb8, Itga8, Itga7, Thbs2, Spp1, Col1a1, Col1a2, Col3a1, Col5a1, Col5a2, Col6a1, Col6a2, Col6a3, Tnc, Col5a3, Tnxb, Cd36, Sdc3, Sv2c, Hspg2

Focal adhesion

Itga2b, Fn1, Lamc1, Col4a1, Col4a2, Lama4, Lama5, Lamb1, Lamb2, Itga1, Itga5, Itgb3, Itga9, Itgb8, Itga8, Itga7, Thbs2, Spp1, Col1a1, Col1a2, Col3a1, Col5a1, Col5a2, Col6a1, Col6a2, Col6a3, Tnc, Col5a3, Tnxb, Rac2, Pik3cg, Pik3r5, Pdgfra, Prkcb, Pak3, Pak6, Myl9, Vav1, Pip5k1c, Flt1, Flt4, Flna, Parvb, Cav2

Pathways in Cancer

Itga2b, Fn1, Lamc1, Col4a1, Col4a2, Lama4, Lama5, Lamb1, Lamb2, Rac2, Pik3cg, Pik3r5, Pdgfra, Prkcb, Tgfb1, Fgfr2, Ptgs2, Ccne2, Skp2, Rarb, Kit, Kitlg, Tcf7, Fzd10, Fzd2, Fzd4, Mmp2, Mmp9, Ptch1, Smo, Msh2, Brca2

Axon guidance

Rac2, Pak3, Pak6, Gnai1, Sema4f, Sema4d, Epha7, Ephb3, Ephb4, Srgap2, Plxnb1, Sema4c, Sema3g, Ntn4, Robo1, Sema3f, Sema5a, Slit2, Ntn1, Srgap3

Dilated cardiomyopathy

Itga2b, Itga1, Itga5, Itgb3, Itga9, Itgb8, Itga8, Itga7, Tgfb1, Prkacb, Adcy8, Adcy1, Adcy3, Adcy5, Cacna1c, Slc8a1, Tnnt2

Regulation of actin cytoskeleton

Itga2b, Fn1, Itga1, Itga5, Itgb3, Itga9, Itgb8, Itga8, Itga7, Rac2, Pik3cg, Pik3r5, Pdgfra, Pak3, Pak6, Myl9, Vav1, Pip5k1c, Fgfr2, F2r, Msn, Wasf1, Rdx

Small cell lung cancer

Itga2b, Fn1, Lamc1, Col4a1, Col4a2, Lama4, Lama5, Lamb1, Lamb2, Pik3cg, Pik3r5, Ptgs2, Ccne2, Skp2, Rarb

Melanogenesis

Prkcb, Kit, Kitlg, Tcf7, Fzd10, Fzd2, Fzd4, Gnai1, Prkacb, Adcy8, Adcy1, Adcy3, Adcy5, Plcb4, Edn1

Calcium signaling pathway

Pdgfra, Prkcb, Prkacb, Adcy8, Adcy1, Adcy3, Cacna1c, Slc8a1, F2r, Plcb4, Itpr1, Itpkb, Sphk1, Nos3, Cacna1h, Nos1, P2rx7, Slc25a4, Atp2b4

Vascular smooth muscle contraction

Prkcb, Myl9, Prkacb, Adcy8, Adcy1, Adcy3, Adcy5, Cacna1c, Plcb4, Itpr1, Npr1, Calcr1, Mrvi1, Actg2, Ppp1r14a

Related to 14d:

Functional categories (mSigDB Hallmark gene sets) overrepresented among mRNAs up-regulated in adenomas of *Apc^{Min}/Ap4^{ΔIEC}* vs *Apc^{Min}/Ap4^{fl/fl}* mice

Interferon gamma response

Irf7, Tap1, B2m, Rtp4, Bst2, Nmi, Casp1, Casp8, Ube2l6, Ifih1, Stat2, Psmb9, Psmb8, Rsad2, Ifi44, Usp18, Batf2, Tdrd7, Ifi27, Ifi35, Sp110, Parp14, Herc6, Ddx60, Psme2, Parp12, Dhx58, Oasl, Epsti1, Isg15, Stat1, Hla-Dqa1, Cdkn1a, Upp1, Cd38, Casp7, Casp4, Ddx58, Cd274, Ifit1, Il18bp, Gbp6, Ido1, Mx2, Oas2, Oas3, Xaf1, Rnf213, Zbp1, Nlrc5

Interferon alpha response

Irf7, Tap1, B2m, Rtp4, Bst2, Nmi, Casp1, Casp8, Ube2l6, Ifih1, Stat2, Psmb9, Psmb8, Rsad2, Ifi44, Usp18, Batf2, Tdrd7, Ifi27, Ifi35, Sp110, Parp14, Herc6, Ddx60, Psme2, Parp12, Dhx58, Oasl, Epsti1, Isg15, Mov10, Oas1, Tmem140, Uba7, Parp9, Trim5

Cholesterol homeostasis

Ldlr, Idi1, Hmgcs1, Hmgcr, Sqle, Cyp51a1, Hsd17b7, Mvd, Fdft1, Pmvk, Antxr2, Anxa13, Lss

Allograft rejection

Irf7, Tap1, B2m, Stat1, Hla-Dqa1, Il18, Tlr1, Ccnd2, Cdkn2a, C2, Gcnt1, Hla-Dmb, Hla-E, Nos2, Tap2, Cd3g, Cd8a

Inflammatory response

Irf7, Rtp4, Bst2, Nmi, Cdkn1a, Ldlr, Il18, Tlr1, Cd82, Mep1a, Hrh1, Slc4a4

Xenobiotic metabolism

Upp1, Slc35d1, Tnfrsf1a, Acox2, Enpep, Slc46a3, Gsta3, Abhd6, Ccl25, Xdh, Abcc3, Entpd5

MTORC1 signaling

Cdkn1a, Ldlr, Idi1, Hmgcs1, Hmgcr, Sqle, Cyp51a1, Dhcr24, Insig1, Elovl6, Ifrd1

p53 pathway

Tap1, Casp1, Cdkn1a, Upp1, Ccnd2, Cdkn2a, Cd82, Slc35d1, S100a10, Stom, Eps8l2

Apoptosis

Tap1, Casp1, Casp8, Cdkn1a, Cd38, Casp7, Casp4, Il18, Ccnd2

Fatty acid metabolism

Ube2l6, Idi1, Hmgcs1, Hsd17b7, Dhcr24, S100a10, Aldh1a1, Acsl5

Related to Figure 14d:

Functional categories (KEGG pathways) overrepresented among mRNAs up-regulated in adenomas of *Apc^{Min}/Ap4^{ΔIEC}* vs *Apc^{Min}/Ap4^{fl/fl}* mice

Steroid biosynthesis

Hsd17b7, Cyp51a1, Dhcr24, Fdft1, Lss, Sqle, Soat2

Antigen processing and presentation

Hla-Dmb, Hla-Dqa1, Hla-Dqb1, Hla-E, Tap1, Tap2, Cd8a, Psme2, B2m

Terpenoid backbone biosynthesis

Pmvk, Hmgcs1, Hmgcr, Idi1, Mvd

Rig I like receptor signaling pathway

Casp8, Irf7, Ddx58, Ifih1, Dhx58, Isg15

Viral myocarditis

Hla-Dmb, Hla-Dqa1, Hla-Dqb1, Hla-E, Casp8, Actb

ABC transporters

Tap1, Tap2, Abcb11, Abcc3, Abcg2

Glycerophospholipid metabolism

Dgkq, Mboat1, Agpat4, Agpat9, Cds1, Pla2g2e

Glutathione metabolism

Anpep, Gsta3, Mgst1, Mgst2, Ggt1

Cytosolic DNA sensing pathway

Irf7, Ddx58, Casp1, Il18, Zbp1

Systemic lupus erythematosus

Hla-Dmb, Hla-Dqa1, Hla-Dqb1, C2, Hist1h2ae, Hist1h2ai, Hist1h2al

Related to Figure 24d:

Functional categories (mSigDB Hallmark gene sets) overrepresented among mRNAs down-regulated in organoids derived from *Villin-Cre-ERT2/Ap4^{fl/fl}* vs *Villin-Cre-ERT2* mice.

UV response

Cap2, Tfpi, Mgl1, Fzd2, Amph, Kit, Plcb4

KRAS signaling

Igfbp2, Myh7, Fam46c, Adck3, Atp6v1b1, Capn9, Clps, Tff2

Pancreas beta cells

Chga, Insm1, Nkx2-2, Syt13

Wnt/ β -catenin signaling

Notch1, Dll1, Axin2, Nkd1

EMT

Cap2, Igfbp2, Eno2, Jun, Timp3, Gas1, Pthlh

Estrogen response early

Tiam1, Tpbg, Tff3, Celsr1, Tubb2b, Mreg, Tgif2

IL2/STAT5 signaling

Tiam1, Ifitm3, Tnfsf10, Cd83, Itih5, Plagl1, Slc39a8

Glycolysis

Eno2, Tpbg, Tff3, Cacna1h, Efna3, Nanp

Myogenesis

Myh7, Notch1, Cacna1h, Spdef, Dmpk, Myl7

Apoptosis

Eno2, Jun, Timp3, Ifitm3, Tnfsf10

Related to Figure 24d:

Functional categories (KEGG pathways) overrepresented among mRNAs down-regulated in organoids derived from *Villin-Cre-ERT2/Ap4^{f/f}* vs *Villin-Cre-ERT2* mice.

Axon guidance

Efna3, Efna4, Sema4c, Dpysl5, Ntn4, Sema5a, Srgap3

Wnt signaling pathway

Wnt3, Fzd2, Axin2, Jun, Plcb4, Sfrp5, Nkd1

Leukocyte transendothelial migration

Rassf5, Myl7, Ncf2, Rapgef3, Esam, Nox1

Pathways in cancer

Wnt3, Fzd2, Axin2, Jun, Rassf5, Kit, Nos2, Pdgfa, Fgfr2

Melanogenesis

Wnt3, Fzd2, Plcb4, Kit, Creb3l4

Arachidonic acid metabolism

Pla2g10, Ggt7, Ptgds, Cyp4f2

Calcium signaling pathway

Plcb4, Nos2, Mylk3, Chrm1, Cacna1h, Itpkb

Regulation of actin cytoskeleton

Myl7, Pdgfa, Fgfr2, Mylk3, Chrm1, Tiam1

Notch signaling pathway

Notch1, Dll3, Dll1

Related to Figure 24d:

Functional categories (mSigDB Hallmark gene sets) overrepresented among mRNAs up-regulated in organoids derived from *Villin-Cre-ERT2/Ap4^{fl/fl}* vs *Villin-Cre-ERT2* mice.

Xenobiotic metabolism

Ca2, Cd36, Acox1, Adh1c, Fabp1, Fas, Gcnt2, Papss2, Leap2, Abcc2, Cyp2j2, Enpep, G6pc, Slc46a3, Arg2, Xdh

KRAS signaling

Ca2, Ptgs2, Ereg, Angptl4, Prrx1, Aldh1a3, Mafb, Ace, Spon1, Anxa10, Ptpr, Mall, Hkdc1, Il33

Fatty acid metabolism

Ca2, Cd36, Acox1, Adh1c, Fabp1, Me1, Aldh1a1, Fabp2, Aqp7, Tp53inp2

Coagulation

Gp1ba, Mmp15, Apoa1, Ctse, Gsn, Crip2, Apoc3, Proz, Gda

Complement

Ca2, Cd36, Me1, Gp1ba, Mmp15, Irf7, Lgals3, F5, Apoa4, Lipa

Interferon gamma response

Fas, Ptgs2, Irf7, Hif1a, Mx1, Oasl, Isg15, Ifit1, Oas3

Bile acid metabolism

Aldh1a1, Apoa1, Ephx2, Gstk1, Abca8, Sult1b1, Bbox1

Inflammatory response

Ereg, Gp1ba, Irf7, Hif1a, Il18, Mxd1, Rnf144b, Ptafr

Allograft rejection

Fas, Ereg, Irf7, Hif1a, Il18, Capg, Gcnt1

Heme metabolism

Ca2, Ctse, Slc7a11, Aqp3, Cdr2, Mpp1, Nfe2

Related to Figure 24d:

Functional categories (KEGG pathways) overrepresented among mRNAs up-regulated in organoids derived from *Villin-Cre-ERT2/Ap4^{fl/fl}* vs *Villin-Cre-ERT2* mice.

PPAR signaling pathway

Pck1, Acox1, Me1, Cd36, Gk, Fabp1, Fabp2, Slc27a6, Apoa1, Apoc3, Aqp7, Angptl4, Pltp

Drug metabolism cytochrome P450

Cyp2c8, Adh1c, Ugt2b10, Cyp3a4, Aldh1a3, Gstk1, Gsta1, Gsta2, Maob, Cyp2d6, Fmo5

Metabolism of xenobiotics by cytochrome P450

Cyp2c8, Adh1c, Ugt2b10, Cyp3a4, Aldh1a3, Gstk1, Gsta1, Gsta2, Cyp1b1

Arachidonic acid metabolism

Cyp2c8, Ggt1, Cyp2j2, Ephx2, Ptgs2, Alox5

Retinol metabolism

Cyp2c8, Adh1c, Ugt2b10, Cyp3a4, Dhhrs9, Aldh1a1

Renin angiotensin system

Mme, Ace, Enpep, Ace2

Glycolysis gluconeogenesis

Pck1, Adh1c, Aldh1a3, G6pc, Aldob

Glutathione metabolism

Gstk1, Gsta1, Gsta2, Ggt1

Starch and sucrose metabolism

Ugt2b10, G6pc, Enpp3, Treh

Glycosphingolipid biosynthesis

Gcnt2, St3gal4, B3gnt5

11.2 Supplemental Data 2

Related to Figure 15a,b and 25a,b

Significantly regulated mRNAs associated with distinct signatures as identified by GSEA.

Related to Figure 15a,b:

Combined stem cell signature, *Apc^{Min}* adenoma

Gene ID	Mean <i>AP4^{Wt}</i>	Mean <i>AP4^{ΔIEC}</i>	fc - <i>AP4^{ΔIEC}</i> vs <i>AP4^{Wt}</i>	P-value
<i>Cbx6</i>	2.833	0.280	0.099	0.005
<i>Cyp11a1</i>	0.789	0.082	0.104	< 0.001
<i>Tfpi</i>	1.289	0.215	0.167	0.008
<i>Rdh1</i>	0.204	0.035	0.170	0.001
<i>Tgif2</i>	2.079	0.390	0.188	0.001
<i>Nrn1</i>	1.677	0.334	0.199	0.013
<i>Slc14a1</i>	2.216	0.457	0.206	0.007
<i>Tmem182</i>	0.182	0.040	0.221	0.040
<i>Clic6</i>	6.413	1.509	0.235	< 0.001
<i>Ifitm1</i>	107.524	26.247	0.244	< 0.001
<i>Adra2a</i>	2.151	0.538	0.250	0.002
<i>Zbtb16</i>	0.183	0.050	0.272	0.034
<i>Cgnl1</i>	4.831	1.333	0.276	0.002
<i>Prelp</i>	4.220	1.167	0.277	0.011
<i>Slc27a2</i>	1.600	0.453	0.283	0.023
<i>Limch1</i>	2.531	0.724	0.286	0.004
<i>Olfm4</i>	48.682	14.460	0.297	0.001
<i>Fstl1</i>	5.094	1.519	0.298	0.026
<i>Lgr5</i>	2.396	0.736	0.307	0.002
<i>Rassf5</i>	0.180	0.056	0.312	0.027
<i>Fscn1</i>	4.205	1.332	0.317	0.007
<i>Rasl11b</i>	2.011	0.658	0.327	0.027
<i>Ptprm</i>	0.561	0.186	0.331	0.046
<i>Vwa2</i>	0.396	0.133	0.337	0.020
<i>Fzd2</i>	2.494	0.872	0.350	0.021
<i>Agr3</i>	1.173	0.417	0.355	0.021
<i>Wwtr1</i>	2.996	1.071	0.358	0.038
<i>Kif26b</i>	0.985	0.353	0.358	0.005
<i>Fam188b</i>	0.369	0.137	0.371	0.012
<i>Zfp618</i>	1.158	0.436	0.376	0.007
<i>Smoc2</i>	25.019	9.607	0.384	0.002
<i>Slc1a2</i>	0.038	0.015	0.384	0.006
<i>Lfng</i>	12.067	4.709	0.390	0.001
<i>Mex3a</i>	4.685	1.850	0.395	0.001
<i>Notch1</i>	1.845	0.731	0.396	0.001
<i>Cited4</i>	12.147	4.836	0.398	0.017

<i>Sorbs2</i>	0.750	0.299	0.399	0.013
<i>Arid5b</i>	3.783	1.529	0.404	0.007
<i>St3gal3</i>	4.975	2.011	0.404	0.001
<i>Mnx1</i>	0.875	0.357	0.408	0.026
<i>Fam64a</i>	3.867	1.594	0.412	0.005
<i>Pthlh</i>	4.590	1.907	0.415	0.002
<i>Dct</i>	0.184	0.077	0.416	0.001
<i>Dmpk</i>	33.174	14.091	0.425	0.004
<i>Sorcs2</i>	3.870	1.672	0.432	0.005
<i>Prkd3</i>	1.615	0.700	0.433	0.005
<i>Chst11</i>	3.187	1.383	0.434	0.010
<i>Smo</i>	7.955	3.497	0.440	0.004
<i>Soat1</i>	6.933	3.051	0.440	0.002
<i>Esam</i>	3.357	1.485	0.442	0.035
<i>Klhl8</i>	2.576	1.144	0.444	0.002
<i>Tcf7</i>	9.897	4.419	0.446	0.009
<i>Igfbp4</i>	120.004	54.950	0.458	0.002
<i>Pde3b</i>	3.346	1.548	0.463	0.021
<i>Pxdn</i>	5.727	2.650	0.463	0.007
<i>Pls3</i>	20.028	9.301	0.464	0.002
<i>Nrtn</i>	9.054	4.211	0.465	0.044
<i>Slco3a1</i>	1.639	0.763	0.465	0.006
<i>Maged1</i>	21.926	10.215	0.466	0.007
<i>Cachd1</i>	2.783	1.298	0.467	0.001
<i>Ppm1f</i>	2.196	1.029	0.469	0.004
<i>Atp11a</i>	2.796	1.322	0.473	0.004
<i>Cnn3</i>	41.713	19.768	0.474	0.001
<i>Ascl2</i>	15.204	7.233	0.476	0.023
<i>Fads1</i>	17.967	8.565	0.477	0.003
<i>Arl4c</i>	11.483	5.497	0.479	0.002
<i>Man2a2</i>	1.211	0.581	0.480	0.011
<i>Ccdc3</i>	18.479	8.920	0.483	0.018
<i>Ifitm3</i>	443.447	215.744	0.487	0.001
<i>Znrf3</i>	4.953	2.414	0.487	0.002
<i>Ifitm2</i>	349.080	170.144	0.487	0.006
<i>Fmnl2</i>	3.450	1.687	0.489	0.015
<i>Gkap1</i>	3.804	1.863	0.490	0.015
<i>Bcl7a</i>	2.193	1.080	0.492	0.004
<i>Rhobtb3</i>	1.054	0.519	0.493	0.008
<i>Kank1</i>	3.380	1.668	0.494	0.013
<i>Alms1</i>	0.581	0.288	0.497	0.014
<i>Ttc21b</i>	1.157	0.578	0.500	0.008
<i>Pole</i>	2.080	1.046	0.503	0.012
<i>Brca2</i>	0.554	0.279	0.504	0.008
<i>Zfp12</i>	1.519	0.766	0.504	0.012
<i>Evl</i>	8.612	4.362	0.506	0.004

<i>Sertad4</i>	0.360	0.183	0.509	0.044
<i>Iffo2</i>	7.661	3.910	0.510	0.034
<i>Rgs19</i>	2.891	1.479	0.512	0.004
<i>Kif20a</i>	10.188	5.252	0.516	0.014
<i>Ung</i>	4.738	2.448	0.517	0.001
<i>Fam65b</i>	0.417	0.216	0.517	0.031
<i>Ptpns</i>	7.694	3.979	0.517	0.016
<i>Tead2</i>	6.553	3.392	0.518	0.006
<i>Prkacb</i>	5.437	2.822	0.519	0.036
<i>Aspm</i>	1.700	0.885	0.521	0.006
<i>Cit</i>	1.095	0.571	0.522	0.011
<i>Prrc2b</i>	11.454	6.021	0.526	0.007
<i>Kcnq1</i>	24.450	12.972	0.531	0.004
<i>Plxnb1</i>	7.280	3.872	0.532	0.009
<i>Lcp1</i>	3.143	1.678	0.534	0.023
<i>Ppat</i>	7.629	4.074	0.534	0.018
<i>Ephb3</i>	13.909	7.498	0.539	0.017
<i>Nap111</i>	42.931	23.236	0.541	0.006
<i>Slit2</i>	0.541	0.294	0.543	0.010
<i>Myo1b</i>	5.102	2.786	0.546	0.014
<i>Trim44</i>	5.776	3.154	0.546	0.008
<i>Zc3hav1l</i>	0.766	0.419	0.547	0.002
<i>Rccd1</i>	1.232	0.674	0.548	0.014
<i>Rassf4</i>	1.268	0.695	0.548	0.027
<i>Cep192</i>	2.670	1.465	0.549	0.014
<i>Rprd1a</i>	4.917	2.702	0.550	0.002
<i>Cd320</i>	5.476	3.013	0.550	0.015
<i>Il17rd</i>	1.256	0.692	0.551	0.003
<i>Phlpp1</i>	2.010	1.117	0.556	0.013
<i>Pds5b</i>	2.190	1.219	0.556	0.010
<i>Clu</i>	376.724	210.033	0.558	0.042
<i>Zmym1</i>	1.623	0.909	0.560	0.026
<i>Gemin8</i>	1.104	0.620	0.562	0.005
<i>Dtl</i>	1.788	1.006	0.563	0.006
<i>Clca1</i>	234.069	131.917	0.564	0.033
<i>Sox4</i>	58.085	32.781	0.564	0.009
<i>Arhgap39</i>	1.884	1.064	0.564	0.018
<i>Hirip3</i>	6.611	3.734	0.565	0.017
<i>Hmga2</i>	1.437	0.812	0.565	0.044
<i>Nfic</i>	5.047	2.853	0.565	0.010
<i>Cc2d2a</i>	0.820	0.464	0.565	0.037
<i>Mpzl1</i>	23.847	13.512	0.567	0.010
<i>Ilf3</i>	9.584	5.454	0.569	0.016
<i>Nav1</i>	2.194	1.251	0.570	0.019
<i>Esp1</i>	3.029	1.727	0.570	0.018
<i>Cfi</i>	92.039	52.544	0.571	0.050

<i>Palb2</i>	0.985	0.564	0.573	0.029
<i>Spag5</i>	4.246	2.436	0.574	0.024
<i>Irs1</i>	0.672	0.387	0.576	0.003
<i>Fbxo21</i>	4.251	2.452	0.577	0.022
<i>Tnfrsf19</i>	14.029	8.106	0.578	0.008
<i>Shisa2</i>	9.889	5.719	0.578	0.011
<i>Cenpf</i>	3.330	1.929	0.579	0.021
<i>Msi1</i>	2.891	1.675	0.579	0.027
<i>Zfp503</i>	8.260	4.807	0.582	0.006
<i>Klhl24</i>	4.655	2.717	0.584	0.029
<i>Zbtb25</i>	0.939	0.550	0.586	0.034
<i>Mcm8</i>	1.961	1.150	0.586	0.044
<i>Ckap2</i>	4.818	2.827	0.587	0.003
<i>Hebp2</i>	10.149	5.958	0.587	0.009
<i>Mfge8</i>	18.538	10.944	0.590	0.022
<i>Myc</i>	25.849	15.303	0.592	0.034
<i>Apcdd1</i>	3.711	2.198	0.592	0.030
<i>Dach1</i>	1.242	0.736	0.593	0.018
<i>Srpk2</i>	1.531	0.909	0.594	0.043
<i>Nedd4</i>	31.340	18.632	0.595	0.014
<i>Rnf43</i>	18.439	10.970	0.595	0.023
<i>Psrc1</i>	1.483	0.882	0.595	0.035
<i>Slc12a2</i>	41.119	24.558	0.597	0.016
<i>Phc1</i>	2.284	1.368	0.599	0.002
<i>Efna4</i>	10.567	6.330	0.599	0.047
<i>Isyna1</i>	27.972	16.829	0.602	0.049
<i>Wipi1</i>	3.979	2.411	0.606	0.002
<i>Cdc42ep1</i>	13.457	8.192	0.609	0.026
<i>Mdn1</i>	1.188	0.727	0.612	0.032
<i>Ppp1r9a</i>	1.243	0.763	0.614	0.025
<i>Tiam1</i>	3.317	2.052	0.619	0.042
<i>Ccdc18</i>	0.569	0.353	0.619	0.048
<i>Rnf219</i>	3.001	1.860	0.620	0.038
<i>Timeless</i>	2.721	1.691	0.621	0.006
<i>Lrig1</i>	15.265	9.521	0.624	0.025
<i>Tns3</i>	15.998	9.987	0.624	0.003
<i>Pogk</i>	2.099	1.316	0.627	0.041
<i>Cdca7</i>	27.066	17.010	0.628	0.004
<i>Tbc1d9</i>	1.949	1.231	0.632	0.028
<i>Notch4</i>	1.812	1.145	0.632	0.034
<i>Paics</i>	29.262	18.521	0.633	0.023
<i>Sox9</i>	29.670	18.781	0.633	0.014
<i>Ttc23</i>	1.019	0.646	0.634	0.001
<i>Cdca7l</i>	6.817	4.320	0.634	0.046
<i>Mpp3</i>	0.521	0.331	0.635	0.037
<i>Slc39a10</i>	4.222	2.689	0.637	0.032

<i>Id2</i>	49.195	31.379	0.638	0.008
<i>Mif</i>	256.148	163.402	0.638	0.047
<i>Tbc1d4</i>	0.799	0.510	0.638	0.049
<i>Sesn3</i>	2.992	1.915	0.640	0.002
<i>Tgif1</i>	15.646	10.084	0.645	0.022
<i>Napepld</i>	4.053	2.616	0.645	0.025
<i>Lipt2</i>	15.168	9.840	0.649	0.035
<i>Tubb2b</i>	22.037	14.342	0.651	0.013
<i>Ddit4</i>	73.921	48.138	0.651	0.017
<i>Rasa3</i>	2.869	1.871	0.652	0.049
<i>Etv6</i>	13.585	8.877	0.653	0.018
<i>Csnk1e</i>	9.082	5.935	0.654	0.020
<i>Notch2</i>	2.867	1.883	0.657	0.045
<i>Dctd</i>	3.878	2.547	0.657	0.044
<i>Dlgap1</i>	0.168	0.110	0.659	0.028
<i>Zfhx3</i>	1.432	0.946	0.661	0.015
<i>Pabpc1</i>	270.241	179.318	0.664	0.007
<i>Haus4</i>	11.656	7.743	0.664	0.011
<i>Nfia</i>	3.282	2.200	0.670	0.007
<i>Trim37</i>	3.634	2.448	0.674	0.041
<i>Dtx4</i>	3.103	2.095	0.675	0.044
<i>Cdk6</i>	2.404	1.630	0.678	0.035
<i>Mcc</i>	1.025	0.698	0.681	0.046
<i>Mecom</i>	7.895	5.391	0.683	0.042
<i>Irf2bp2</i>	26.034	17.879	0.687	0.033
<i>Farp1</i>	6.628	4.585	0.692	0.018
<i>Lysmd2</i>	11.387	7.897	0.694	0.003
<i>Zfp341</i>	1.738	1.208	0.695	0.028
<i>Sfpq</i>	54.134	37.686	0.696	0.015
<i>Slc30a2</i>	18.234	12.746	0.699	0.037
<i>Pik3r1</i>	10.178	7.156	0.703	0.010
<i>Psd3</i>	1.207	0.849	0.703	0.042
<i>Tmem209</i>	2.748	1.958	0.712	0.047
<i>Nin</i>	1.616	1.152	0.713	0.017
<i>Pla2g5</i>	2.213	1.596	0.721	0.012
<i>Socs2</i>	4.172	3.010	0.721	0.021
<i>Sestd1</i>	6.436	4.693	0.729	0.045
<i>Wwp1</i>	2.883	2.107	0.731	0.038
<i>Sdc4</i>	56.427	41.795	0.741	0.034
<i>Tspan5</i>	9.061	6.753	0.745	0.001
<i>Hmbox1</i>	2.401	1.836	0.765	0.011
<i>Pbx1</i>	4.037	3.092	0.766	0.032
<i>Yap1</i>	14.531	11.201	0.771	0.040
<i>Ccnd3</i>	6.943	5.371	0.774	0.031
<i>Mlxip</i>	6.624	5.238	0.791	0.034
<i>Utrn</i>	6.492	5.292	0.815	0.044

Combined Wnt signature, *Apc*^{Min} adenoma

Gene ID	Mean <i>AP4</i> ^{Wt}	Mean <i>AP4</i> ^{ΔIEC}	fc - <i>AP4</i> ^{ΔIEC} <i>AP4</i> ^{Wt} vs	P-value
<i>Jag2</i>	4.297	1.038	0.241	0.001
<i>Gnai1</i>	1.972	0.726	0.368	0.016
<i>Notch1</i>	1.845	0.731	0.396	0.001
<i>Hey1</i>	2.135	0.858	0.402	0.006
<i>Tcf7</i>	9.897	4.419	0.446	0.009
<i>Skp2</i>	1.609	0.753	0.468	0.007
<i>Ascl2</i>	15.204	7.233	0.476	0.023
<i>Ifitm2</i>	349.080	170.144	0.487	0.006
<i>Fzd1</i>	2.434	1.189	0.489	0.033
<i>Rhobtb3</i>	1.054	0.519	0.493	0.008
<i>Ptch1</i>	2.359	1.217	0.516	0.007
<i>Dvl2</i>	2.119	1.176	0.555	0.015
<i>Sox4</i>	58.085	32.781	0.564	0.009
<i>Trp53</i>	20.202	11.806	0.584	0.019
<i>Ankrd10</i>	5.648	3.306	0.585	0.003
<i>Myc</i>	25.849	15.303	0.592	0.034
<i>Nkd1</i>	55.307	33.244	0.601	0.032
<i>Ncor2</i>	7.104	4.317	0.608	0.029
<i>Tiam1</i>	3.317	2.052	0.619	0.042
<i>Jag1</i>	3.298	2.046	0.620	0.005
<i>Hdac2</i>	19.662	12.201	0.621	0.013
<i>Notch4</i>	1.812	1.145	0.632	0.034
<i>Maml1</i>	3.154	2.038	0.646	0.022
<i>Rasa3</i>	2.869	1.871	0.652	0.049
<i>Csnk1e</i>	9.082	5.935	0.654	0.020
<i>Smyd5</i>	4.624	3.027	0.655	0.037
<i>Notch2</i>	2.867	1.883	0.657	0.045
<i>Fzd8</i>	1.349	0.892	0.661	0.022
<i>Rbpj</i>	4.386	2.973	0.678	0.003
<i>Kat2a</i>	11.300	7.682	0.680	0.031
<i>Lef1</i>	1.495	1.027	0.687	0.019
<i>Msi2</i>	3.897	2.699	0.693	0.023
<i>Smarca5</i>	17.185	11.937	0.695	0.044
<i>Rnf138</i>	7.062	5.032	0.713	0.027
<i>Smyd2</i>	13.706	10.088	0.736	0.039
<i>Adam17</i>	7.137	5.647	0.791	0.045
<i>Axin1</i>	13.177	11.139	0.845	0.025
<i>Ccnd2</i>	21.270	29.703	1.396	0.006

Combined Notch signature, *Apc*^{Min} adenoma

Gene ID	Mean <i>AP4</i> ^{Wt}	Mean <i>AP4</i> ^{ΔIEC}	fc - <i>AP4</i> ^{ΔIEC} vs <i>AP4</i> ^{Wt}	P-value
<i>Jag2</i>	4.297	1.038	0.241	0.001
<i>Lfng</i>	12.067	4.709	0.390	0.001
<i>Notch1</i>	1.845	0.731	0.396	0.001
<i>Fzd1</i>	2.434	1.189	0.489	0.033
<i>St3gal6</i>	5.465	2.977	0.545	0.003
<i>Dvl2</i>	2.119	1.176	0.555	0.015
<i>Sap30</i>	19.381	11.657	0.601	0.008
<i>Ncor2</i>	7.104	4.317	0.608	0.029
<i>Jag1</i>	3.298	2.046	0.620	0.005
<i>Hdac2</i>	19.662	12.201	0.621	0.013
<i>Notch4</i>	1.812	1.145	0.632	0.034
<i>Hes1</i>	40.017	25.495	0.637	0.006
<i>Maml1</i>	3.154	2.038	0.646	0.022
<i>Notch2</i>	2.867	1.883	0.657	0.045
<i>Dtx4</i>	3.103	2.095	0.675	0.044
<i>Rbpj</i>	4.386	2.973	0.678	0.003
<i>Kat2a</i>	11.300	7.682	0.680	0.031
<i>Dvl3</i>	6.340	4.384	0.692	0.030
<i>Ep300</i>	7.420	5.795	0.781	0.008
<i>Hdac1</i>	36.556	28.566	0.781	0.008
<i>Rbx1</i>	37.968	29.875	0.787	0.006
<i>Adam17</i>	7.137	5.647	0.791	0.045
<i>Snw1</i>	26.577	21.174	0.797	0.039
<i>Ctbp1</i>	46.874	40.030	0.854	0.024
<i>Prkca</i>	7.283	8.429	1.157	0.026
<i>Tcf7l2</i>	6.023	8.102	1.345	0.002

c-Myc target genes, *Apc^{Min}* adenoma

Gene ID	Mean <i>AP4^{Wt}</i>	Mean <i>AP4^{ΔIEC}</i>	fc - <i>AP4^{ΔIEC}</i> vs <i>AP4^{Wt}</i>	P-value
<i>Ung</i>	4.738	2.448	0.517	0.001
<i>Tcof1</i>	11.749	6.444	0.548	0.009
<i>Pprc1</i>	5.890	3.248	0.551	0.019
<i>Plk4</i>	3.399	1.914	0.563	0.015
<i>Utp20</i>	4.344	2.534	0.583	0.023
<i>Mcm5</i>	21.579	12.621	0.585	0.023
<i>Rcl1</i>	12.163	7.139	0.587	0.016
<i>Nolc1</i>	20.655	12.198	0.591	0.028
<i>Myc</i>	25.849	15.303	0.592	0.034
<i>Mcm4</i>	19.945	11.909	0.597	0.010
<i>Mybbp1a</i>	25.928	15.493	0.598	0.024
<i>Gnl3</i>	22.669	13.750	0.607	0.018
<i>Plk1</i>	29.279	17.793	0.608	0.016
<i>Slc19a1</i>	4.350	2.671	0.614	0.017
<i>Cdk4</i>	53.455	33.091	0.619	0.018
<i>Srm</i>	25.398	16.212	0.638	0.047
<i>Cbx3</i>	34.089	21.860	0.641	0.014
<i>Ddx18</i>	22.394	14.787	0.660	0.037
<i>Ndufaf4</i>	6.584	4.382	0.666	0.024
<i>Mphosph10</i>	7.746	5.227	0.675	0.018
<i>Las1l</i>	6.113	4.128	0.675	0.031
<i>Wdr43</i>	18.349	12.592	0.686	0.042
<i>Tfb2m</i>	8.685	5.974	0.688	0.025
<i>Slc29a2</i>	0.843	0.581	0.689	0.019
<i>Prmt3</i>	3.399	2.363	0.695	0.043
<i>Mrto4</i>	14.026	9.804	0.699	0.018
<i>Nip7</i>	10.704	7.597	0.710	0.015
<i>Hspe1</i>	83.661	62.280	0.744	0.016
<i>Imp4</i>	7.404	5.681	0.767	0.047

Related to Figure 25a,b:

Combined stem cell signature, organoids

Gene ID	Mean <i>AP4</i> ^{Wt}	Mean <i>AP4</i> ^{ΔIEC}	fc - <i>AP4</i> ^{ΔIEC} vs <i>AP4</i> ^{Wt}	P-value
<i>Vwa2</i>	0.702	0.142	0.202	0.001
<i>Slc14a1</i>	0.067	0.015	0.226	0.006
<i>Ptgds</i>	2.898	0.670	0.231	< 0.001
<i>Apcdd1</i>	0.860	0.264	0.307	0.030
<i>Pcdh8</i>	2.049	0.654	0.319	0.006
<i>Sfrp5</i>	2.008	0.651	0.324	0.001
<i>Olfm4</i>	401.814	133.163	0.331	< 0.001
<i>Rassf5</i>	0.247	0.084	0.338	0.008
<i>Adra2a</i>	6.777	2.294	0.338	< 0.001
<i>Cap2</i>	0.617	0.214	0.347	0.002
<i>Dmpk</i>	2.598	0.908	0.350	< 0.001
<i>St3gal3</i>	5.681	1.997	0.351	< 0.001
<i>Limch1</i>	0.139	0.051	0.365	0.003
<i>Ccdc3</i>	2.314	0.850	0.367	0.024
<i>Tmem182</i>	0.557	0.211	0.378	0.007
<i>Mylk3</i>	0.614	0.236	0.384	0.002
<i>Angpt2</i>	0.359	0.138	0.385	0.009
<i>Nr2e3</i>	5.020	1.937	0.386	< 0.001
<i>Prelp</i>	2.416	0.980	0.406	0.001
<i>Chst11</i>	2.465	1.000	0.406	< 0.001
<i>Kif26b</i>	0.250	0.102	0.407	0.036
<i>Cbs</i>	5.791	2.382	0.411	0.001
<i>Slco3a1</i>	0.332	0.146	0.439	0.003
<i>Cfi</i>	8.813	3.970	0.450	0.002
<i>H2-Eb1</i>	0.180	0.081	0.451	0.004
<i>Dct</i>	0.243	0.111	0.455	0.005
<i>Hemgn</i>	0.823	0.381	0.463	0.004
<i>Sdr16c5</i>	0.612	0.294	0.481	0.015
<i>Fzd2</i>	4.407	2.166	0.491	0.002
<i>Casp12</i>	0.296	0.148	0.500	0.023
<i>Msi1</i>	4.356	2.209	0.507	0.003
<i>Cttnbp2</i>	1.387	0.704	0.507	< 0.001
<i>Tubb2b</i>	28.482	14.493	0.509	< 0.001
<i>Ifitm3</i>	83.380	42.483	0.510	0.001
<i>Tead2</i>	2.694	1.388	0.515	0.003
<i>Kif12</i>	8.281	4.467	0.539	0.001
<i>Wfdc15b</i>	0.650	0.351	0.540	0.048
<i>Tgif2</i>	5.037	2.721	0.540	0.004
<i>Hebp2</i>	1.735	0.942	0.543	0.004

<i>Rgmb</i>	9.241	5.061	0.548	0.006
<i>Pgc</i>	4.296	2.355	0.548	0.003
<i>Fam65b</i>	0.567	0.316	0.558	0.001
<i>Nrtn</i>	17.617	9.859	0.560	0.017
<i>Gkn3</i>	9.091	5.145	0.566	< 0.001
<i>Klh23</i>	2.133	1.209	0.567	0.002
<i>Cyp11a1</i>	0.115	0.066	0.570	0.010
<i>Smoc2</i>	97.596	55.792	0.572	0.001
<i>Jun</i>	52.195	29.922	0.573	0.003
<i>Esam</i>	2.464	1.445	0.586	0.010
<i>Efna4</i>	19.125	11.221	0.587	0.001
<i>Cited4</i>	10.291	6.075	0.590	0.005
<i>Fam20c</i>	4.595	2.714	0.591	0.006
<i>Tlr2</i>	0.648	0.384	0.593	0.010
<i>Notch1</i>	4.456	2.651	0.595	< 0.001
<i>Ptpro</i>	1.473	0.877	0.595	0.015
<i>Tnfrsf10</i>	1.713	1.020	0.596	0.008
<i>Pthlh</i>	3.205	1.919	0.599	0.001
<i>Axin2</i>	41.383	24.969	0.603	0.005
<i>Lgr5</i>	29.496	17.944	0.608	0.002
<i>Ldhb</i>	0.933	0.571	0.613	0.004
<i>Pdgfra</i>	49.397	30.625	0.620	0.002
<i>Tiam1</i>	5.348	3.322	0.621	0.004
<i>Ascl2</i>	20.796	13.143	0.632	0.002
<i>Dapk2</i>	9.239	5.876	0.636	0.001
<i>Lfng</i>	8.832	5.625	0.637	0.008
<i>Cdc42ep1</i>	22.573	14.399	0.638	0.002
<i>Cnn3</i>	48.763	31.157	0.639	< 0.001
<i>4933406C10Rik</i>	1.371	0.876	0.639	0.006
<i>Tacc1</i>	0.730	0.467	0.639	0.012
<i>Fgd1</i>	1.382	0.887	0.642	0.016
<i>Zfp618</i>	1.373	0.882	0.642	0.002
<i>Slc27a2</i>	11.642	7.520	0.646	0.001
<i>Cachd1</i>	7.104	4.614	0.649	0.005
<i>Cyp2e1</i>	2.555	1.666	0.652	0.001
<i>Sorcs2</i>	7.045	4.607	0.654	0.003
<i>Rgs12</i>	2.243	1.471	0.656	0.008
<i>Il17rd</i>	1.943	1.298	0.668	0.009
<i>Iffo2</i>	9.664	6.463	0.669	0.001
<i>Mpp3</i>	4.036	2.718	0.673	0.016
<i>Sox4</i>	64.237	43.346	0.675	0.008
<i>Nod1</i>	1.966	1.332	0.678	0.008
<i>1700040L02Rik</i>	3.305	2.243	0.679	0.012

<i>Atg16l2</i>	1.296	0.880	0.679	0.011
<i>Ddit4</i>	88.085	60.079	0.682	0.008
<i>Ptprm</i>	0.916	0.627	0.684	0.016
<i>Notch4</i>	0.869	0.594	0.684	0.008
<i>Cdca7</i>	64.325	44.232	0.688	< 0.001
<i>Zfp341</i>	2.612	1.799	0.689	< 0.001
<i>Sesn3</i>	4.417	3.042	0.689	0.006
<i>Grb7</i>	39.013	26.891	0.689	0.002
<i>Pold1</i>	17.986	12.419	0.691	0.006
<i>Arl4c</i>	1.787	1.235	0.691	0.004
<i>Sema7a</i>	31.048	21.477	0.692	0.003
<i>Lysmd2</i>	5.601	3.881	0.693	< 0.001
<i>Zfp503</i>	17.115	11.867	0.693	0.013
<i>Fgfr1</i>	14.118	9.796	0.694	0.004
<i>Smarcd3</i>	0.579	0.402	0.694	0.032
<i>Evl</i>	4.520	3.144	0.695	0.024
<i>Cib2</i>	4.401	3.064	0.696	0.008
<i>Vav3</i>	1.391	0.973	0.699	0.042
<i>Zfp90</i>	2.470	1.731	0.701	0.010
<i>Wipi1</i>	7.058	4.959	0.703	0.001
<i>Aqp4</i>	15.463	10.926	0.707	0.004
<i>Lrig1</i>	54.543	38.541	0.707	0.001
<i>Ephb3</i>	15.258	10.790	0.707	0.004
<i>Ung</i>	12.647	8.946	0.707	0.010
<i>Sdc4</i>	72.832	51.648	0.709	0.001
<i>Isyna1</i>	55.774	39.925	0.716	0.006
<i>Pla2g4a</i>	7.253	5.213	0.719	0.009
<i>Arhgap39</i>	4.517	3.248	0.719	0.005
<i>D930015E06Rik</i>	3.648	2.629	0.721	0.003
<i>Fbxo21</i>	6.634	4.792	0.722	0.013
<i>Fhdc1</i>	5.190	3.756	0.724	0.002
<i>Smo</i>	14.499	10.544	0.727	0.003
<i>Igfbp4</i>	58.600	42.725	0.729	0.007
<i>Spata24</i>	9.425	6.877	0.730	0.012
<i>Fam64a</i>	5.239	3.825	0.730	0.005
<i>Rnf43</i>	34.601	25.325	0.732	0.002
<i>Irf2bp2</i>	64.700	47.466	0.734	0.032
<i>Soat1</i>	14.996	11.039	0.736	0.002
<i>Sertad4</i>	2.360	1.738	0.736	0.002
<i>Phc1</i>	2.300	1.696	0.737	0.005
<i>Wwtr1</i>	2.595	1.915	0.738	0.006
<i>Aqp1</i>	53.646	39.653	0.739	0.017
<i>Ttc21b</i>	1.899	1.413	0.744	0.006

<i>Zfp956</i>	5.813	4.329	0.745	< 0.001
<i>Kcnq1</i>	57.142	42.575	0.745	0.005
<i>Timeless</i>	6.475	4.828	0.746	< 0.001
<i>Acvr2b</i>	3.619	2.699	0.746	< 0.001
<i>Rassf10</i>	1.270	0.947	0.746	0.004
<i>Hunk</i>	19.820	14.793	0.746	0.001
<i>Sox9</i>	44.149	33.015	0.748	0.002
<i>Arhgef4</i>	0.385	0.288	0.749	0.024
<i>Mpzl1</i>	20.591	15.463	0.751	< 0.001
<i>Qsox2</i>	18.237	13.713	0.752	0.008
<i>Ifitm2</i>	198.896	149.751	0.753	0.003
<i>Engase</i>	26.287	19.868	0.756	0.006
<i>Greb1</i>	6.113	4.621	0.756	0.002
<i>Clic6</i>	35.039	26.492	0.756	< 0.001
<i>Gpld1</i>	17.060	12.913	0.757	< 0.001
<i>Farp1</i>	13.258	10.063	0.759	0.001
<i>Etv6</i>	21.313	16.188	0.760	0.001
<i>Rccd1</i>	3.521	2.675	0.760	0.011
<i>Sorbs2</i>	3.397	2.584	0.761	0.006
<i>Ptprs</i>	22.069	16.822	0.762	0.010
<i>Gas6</i>	102.714	78.316	0.762	0.003
<i>Fam49a</i>	1.817	1.387	0.764	0.025
<i>Pole</i>	6.247	4.796	0.768	< 0.001
<i>Dtx4</i>	13.068	10.032	0.768	0.003
<i>Dgkg</i>	1.156	0.888	0.768	0.018
<i>Rhbdf1</i>	12.681	9.742	0.768	0.008
<i>Plekhb1</i>	1.451	1.118	0.771	0.022
<i>Mcc</i>	2.286	1.764	0.771	0.004
<i>Zkscan17</i>	12.633	9.754	0.772	0.005
<i>Pde3b</i>	2.329	1.799	0.772	0.005
<i>Napepld</i>	5.904	4.562	0.773	< 0.001
<i>Pacsin3</i>	2.024	1.565	0.773	0.012
<i>Fam43a</i>	0.613	0.474	0.773	0.033
<i>Gramd1a</i>	1.322	1.024	0.774	0.025
<i>1110051M20Rik</i>	4.432	3.432	0.774	0.009
<i>Gins1</i>	6.734	5.225	0.776	0.034
<i>Zbtb38</i>	5.514	4.279	0.776	0.001
<i>Fads1</i>	66.039	51.371	0.778	< 0.001
<i>Bcl7a</i>	4.120	3.209	0.779	0.002
<i>Espl1</i>	6.491	5.058	0.779	0.007
<i>Cit</i>	3.219	2.509	0.779	0.003
<i>Dbp</i>	13.260	10.362	0.781	0.004
<i>Lcp1</i>	12.024	9.436	0.785	0.002

<i>Mnx1</i>	5.302	4.163	0.785	0.048
<i>Tmem9</i>	10.408	8.181	0.786	0.007
<i>Phlpp1</i>	5.967	4.703	0.788	0.004
<i>Zc3hav1l</i>	1.300	1.025	0.789	0.001
<i>Rasa3</i>	7.163	5.655	0.789	0.001
<i>Adrbk2</i>	3.678	2.919	0.794	0.007
<i>Tcf7</i>	4.213	3.348	0.795	0.029
<i>Fras1</i>	2.047	1.631	0.797	0.036
<i>Plxnb1</i>	4.983	3.983	0.799	0.010
<i>Cd320</i>	4.121	3.295	0.800	0.021
<i>Fam171a1</i>	10.353	8.283	0.800	< 0.001
<i>Pde8b</i>	0.927	0.746	0.804	0.018
<i>Mif</i>	974.795	786.847	0.807	0.032
<i>Dtl</i>	5.768	4.678	0.811	0.022
<i>Ilf3</i>	20.691	16.805	0.812	< 0.001
<i>Phlda1</i>	110.713	89.925	0.812	0.012
<i>Atp11a</i>	3.754	3.051	0.813	0.001
<i>Zfp783</i>	2.348	1.916	0.816	0.004
<i>Hirip3</i>	10.231	8.358	0.817	0.006
<i>Pbx1</i>	4.062	3.325	0.819	0.032
<i>Gkap1</i>	4.085	3.346	0.819	0.048
<i>Znrf3</i>	4.325	3.550	0.821	0.020
<i>Impdh2</i>	76.542	62.866	0.821	0.003
<i>Nfic</i>	9.383	7.713	0.822	0.050
<i>Gemin8</i>	1.377	1.136	0.825	0.005
<i>Afap1</i>	2.165	1.789	0.826	0.003
<i>Fzd7</i>	13.396	11.071	0.826	0.020
<i>Csad</i>	8.655	7.156	0.827	0.007
<i>Ets2</i>	64.227	53.267	0.829	0.011
<i>Mlxip</i>	13.268	11.020	0.831	< 0.001
<i>Srl</i>	3.124	2.599	0.832	0.015
<i>Zfp704</i>	5.650	4.708	0.833	0.004
<i>Adora1</i>	8.805	7.344	0.834	0.017
<i>Socs2</i>	4.751	3.968	0.835	< 0.001
<i>Blnk</i>	6.831	5.731	0.839	0.001
<i>AU020206</i>	6.421	5.387	0.839	0.050
<i>Zfp12</i>	2.566	2.153	0.839	0.011
<i>Maged1</i>	20.344	17.087	0.840	0.038
<i>Spice1</i>	2.084	1.754	0.842	0.036
<i>Vdr</i>	31.001	26.098	0.842	0.001
<i>Psrc1</i>	13.462	11.343	0.843	0.015
<i>Nin</i>	1.134	0.957	0.844	0.007
<i>App</i>	193.920	163.702	0.844	0.002

<i>BC021891</i>	16.478	13.914	0.844	0.002
<i>Cdca7l</i>	13.578	11.476	0.845	0.018
<i>Pla2g5</i>	11.321	9.596	0.848	0.005
<i>Limk2</i>	46.715	39.660	0.849	0.009
<i>Zfhx3</i>	3.237	2.754	0.851	0.027
<i>Slc44a2</i>	12.639	10.755	0.851	0.003
<i>Lipt2</i>	5.205	4.455	0.856	0.034
<i>Pck2</i>	49.534	42.484	0.858	0.030
<i>Cdk6</i>	15.286	13.121	0.858	0.019
<i>Tgif1</i>	14.378	12.351	0.859	0.010
<i>Dctd</i>	9.144	7.875	0.861	0.004
<i>Rprd1a</i>	5.197	4.478	0.862	0.016
<i>Sept6</i>	2.380	2.053	0.862	0.044
<i>Kif20a</i>	12.774	11.017	0.862	0.016
<i>Sfpq</i>	65.732	56.796	0.864	0.004
<i>Myc</i>	76.280	65.983	0.865	0.013
<i>Hmbox1</i>	5.374	4.656	0.866	0.017
<i>Spag5</i>	8.510	7.383	0.868	0.009
<i>Gabbr1</i>	4.255	3.693	0.868	0.002
<i>Marveld1</i>	3.917	3.407	0.870	0.028
<i>Ckap2</i>	13.409	11.673	0.871	0.037
<i>Zfp462</i>	1.801	1.568	0.871	0.015
<i>Prkd3</i>	2.252	1.966	0.873	0.034
<i>Kank1</i>	7.130	6.266	0.879	0.008
<i>Arid5b</i>	11.172	9.858	0.882	< 0.001
<i>Nfia</i>	4.597	4.076	0.887	0.025
<i>Hdac11</i>	17.254	15.330	0.888	0.028
<i>Ces1d</i>	16.484	14.670	0.890	0.013
<i>Rpl22</i>	141.929	127.180	0.896	0.016
<i>Tbc1d9</i>	6.907	6.190	0.896	0.009
<i>4933431E20Rik</i>	2.049	1.841	0.899	0.027
<i>Emp2</i>	46.719	42.252	0.904	0.001
<i>Tns3</i>	13.860	12.536	0.904	0.050
<i>Aldh7a1</i>	4.823	4.376	0.907	0.025
<i>Utrn</i>	11.402	10.423	0.914	0.045
<i>Pabpc1</i>	257.050	235.469	0.916	0.019
<i>Klhl13</i>	0.979	1.071	1.094	0.048
<i>Lamb3</i>	35.654	41.027	1.151	0.047
<i>Mipol1</i>	0.860	0.998	1.160	0.010
<i>Rpe</i>	16.136	19.183	1.189	0.001
<i>Atm</i>	3.415	4.282	1.254	0.035
<i>Id2</i>	12.635	16.023	1.268	0.032
<i>Vnn1</i>	2.774	3.617	1.304	0.023

<i>Phldb2</i>	4.520	5.909	1.307	0.008
---------------	-------	-------	-------	-------

Combined Wnt signature, organoids

Gene ID	Mean <i>AP4^{Wt}</i>	Mean <i>AP4^{ΔIEC}</i>	fc - <i>AP4^{ΔIEC}</i> vs <i>AP4^{Wt}</i>	P-value
<i>Notch1</i>	4.456	2.651	0.595	< 0.001
<i>Axin2</i>	41.383	24.969	0.603	0.005
<i>Dll1</i>	8.058	4.963	0.616	< 0.001
<i>Tiam1</i>	5.348	3.322	0.621	0.004
<i>Ascl2</i>	20.796	13.143	0.632	0.002
<i>Rgs12</i>	2.243	1.471	0.656	0.008
<i>Sox4</i>	64.237	43.346	0.675	0.008
<i>Notch4</i>	0.869	0.594	0.684	0.008
<i>Bcl7c</i>	3.757	2.810	0.748	0.010
<i>Trp53</i>	32.987	24.785	0.751	0.005
<i>Ptch1</i>	4.224	3.176	0.752	0.002
<i>Ifitm2</i>	198.896	149.751	0.753	0.003
<i>Frat1</i>	9.286	7.054	0.760	0.008
<i>Dvl2</i>	5.021	3.848	0.766	0.025
<i>Jag2</i>	12.974	10.117	0.780	0.036
<i>Apex1</i>	47.816	37.389	0.782	0.006
<i>Hdac5</i>	6.714	5.282	0.787	0.041
<i>Rasa3</i>	7.163	5.655	0.789	0.001
<i>Tcf7</i>	4.213	3.348	0.795	0.029
<i>Smyd2</i>	34.225	28.006	0.818	0.003
<i>Impdh2</i>	76.542	62.866	0.821	0.003
<i>Kat2a</i>	15.867	13.142	0.828	0.027
<i>Psen2</i>	3.230	2.723	0.843	0.015
<i>Smyd5</i>	10.884	9.287	0.853	0.013
<i>Axin1</i>	18.539	15.889	0.857	0.017
<i>Tox</i>	4.635	3.992	0.861	0.034
<i>Skp2</i>	2.170	1.872	0.862	0.022
<i>Myc</i>	76.280	65.983	0.865	0.013
<i>Ccnd2</i>	66.420	57.730	0.869	0.011
<i>Hdac11</i>	17.254	15.330	0.888	0.028
<i>Numb</i>	14.321	13.698	0.957	0.005

Combined Notch signature, organoids

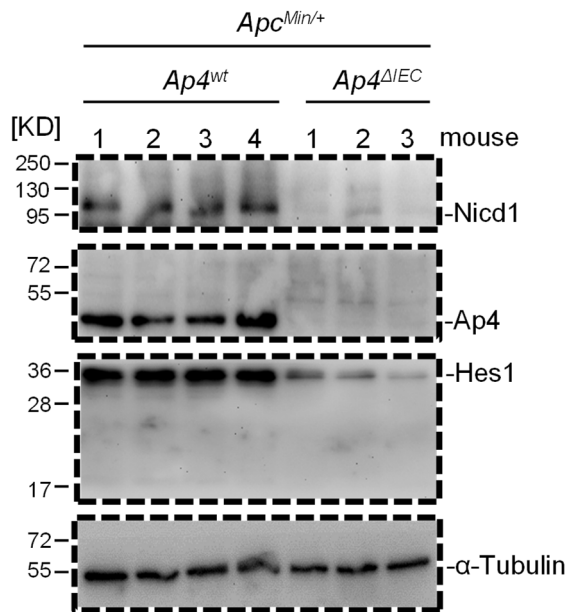
Gene ID	Mean <i>AP4^{Wt}</i>	Mean <i>AP4^{ΔIEC}</i>	fc - <i>AP4^{ΔIEC}</i> vs <i>AP4^{Wt}</i>	P-value
<i>Dll3</i>	0.700	0.376	0.537	0.006
<i>Notch1</i>	4.456	2.651	0.595	< 0.001
<i>Dll1</i>	8.058	4.963	0.616	< 0.001
<i>Lfng</i>	8.832	5.625	0.637	0.008
<i>Notch3</i>	2.124	1.353	0.637	0.001
<i>Mfng</i>	0.298	0.202	0.678	0.007
<i>Dll4</i>	3.637	2.472	0.680	< 0.001
<i>Notch4</i>	0.869	0.594	0.684	0.008
<i>Gm9840</i>	0.286	0.195	0.685	0.012
<i>Dtx3</i>	2.876	2.037	0.708	0.018
<i>Hes1</i>	58.314	44.004	0.755	0.009
<i>Dvl2</i>	5.021	3.848	0.766	0.025
<i>Dtx4</i>	13.068	10.032	0.768	0.003
<i>Jag2</i>	12.974	10.117	0.780	0.036
<i>Ccnd1</i>	42.258	33.371	0.790	< 0.001
<i>Maml3</i>	3.037	2.481	0.817	0.001
<i>Ctbp1</i>	54.850	44.844	0.818	0.016
<i>Dtx2</i>	1.704	1.394	0.818	0.044
<i>Fzd7</i>	13.396	11.071	0.826	0.020
<i>Kat2a</i>	15.867	13.142	0.828	0.027
<i>Psen2</i>	3.230	2.723	0.843	0.015
<i>Rbx1</i>	34.554	29.270	0.847	0.006
<i>Sap30</i>	19.486	16.908	0.868	0.045
<i>Hdac1</i>	27.162	24.273	0.894	0.002
<i>Numb</i>	14.321	13.698	0.957	0.005
<i>Psen1</i>	28.568	30.631	1.072	0.002
<i>Arrb1</i>	11.541	12.788	1.108	0.017
<i>Dtx3l</i>	3.833	4.799	1.252	0.010

c-Myc target genes, organoids

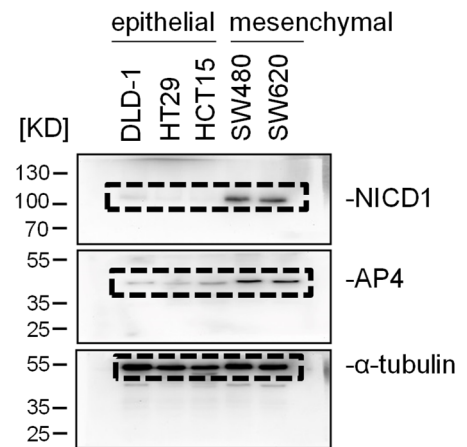
Gene ID	Mean <i>AP4</i> ^{Wt}	Mean <i>AP4</i> ^{ΔIEC}	fc - <i>AP4</i> ^{ΔIEC} vs <i>AP4</i> ^{Wt}	P-value
<i>Ung</i>	12.647	8.946	0.707	0.010
<i>Mcm5</i>	36.978	27.227	0.736	0.002
<i>Plk1</i>	35.717	27.060	0.758	< 0.001
<i>Tcof1</i>	15.961	12.203	0.765	0.004
<i>Mcm4</i>	29.387	22.827	0.777	0.008
<i>Dctpp1</i>	51.572	40.219	0.780	0.020
<i>Cdk4</i>	77.414	60.999	0.788	0.006
<i>Pus1</i>	29.030	23.018	0.793	0.010
<i>Rcl1</i>	22.011	17.535	0.797	< 0.001
<i>Slc19a1</i>	18.863	15.570	0.825	0.002
<i>Pprc1</i>	12.816	10.754	0.839	0.006
<i>Plk4</i>	4.608	3.935	0.854	0.007
<i>Mrto4</i>	16.938	14.524	0.857	0.016
<i>Myc</i>	76.280	65.983	0.865	0.013
<i>Noc4l</i>	15.664	13.592	0.868	0.050
<i>Rrp12</i>	9.255	8.047	0.869	0.042
<i>Nolc1</i>	39.795	35.251	0.886	0.011
<i>Hk2</i>	13.263	11.822	0.891	0.021
<i>Hspe1</i>	105.098	95.664	0.910	0.012
<i>Mybbp1a</i>	52.743	48.050	0.911	0.014
<i>Pes1</i>	36.673	33.527	0.914	0.013
<i>Rabepk</i>	4.127	3.780	0.916	0.030
<i>Tmem97</i>	85.989	79.351	0.923	0.002
<i>Tbrg4</i>	27.708	25.648	0.926	0.046
<i>Nip7</i>	12.845	12.195	0.949	0.009

11.3 Supplemental Data 3: related to Figure 17e, 26a, b, d

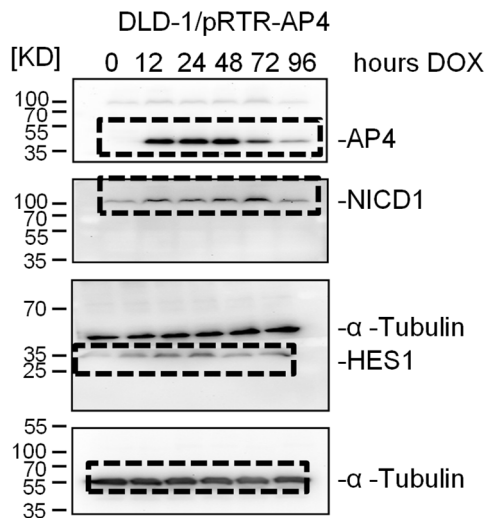
Figure 17e



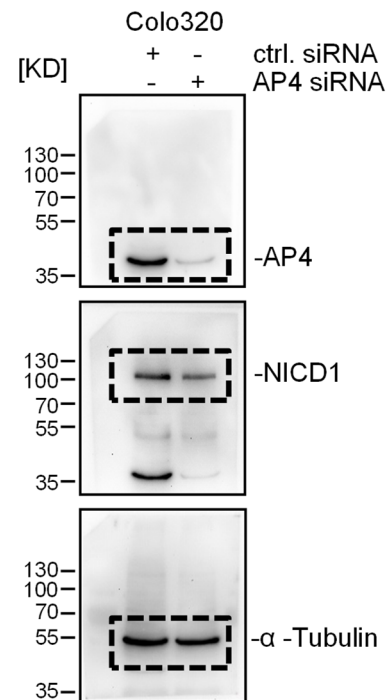
Supplementary Figure 26a



Supplementary Figure 26b



Supplementary Figure 26d



Supplemental Data 3. Uncropped Western blot membranes

Corresponding uncropped membranes of western blots shown in Figure 17e and 26a,b,d. Membranes were cut to enable blotting for multiple antibodies. The protein standards are depicted to the left. The part of the membranes shown in the stated figures is represented by dashed lines.